2010

Electrophysiological Analysis in an Animal Model of Dystonia

Kunal Chaniary
Virginia Commonwealth University

Follow this and additional works at: http://scholarscompass.vcu.edu/etd

Part of the Biomedical Engineering and Bioengineering Commons

Downloaded from
http://scholarscompass.vcu.edu/etd/93

ELECTROPHYSIOLOGICAL ANALYSIS IN AN ANIMAL MODEL OF DYSTONIA

A Dissertation submitted in partial fulfillment of the requirements for the degree of
DOCTOR OF PHILOSOPHY at Virginia Commonwealth University.

by

KUNAL DILIP CHANIARY
MASTER OF SCIENCE, VIRGINIA COMMONWEALTH UNIVERSITY, 2008
BACHELOR OF ENGINEERING, UNIVERSITY OF MUMBAI, INDIA, 2005

Director: DR. PAUL A. WETZEL
ASSOCIATE PROFESSOR, DEPARTMENT OF BIOMEDICAL ENGINEERING

Virginia Commonwealth University
Richmond, Virginia
May 2010

Acknowledgements

Firstly, I would like to thank my advisor, Dr. Wetzel for his guidance throughout this project and his encouragement in pursuing this exciting line of research. His insights in digital signal processing have helped me tremendously in this project.

I would like to express my gratitude to Dr. Shapiro for giving me with an opportunity to work on this research. His in-depth knowledge and logical way of thinking has been of great help to me. His extensive discussions around my work and constructive comments have been very helpful throughout this project.

I am extremely thankful to Dr. Mark Baron whose help, suggestions, patience and encouragement has helped me at all times during this research project. His perpetual energy and enthusiasm in research has motivated me to work harder towards my research. Throughout the entire project he has encouraged me to develop independent thinking and research skills.

I would like to thank Dr. Ann Rice for all her invaluable suggestions and guidance throughout this project and for the efforts she has put in helping me understand the field of neuroscience better. Her detailed review, constructive criticism and excellent advice have helped me immensely in improving my skills for technical writing. I would

also like to thank my committee members, Dr. Bai and Dr. Fei for all the guidance and support throughout this project.

Last and most importantly, I would like to thank my parents for their enduring love and support throughout my life in achieving my dreams. None of this would have been possible without their blessings and encouragement. To them I dedicate this thesis. Also, I would like to thank my friends who have been a constant source of encouragement throughout my graduate study.

Table of Contents

List of Tables

List of Figures

List of Abbreviations

DBS	Deep brain stimulation
GPi	Globus pallidus internus
DYT1	Dystonia 1 gene
UDGT	Uridine diphosphate glucuronosyl transferase
MRI	Magnetic resonance imaging
BAEP	Brainstem auditory evoked potentials
STN	Subthalamic nucleus
GPe	Globus pallidus externus
SNr	Substantia nigra pars reticulata
GP	Globus pallidus (rat equivalent of GPe)
EP	Entopeduncular nucleus (rat equivalent of GPi)
Sulfa	Sulfadimethoxine
jj	Jaundiced rat
Nj	Non-jaundiced rat
GABA	Gamma aminobutyric acid
dt^{sz}	Dystonic hamster model
EMG	Electromyography
IACUC	Institutional animal care and use committee
CS	Clinical Scores
DWT	Discrete wavelet transform
ANOVA	Analysis of variance
SLR	Step length ratio
SSR	Stance to swing ratio
PCA	Principal Component Analysis
MER	Microelectrode recordings
ISI	Interspike interval
SD	Standard deviation
CV	Coefficient of variation
PETH	Perievent histograms

<u>Abstract</u>

ELECTROPHYSIOLOGICAL ANALYSIS IN AN ANIMAL MODEL OF DYSTONIA

By Kunal Dilip Chaniary, Ph.D.

A Dissertation submitted in partial fulfillment of the requirements for the degree of Doctor of Philosophy at Virginia Commonwealth University.

Virginia Commonwealth University, 2010

Director: Paul A. Wetzel, Ph.D.
Associate Professor, Department of Biomedical Engineering

Dystonia is a movement disorder characterized by patterned, repetitive, and sustained muscle contractions that cause ineffective and often painful movements. The overall goal of this project was to understand the physiological mechanisms of dystonia in a rodent model as a basis for developing innovative treatments for secondary dystonias. The first half of the project was focused at developing essential techniques for systematically investigating the movement disorder in these animals. For achieving this, an innovative, multi-faceted approach was pursued starting with electromyographic (EMG) analysis for animal model validation, gait analysis for dystonia quantification, and development of a novel stereotaxic apparatus for recording brain activity during awake conditions. The later half of the project was focused on understanding how brain circuitry produces abnormal

motor control in dystonia. Single and multi-unit neuronal activity was collected from individual basal ganglia nuclei along with EMG recordings to characterize the abnormal patterns of firing in dystonic animals and determine how neurons within individual nuclei communicate in dystonia, respectively. The findings of the current project have lead to new insights into the pathophysiology and treatment of secondary kernicteric dystonia and other secondary dystonia in humans.

CHAPTER 1 INTRODUCTION

1.1. DYSTONIA:

Dystonia is a heterogeneous group of movement disorder that produces patterned, repetitive, and often sustained muscle contractions thereby causing ineffective and often painful movements (1). It is characterized physiologically by co-contractions of antagonistic muscles and overflow contractions of nearby muscles (2, 3). Dystonic movements can occur in all regions of the body and may occur when the body part is at rest or engaged in voluntary motor function. The underlying pathophysiology of dystonia is poorly understood and treatments are inadequate (4, 5). Therefore, experimental studies in animal models are critically necessary towards understanding the underlying pathophysiological mechanisms and ultimately developing better therapies (6).

Dystonia can be classified based on the anatomical distribution, age of onset, and etiology (7, 8). Classification by anatomical distribution includes focal dystonia in which only a single body part is affected, multifocal dystonia where two or more non-adjacent body are involved, segmental dystonia where two or more body adjacent body parts are involved, hemidystonia which involves one side of the body and generalized dystonia

characterized by involvement of muscles throughout the body (3). Based on the age of onset, dystonia can be classified as early-onset dystonia (<20 yrs) in which symptoms begin during childhood or adolescence and the disorder eventually becomes generalized causing severe twisting of the trunk and the extremities. In contrast, in late-onset dystonia the symptoms begin at older age and tend to remain localized to a single region, such as the neck and the hand. Another way to classify dystonia is based on etiology, including primary dystonia *describing* inherited or sporadic cases and secondary dystonia, which, for example, can result from strokes or the effects of drugs (3).

Dystonia is one of the most challenging movement disorders to treat. Although presently there is no way to cure dystonia, there are multiple treatment options using pharmacological, surgical and physical therapy to help ease the severity of symptoms (1). As the disease progresses, one or a combination of these methods could be used for treatment depending on severity of symptoms. For patients with severe dystonia who fail to respond to oral medications, the use of deep brain stimulation (DBS) can improve the dystonic symptoms and enhance functional capacity. In deep brain stimulation, an implanted medical electrode sends electrical signals to specific regions in the brain that are abnormally functioning. The electrical stimulation reorganizes the brain's electrical impulses thereby allowing the brain to function more normally. Over the years, bilateral globus pallidus internus (GPi)-DBS procedures have been highly successful for treating primary generalized dystonia, especially the early-onset primary dystonia (DYT1 type) (9). In contrast, patients with secondary dystonia undergoing bilateral GPi-DBS often display

lesser and more variable degree of improvement (10). One possible reason for this disparity could be because secondary dystonias result from strokes, metabolic abnormalities; cerebral palsy etc., each of which involves different brain regions (11). It is possible that secondary forms of dystonia may involve pathology within single or multiple motor pathways. To date, in spite of years of research, scientists have failed to understand how abnormal brain signaling triggers distorted motor control in dystonia. Thus, major advances in the knowledge of pathophysiology of dystonia are critically needed in the pursuit of more effective therapies for this devastating movement disorder. The overall aim in this project was to elucidate the underlying pathophysiology of dystonia in jaundiced Gunn rat model as a basis for developing novel therapies for secondary, as well as primary dystonias.

1.2. KERNICTERUS:

In newborn infants, the red blood cell volume is high and specific liver enzyme function that conjugates bilirubin in order to eliminate it is low. After birth their body begins to rapidly destroy the red blood cells containing the fetal-type hemoglobin and replaces them with red blood cells containing the adult-type hemoglobin. Bilirubin, an end product of heme catabolism is lipid soluble, water-insoluble and neurotoxic. Under normal circumstances, unconjugated bilirubin in the blood is bound to albumin is transported to the liver and is broken down by uridine diphosphate glucuronosyl transferase (UDGT) and excreted in bile. However, in newborn infants, due to immaturity of the liver enzymes the

bilirubin in blood cannot be completely metabolized. Therefore, neonatal jaundice is a common problem among newborn infants during the first week of life. Most infants develop only mild jaundice (physiological jaundice) due to the elevation of bilirubin concentration (12). In most cases, the jaundice disappears after the first few days without any special treatment as UDGT matures.

On the other hand, many newborn infants develop severe jaundice, putting them at risk of developing kernicterus (13). Excessive hyperbilirubinemia especially can cause severe, permanent brain damage known as kernicterus (14). In preterm and low weight infants, the bilirubin binding capacity of serum albumin is exceeded and the levels of unconjugated-indirect bilirubin in the blood increases. This extra amount of bilirubin if not effectively reduced using phototherapy and/or exchange transfusion can cross the blood-brain barrier and penetrate the brain to cause permanent brain damage. The basal ganglia and the auditory system are most susceptible to damage from the bilirubin toxicity (15, 16). Damage to the auditory system can lead to auditory neuropathy and under prolonged exposures can cause permanent hearing loss. Damage to the basal ganglia results in dystonia, athetosis and spasticity. The syndrome in term infants can be identified by high pitched cry, poor sucking or nursing, weakness, abnormalities of muscle tone including increased muscle tone (hypertonia) and decreased muscle tone (hypotonia), lethargy, arching of the back and spine, fever and abnormal auditory brainstem potentials (17).

Permanent neurological damage in kernicterus can be prevented if detection and diagnosis is done at an early stage. Currently the clinical diagnosis in kernicterus can be confirmed using magnetic resonance imaging (MRI) and Brainstem Auditory Evoked Potentials (BAEPs). BAEP's measured in hyperbilirubinemic infants show an increase in interwave interval indicating increased conduction time and decrease in amplitude indicates auditory dys-synchrony (15-17). One commonly used method used for hyperbilirubinemia treatment is phototherapy. In this method light causes photoisomerization of bilirubin into non-toxic water soluble products thereby preventing

A.   **B.**
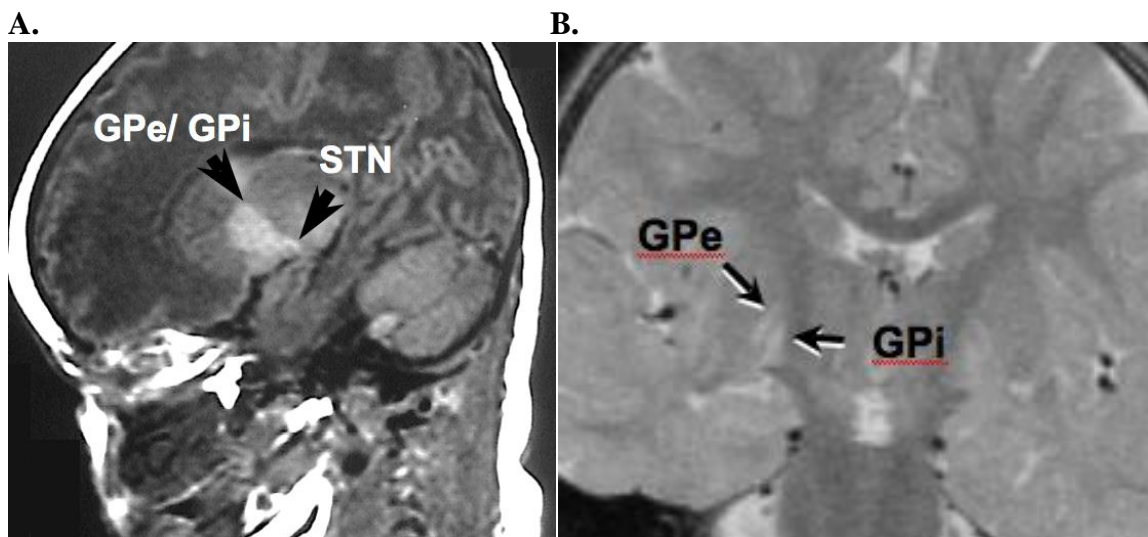
Fig 1. Characteristic focal MRI signal changes in children with kernicterus. A. A 10-day-old; T1 sagittal sequence, and **B**. a 2-year-old; T2 coronal sequence

toxic accumulation of bilirubin in the body to prevent permanent brain damage. Another method used to treat severe hyperbilirubinemia is exchange transfusion. In this therapy the baby's blood is replaced with donor's blood that does not contain bilirubin. The goal of this procedure is to remove enough bilirubin to prevent severe complication of brain damage due to kernicterus (13, 15, 17).

Classic kernicterus include symptoms like hearing loss or deafness due to central auditory processing disorder (auditory neuropathy/dyssynchrony), dystonia due to involvement of basal ganglia, impairment vertical gaze paralysis and enamel dysplasia of primary teeth. Pathologic findings in human autopsies of kernicterus neonates indicate prominent cell loss and gliosis in the globus pallidus externa (GPe, equivalent to the rodent GP), the globus pallidus interna (GPi, equivalent to rodent EP), subthalamic nucleus (STN) and substantia nigra reticulata (SNr), and less consistently in the brainstem auditory nuclei, oculomotor nuclei, hippocampus and cerebellum (12, 18-28). Consistent with pathological findings, MRI studies of kernicterus patients show abnormally high signal intensity in posteromedial border of globus pallidus **(Fig. 1)** (29).

Despites advances in medicine, kernicterus continues to be a threat to newborn infants and a significant risk for central nervous system damage and neurodevelopment disabilities. A better understanding of effects of bilirubin toxicity in basal ganglia will lead to more effective strategies in preventing and treating kernicterus-induced dystonia. This dissertation is focused at understanding the effects of bilirubin toxicity on the basal ganglia so as to develop new efficacious therapies for children suffering with kernicterus.

1.3. GUNN RAT MODEL:

In this dissertation, dystonia has been studied using the Gunn rat model of kernicterus. The spontaneously jaundiced Gunn rat model very closely mimics kernicterus in humans and is presently the best available model of bilirubin encephalopathy (30, 31).

The Gunn rat was first described in 1938 by C.K. Gunn as a mutant jaundiced rat of the Wistar rat strain (Gunn, 1938). The homozygous recessive (jj) Gunn rat lacks the enzyme uridine diphosphate glucuronosyl transferase, which is responsible for the conversion of unconjugated bilirubin to conjugated

Fig. 2: Dystonic Gunn rat.
Dystonic posture in a 21 day old jj Gunn rat. Note the abnormal dystonic posture, especially in the hind limbs.

bilirubin (32, 33). In jj Gunn rats, the plasma bilirubin level peak naturally at about postnatal day 16 and remain moderately elevated throughout the animal's life. Their usually mild bilirubin encephalopathy can be accentuated by injecting the jj rats with sulfadimethoxine (sulfa) on day 16 to displace bilirubin from blood albumin sites into tissues, including the brain (15, 16, 32-35). Within hours after sulfa injection, the rats develop auditory system dysfunction and abnormal prolonged axial and appendicular posturing **(Fig. 2)** (36). Heterozygous non-jaundiced (Nj) rats have about 50% of the normal enzyme activity and are phenotypically normal (37).

Previous studies in jaundiced Gunn rat have focused particularly on the damage in the auditory brainstem pathways (15, 32-35). In contrast; the clinical aspects and the pathophysiological correlate of the movement disorder have never been systematically investigated in this animal model. The experiments included in this dissertation are intended towards advancing the knowledge about physiological mechanisms of dystonia in these animals and how abnormal brain signaling produces distorted motor control in dystonia. The Gunn rat model of kernicterus provides an unique opportunity to investigate

underlying pathophysiological mechanisms of dystonia and potential therapeutic strategies for treating this condition.

1.4. BASAL GANGLIA:

The basal ganglia are a group of nuclei located in the central part of the neuronal loop that receives input from the several areas of the cortex and projects via the thalamus back to the prefrontal and motor cortical areas (38). The basal ganglia comprise the striatum (caudate, putamen and nucleus accumbens), subthalamic nucleus, globus pallidus (external and internal) and substantia nigra

Striatum

The striatum is the main input nucleus of the basal ganglia. The striatum can be divided into three main parts 1) caudate 2) putamen 3) ventral striatum. Of these, the putamen is the primary site for motor-related input. The striatum receives excitatory projections from almost the entire cerebral cortex, especially from the sensorimotor and frontal cortex. The majority of afferent projections synapse upon the medium spiny neurons of the striatum which comprises 96% of the cells in the nucleus (39). Striatal neurons contain gamma aminobutyric acid (GABA) as the neurotransmitter, typically considered to be inhibitory. Based on the traditional basal ganglia models the striatum is considered to regulate activity in GPi, principal output nucleus of the basal ganglia by two pathways, the direct and the indirect (discussed in **section 1.5**.).

Subthalamic nucleus

Subthalamic nucleus (STN) is considered to be an important modulator in the basal ganglia output (40). The STN is a small biconvex shaped structure, densely populated and highly vascularized nucleus (40, 41). STN mainly consist of glutamatergic projection neurons (excitatory). The subthalamic nucleus receives widespread excitatory cortical input from the frontal cortex and cortical somato-motor areas. Additionally, STN has strong reciprocal connections with the globus pallidus externus (GPe) and has been shown to play a role in synchronizing oscillatory activity in GPe (42). In addition to GPe connections, efferent projections from the STN are directed to globus pallidus internus (GPi) and substantia nigra pars reticulata (SNr). *In vivo* single unit recordings have shown that STN cells are tonically active (10-30 Hz) and fire short bursts during movement (43). The average discharge rate is 13-18 Hz in normal rats and 18-25 Hz in non-human primates (43-50).

Globus Pallidus

The pallidum is divided into two parts: the globus pallidus externus (GPe) and globus pallidus internus (GPi).

Globus pallidus externus (GPe)

The GPe is considered to be a relay station along the indirect pathway connecting the input and output structures of the basal ganglia. GPe neurons are GABAergic; therefore, their output is inhibitory. The GPe is reciprocally connected to both the input

structures of the basal ganglia i.e. STN and striatum. In addition, GABAergic projections (inhibitory) of GPe innervate the GPi and SNr. *In vivo* single unit recordings have described two main types of neurons in GPe: 1) The majority of neurons (~85%) exhibit high frequency discharge (40-60Hz) with pauses (0.5 – 1 sec). 2) Remaining 15% neurons exhibit low frequency discharge (~20 Hz) and infrequent bursts. The average discharge rate of GPe neurons has been reported to be 20-25 Hz in rats (Ni 2000 changes in the firing pattern) and 60-70 Hz in non-human primates (45, 51). **The globus pallidus (GP) nucleus is the rodent equivalent of GPe.**

Globus Pallidus internus (GPi)

The GPi is major output nuclei of the basal ganglia. GPi neurons receive inhibitory input from the striatum and GPe and excitatory input from the STN. The GABAergic neurons of GPi project exert tonic inhibitory influence on thalamus (ventral-lateral and ventral-anterior), interlaminar thalamic nuclei, the centeromedian and parafascicular nucleus (52). Most of the anatomical, physiological and biochemical properties of GPi neurons are similar to GPe (39). *In vivo* single-unit recordings in GPi neurons have shown that they are have high frequency discharge (60-70 Hz) with no pauses. **The entopeduncular nucleus (EP) is the rodent equivalent of GPe.**

1.5 BASAL GANGLIA PHYSIOLOGY:

In order to understand the potential role of basal ganglia in dystonia it is important

to review the current models of basal ganglia function (**Fig. 3**). According to these models,

Fig. 3: Traditional model of basal ganglia-thalamocortical motor circuitry. Filled arrows
indicate inhibitory projections while clear arrows indicate excitatory projections
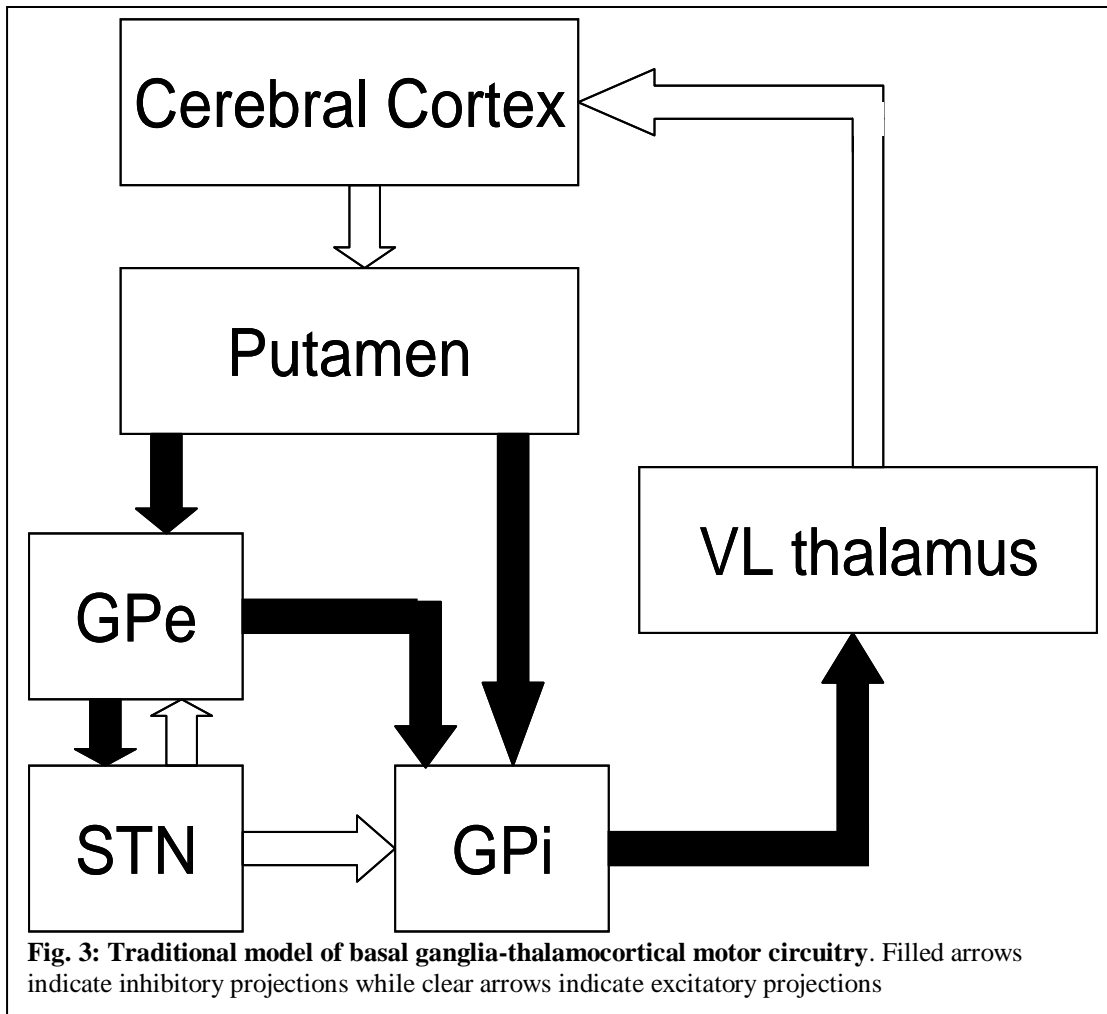
the basal ganglia mediate neuronal activity from the striatum to the GPi, the primary output

of the basal ganglia along the direct and indirect pathways (53, 54). In the direct pathway,

the putamen, the primary nucleus for motor related input, send an inhibitory stimulus to

GPi. In the indirect pathway, putamen sends inhibitory input to the GPe. The GPe is thought to inhibit GPi via inhibition of excitatory STN-GPi projections. The thalamocortical projection is excitatory and this excitation is critical for initiation and proper control of movements by the motor cortex. Activation of the direct pathway facilitates desired movements by disinhibiting the thalamocortical projection. Activation of the indirect pathway suppresses unwanted movements by inhibiting the thalamocortical excitation. Current basal ganglia models predict that alterations in discharge rates within individual nuclei play a crucial role in the development of movement disorders (53, 54)

The current model, however, fails to explain the relationship between GPi output and cortical activity in dystonia. For instance, the sustained improvement in dystonia after GPi pallidotomy is a paradox of traditional basal ganglia models that predict dystonia is caused by decreased basal ganglia output and Parkinsonism is caused by increased output (55). According to the rate model, surgical lesioning of the GPi should worsen dystonia after removal of inhibitory GPi-thalamic pathways. These contrasting findings highlight the limitations of the current model based on tonic firing rates.

1.6. RATIONALE FOR USING THE GUNN RAT MODEL FOR DYSTONIA STUDIES:

A number of animal models have been introduced to investigate pathophysiological aspects of dystonia. The mutant dystonic hamster (dt^{sz}) model (56) shows a close resemblance to generalized paroxysmal dystonia in humans and has been used extensively to investigate neurophysiological correlates of basal ganglia in dystonia. Electrophysiological studies in

this model have revealed a reduction in neuronal firing rates and discharge patterns in EP, the primary output nucleus of basal ganglia (57, 58). These investigators have also reported decreased dopamine D2- and D1-like binding and loss of parvalbumin GABAergic interneurons (59) in the putamen of dt^{sz} hamsters (60) and have suggested that dystonia is associated with excessive dopaminergic activity. Despite the usefulness of this model, these studies are limited in that the animals require prolonged periods of stress to express dystonia, attacks of dystonia are age dependant and neuronal recording studies, to date, have been performed under general anesthesia, such that the neuronal signals are altered by the anesthesia and do not reflect actual dystonic movements.

Another animal model of generalized dystonia is the dystonic (dt) rat (61-63). Expression of dystonia in these rats has been linked to the biochemical abnormalities within the cerebellum. In monkeys, dystonia has been produced by the administration of various toxins, including 4-phenyl-1,2,3,6-tetrahydropyridine (MPTP) and 3-nitropropionic acid. These agents, however, only inconsistently induce dystonia and cannot be targeted effectively towards milder symptoms (64). Byl and colleagues have introduced a chronic model of focal hand dystonia in owl monkeys produced by repetitive hand opening and closing (65). The focal feature of this model offers the advantage of producing less distress than other chronic models; however, this feature would be somewhat limiting for such extracellular recording investigations as intended in this study.

In comparison to these models, the Gunn rats develop persistent dystonia that more closely resembles advanced forms of primary and secondary dystonia. Findings in the

current project will provide a solid basis for understanding the underlying pathophysiology of kernicterus-related dystonia and will serve as a foundation for designing and testing new mechanistic based therapies for this disabling condition.

1.7. DISSERTATION OVERVIEW:

The overall goal of the current project was to understand how abnormal brain signaling in the basal ganglia produces distorted motor control in dystonia. The work included in this dissertation is exploratory and method centric. It is exploratory because when this project was started very little was about the movement disorder in these animals and dystonia in general. Previous studies in Gunn rat model have focused on understanding the auditory processing abnormalities. This project has been divided into two parts. The first half of the project (Chapter 2, 3, 4) has been focused towards developing techniques for systematically investigate the movement disorder in these animals using advanced engineering principles. The second half of the project (Chapter 5, 6) has been focused towards neuronal recordings and analysis to explore the neurophysiological abnormalities that occur in kernicterus-induced dystonia. A systematic approach has been used to study the problem starting with model validation, quantification and then moving over towards neurophysiological data analysis (**Table 1**). At each step of the project a systematic hypothesis was laid out to answer the question of interest. Over the years, studies conducted in this project have made significant contributions towards improving data collection techniques, implementing advanced signal processing techniques and

performing sophisticated data analysis for understanding the neurophysiological

mechanisms of dystonia.

Table 1: Dissertation Overview

Ch.	Objective	Approach
2.	Validate the presence of dystonia	• Established a technique for characterizing the presence of dystonia using EMG recordings • Developing a superior methodology for isolating EMG signals into dystonic frequencies
3.	Objective measure of dystonia	Established a technique for quantifying gait deficits in dystonia
4.	Eliminate the need for anesthesia during neuronal recordings	Design of unique Stereotaxis apparatus (in collaboration with Customs Design and Fabrication)
5.	Understand abnormal brain signaling in dystonia	Recording and analysis of single unit recordings in individual basal ganglia nuclei
6.	Understand how brain circuitry triggers distorted motor output in dystonia	Multi-unit recordings in basal ganglia nuclei along with simultaneous EMG recordings

The dissertation has been organized into chapters. Each chapter starts with an

introduction to the problem and hypothesis under consideration. Next, the key challenges

faced while designing the study have been highlighted. This is primarily aimed at orienting

the reader about the thought process while designing the study. A systematic step-by-step

description of the methods is provided within each chapter. Where ever applicable

additional details about the methods have been included separately in an Appendix at the

end of the dissertation. Descriptions of the results along with detailed statistics are

included in each chapter. At the end of each chapter, discussion summarizes the rationale

for performing the study, interpretation of the results, comparisons with other studies in the

literature and provides direction for future studies.

CHAPTER 2 ELECTROMYOGRAPHIC CHARACTERIZATION IN AN ANIMAL

MODEL OF DYSTONIA

2.1. INTRODUCTION:

Dystonia is characterized by sustained, abnormal stereotyped posturing (7, 8, 66). Co-contractions of antagonistic muscles and overflow contractions of nearby muscles are considered to be cardinal features in some types of dystonia. Electromyographic (EMG) studies are routinely used as part of clinical diagnosis of dystonia. EMG studies help to determine the most actively involved muscle in dystonia, type of involuntary muscle activity and the frequency of dystonic discharges in affected muscle groups. EMG studies in dystonic patients typically show tonic, phasic, tremulous or myoclonic discharges (67, 68). Frequency analysis studies in studies on patients with primary dystonia have shown an abnormal 4-7Hz drive in affected muscle groups (66, 69). Thus, the analysis of muscle activity helps to identify the muscles involved and the pattern with which they are recruited during movements.

A number of animal models have previously been introduced to investigate the pathophysiological aspects of dystonia. However though, to date, the presence of dystonia has never been well characterized via EMG studies in these models. Presence of dystonia

in these models has been evaluated using clinical rating scales which are subjective. Although these scales provide a measure of the severity of motor disability, they fail to provide a definite diagnosis of dystonia. Thus, so far, no objective methods have been developed to identify and measure dystonia in animal models.

Previous studies on the Gunn rat model have focused particularly on the damage in the auditory brainstem pathways (15, 32-35). In contrast; the clinical aspects and the pathophysiological correlate of the movement disorder have never been systematically investigated in this animal model. The purpose of this study was to use electromyographic recordings and coherence analysis to support the clinical impression that the movement disorder in jaundiced Gunn rats represents dystonia. These methods could also importantly be utilized to support the validity of other phenotypic animal models of dystonia.

2. 2. CHALLENGES FACED IN THE PROJECT:

Challenge 1. Develop an objective technique to characterize dystonia:

Prior to this study, the dystonia in Gunn rats was measured using clinical rating scales (70). Although these rating scales provide a measure of the motor disability these scales are subjective and fail to provide a definite diagnosis of dystonia. Thus, EMG recordings have helped to develop a simple, minimally invasive method to characterize the presence of dystonia in these animals.

Challenge 2. To separate the burst and tonic components in the EMG signal:

EMG signals consist of transient short burst that are superimposed on sustained hypertonic activity. The burst (high frequency components) represent the voluntary attempts to move while the sustained hypertonic activity (low frequency components) represent prolong abnormal postures and the background noise in the signal. The main goal of the current study was to understand how muscles activate during voluntary attempts to move by the animal. Also, although the dynamic range of EMG signal is from 0-500 Hz, bursts are dominant in the 50-150 Hz range. Thus, using Discrete Wavelet Transform, EMG signal has been decomposed into the desired frequency bands of interest and burst have been separated from sustained hypertonic activity in the EMG signal.

2.3. MATERIALS AND METHODS:

All animals and procedures used for the study were approved by the Institutional Animal Care and Use Committee (IACUC) at Virginia Commonwealth University. A total of 32 animals were used in this study. Animals from six different litters were used to account for inter-litter variability. The pups were weighed on day 16 and blood samples were drawn via a cheek puncture to determine hematocrit and total plasma bilirubin levels.

2.3.1. Groups and Clinical Assessments

A total of 18 jj animals received an intraperitoneal injection of sulfa (100 mg/kg) on day 16. Five of these animals developed mild-to-moderate motor disability and comprised the experimental group. Of the remaining animals, six were severely affected and did not survive the acute bilirubin encephalopathy, and seven were not affected and were not studied further. Control groups consisted of jjs given saline (n = 5) and Njs given sulfa (n = 5) or no treatment (n = 4). Littermate jjs and Njs were randomly assigned to either experimental sulfa or control groups. All animals were carefully monitored each day for loss of body weight, which was compensated with an oral feeding of kitten milk formula or a subcutaneous injection of 5% dextrose in 0.45% NaCl or a combination of both. Animals were clinically examined daily, and a clinical score (CS) between 0 to 5 was assigned based on the severity of the movement disorder (0- normal, 1- slight limb dystonia & gait abnormality, 2-mild limb dystonia & gait abnormality, and impaired righting reflex, 3- moderate limb dystonia and gait abnormality, with prolonged righting

reflex, 4- severe failure of ambulation, general lack of spontaneous movement with occasional bursts of hyperactivity, and no righting reflex, and 5- moribund, including seizures and agonal respiration) (Shaia 2002), and 0.5 was added to the score of animals appearing to be midway between a category and the next higher one. The five dystonic jj sulfa animals used in this study received scores between 1.0 and 2.5. Six dystonic jj sulfa animals given scores ≥ 3.5, two each at 3.5, 4.0 and 4.5, became severely dystonic and did not survive to 34 days of age; seven additional jj sulfa animals, all receiving scores of 0.5, were clinically unaffected and not used for the study. Thus, for this study, the scale functionally ranges from 0 to 4.

2.3.2. Recording of EMG Activity

EMG activity was recorded on day 34, more than two weeks after sulfa injection. Day 34 was chosen as an optimal age for recording EMG activity to allow sufficient time for the animal to recover from the acute bilirubin encephalopathy and for their neurological symptoms to stabilize, and for the animal to grow larger, allowing easier targeting of muscles for percutaneous insertion of fine wire electrodes.

On the day of recording, the lower backs of the rats were shaved to allow targeting of the muscles for electrode insertion. Rats were lightly anesthetized with an intramuscular injection of ketamine (30 mg/kg) and acepromazine (3 mg/kg). Throughout the recording, the body temperature was monitored with a rectal temperature probe and held at $37 \pm 0.1\,^{\circ}\text{C}$ with a heating pad. Teflon coated 50 μm stainless steel fine wire electrodes (A-

M systems, Carlsborg, WA) were inserted percutaneously into antagonistic hip muscles, the gluteus superficialis (hip flexion) and the gluteus medius (hip extension) via a 30 gauge needle. Hip muscles were chosen for EMG studies because 1) preliminary visual inspection of the movement disorder in these animals showed prominent involvement of hip in abnormal axial and appendicular posturing, 2) the larger proximal muscles are much easier to access with recording wires in pups. Muscles were stimulated electrically (Grass Technologies, West Warwick, RI) and the hip motion was observed in order to verify correct placement of the electrodes. Recordings were assessed as the animals awakened from anesthesia. In the partially sedated state, a small pinch was applied to the toes and EMG activity was recorded in response to this stimulus. Multiple such stimuli were applied and EMG activity was recorded for a minimum of at least 120 sec. The signals were amplified (x 1000) and filtered (10 Hz - 1 KHz) through a differential AC amplifier (A-M Systems, Carlsborg, WA) and digitized through a NI-DAQ card (National Instruments Co., Austin, TX) at a sampling frequency = 4 KHz. EMG activity was monitored continuously on a desktop computer using Sort Client (Plexon Inc., Dallas, TX).

2.3.3. Decomposition of the EMG Signals into Relevant Frequency Bands

Fig. 4: Discrete Wavelet Transform A. Illustration of the Wavelet shrinkage scheme. An input signal with bandwidth of 0-1000 Hz is filtered and downsampled into low frequency (A1, A2…) and high frequency (D1, D2…) components. **B.** Block diagram representation of analysis procedure for Electromyographic (EMG) signals.
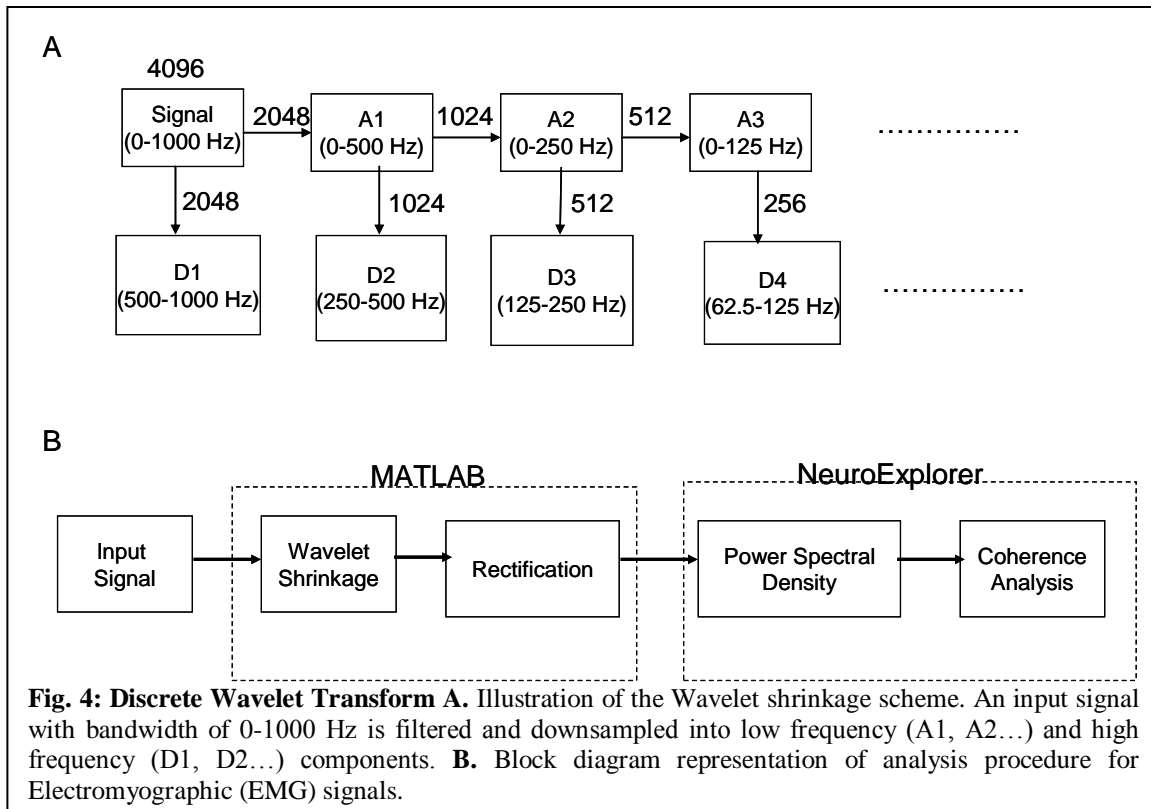
The raw EMG signal in dystonia consists of repetitive bursts superimposed on sustained hypertonic activity (71, 72). For accurate estimation of coherence between antagonist muscle pairs, it is necessary to separate the high frequency bursts from sustained hypertonic muscle activity. An effective way to achieve this separation is to decompose the EMG signal using the Discrete Wavelet Transform (DWT) based multi-resolution approach (71-73). The DWT approach involves passing the EMG signals progressively through a series of filters with different cutoff frequencies; thereby, decomposing the original signals into different frequency bands (73, 74) . At each level of

decomposition, the raw EMG signal is decomposed into approximate (A1, A2...) and detail (D1, D2…) coefficients (**Fig. 4A**). The approximate coefficients are the high scale, low frequency components of the signal obtained by passing the original signal through a highpass scaling filter and downsampling by two. The detail coefficients are the low scale, high frequency coefficients of the signal obtained by passing the original signal through a lowpass scaling filter and downsampling by two. The high pass and low pass filters at each stage are related to each other and are called as quadrature mirror filters. The advantage of using a DWT analysis is that the time localization of frequencies is not lost during the decomposition of the signal (74). Because bursts in EMG signals are dominant in the 50-150 Hz frequency range (Wang 2004, Wang 2003), the raw signals were subjected to level eight decomposition to investigate the pattern of EMG-EMG coherence in 125-250 Hz (D3), 62.5-125 Hz (D4), and 31.25-62.5 Hz (D5) frequency bands. The EMG signals were decomposed and then rectified using Matlab (MathWorks Inc., Natick, MA). Power spectral and coherence analyses were performed using Neuroexplorer (Nex Technologies, Littleton, MA) (**Fig 4B**).A representative decomposition of an EMG signal using Discrete Wavelet Transform is shown in **Fig. 5**.

Note: Filters have been realized using Discrete Wavelet Transform. They are not ideal filters and contain residual spectrum. Care should be taken while interpreting the results.
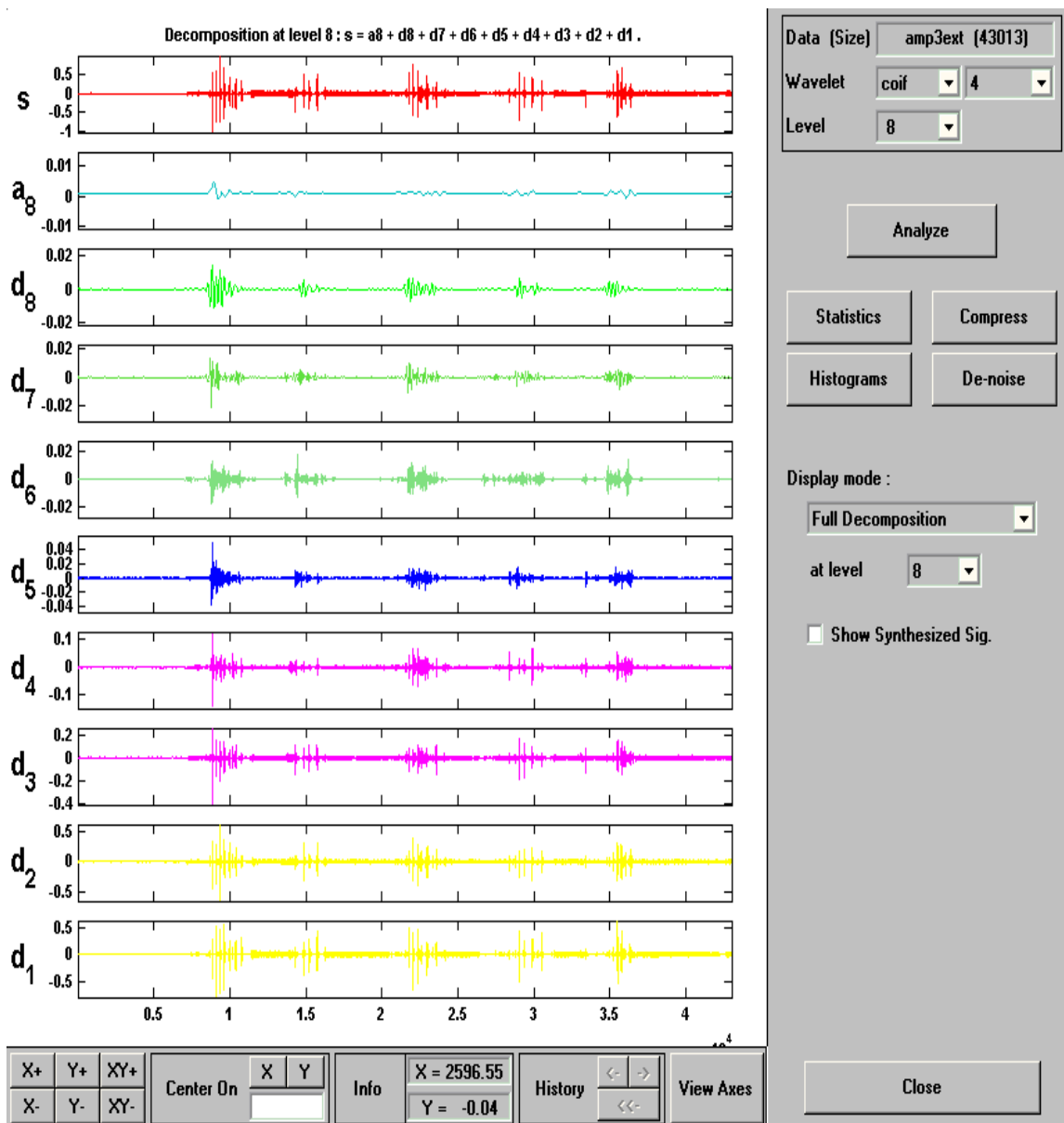
Fig. 5: Representative decomposition of an EMG signal by Discrete Wavelet Transform (DWT) using MATLAB. d1-d8 are the detail coefficients and a8 is approximate coefficient.

2.3.4 Power Spectral Density and Coherence Analysis

Power spectral density is the measure of the average power in a signal per unit of frequency as a function of frequency (75). Coherence provides a measure of how similar

two signals are and the linear association between them (66, 76). Based upon the degree of association, coherence can be assigned values from 0 to 1 in which 0 corresponds to minimal or no coherence and 1 indicates maximal coherence. The coherence estimation of two signals a, b can be represented as

$$\lambda_{ab}(f) = \frac{C_{ab}(f)}{\sqrt{C_{aa}(f) * C_{bb}(f)}}$$

$C_{ab}(f)$= cross spectral density of the two signals, and

$C_{aa}(f)$, $C_{bb}(f)$= auto-spectra of each signal.

The data were smoothed by using a moving average filter and coherence measures were obtained across multiple windows of one second duration along the entire length of each signal. Power spectral and coherence analyses were performed using Neuroexplorer (Nex Technologies, Littleton, MA).

2.3.5 Statistics

Statistical analyses were carried out by the one way analysis of variance (ANOVA) for multiple comparisons followed by Tukey-Kramer honestly significant difference (HSD) test. A probability value of < 0.05 was considered to be statistically significant for making comparisons between groups.

2.4. RESULTS:

Table 2 provides a summary of physiological parameters and clinical scores (CS) for the animals undergoing EMG analysis. Gender was evenly distributed between the jj and Nj groups. Sulfa treated jj animals weighed significantly less than the animals in the other three groups at 34 days of age ($p < 0.001$). **Fig. 6A** depicts a control animal and **Fig. 6B** represents the movement disorder seen in sulfa treated jj rats, characterized by sustained abnormal postures in the trunk and limbs. In sulfa treated animals, gait and balance were also affected in proportion to the degree of abnormal posturing

Table 2: Summary of physiological parameters and clinical scores of animals used for Electromyographic (EMG) characterization.

	Day 16			Day 34	
Group	Weight(gms)	TB(mg/dL)	CS	Weight(gms)	CS
jj sulfa (n=5)	26.1 ± 2.7	9.8 ± 0.8	0.5 ± 0	61 ± 5.5	1.5 ± 0.5
jj saline (n=5)	27.8 ± 2.2	10.33 ± 1.4	0.5 ± 0	79.8 ± 7.6	0.5 ± 0
Nj sulfa (n=5)	27.6 ± 4.4	0 ± 0	0 ± 0	87.5 ± 5.0	0 ± 0
Nj untreated (n=4)	-	-	-	107.5 ± 10.7	0 ± 0

(TB- Total Bilirubin, CS- Clinical Scores)

Under light anesthesia, a tail pinch produced clear volitional movements typically lasting

10-15 seconds. In sulfa-treated animals, these movements closely resembled the abnormal

Fig. 6: Comparison of Electromyographic (EMG) activity in normal and dystonic animal A.
Normal non-jaundiced (Nj) rat 24 hours after sulfa treatment **B.** Dystonic posture in a jaundiced (jj) rat
24 hours after sulfa treatment. Note the abnormal dystonic posture, especially in the hindlimbs **C.** Raw
EMG activity recorded in the Nj rat shows alternating pattern of activation in antagonistic hip muscles
(gluteus superficialis [GS], gluteus medius [GM]) **D.** Raw EMG activity in jj rat shows co-contractions
in antagonistic hip muscles. **E, F.** Magnified view of EMG activity in C, D, respectively.

spontaneous motor activity observed in unanesthetized dystonic animals and clearly

differed from the movements induced in lightly anesthetized control animals. Subsequent

to a tail pinch, EMG activity in all Nj and saline treated jj animals showed a pattern

dominated by alternating activation of agonist and antagonist hip muscles. Representative

EMG activity in a sulfa treated Nj animal is shown in **Fig 6C**. In contrast, co-contractions

were regularly seen in agonist and antagonistic hip muscles in sulfa treated jj animals (**Fig. 6D**).

Fig. 7: Representative power spectral density distribution in a sulfa treated jaundiced (jj) animal. Peak in the spectral density response can be seen at 4.5 Hz in D3 (125-250 Hz) signals and at 5 Hz in D4 (62.5-125 Hz) signals for extensor (e) and flexor (f) muscles.
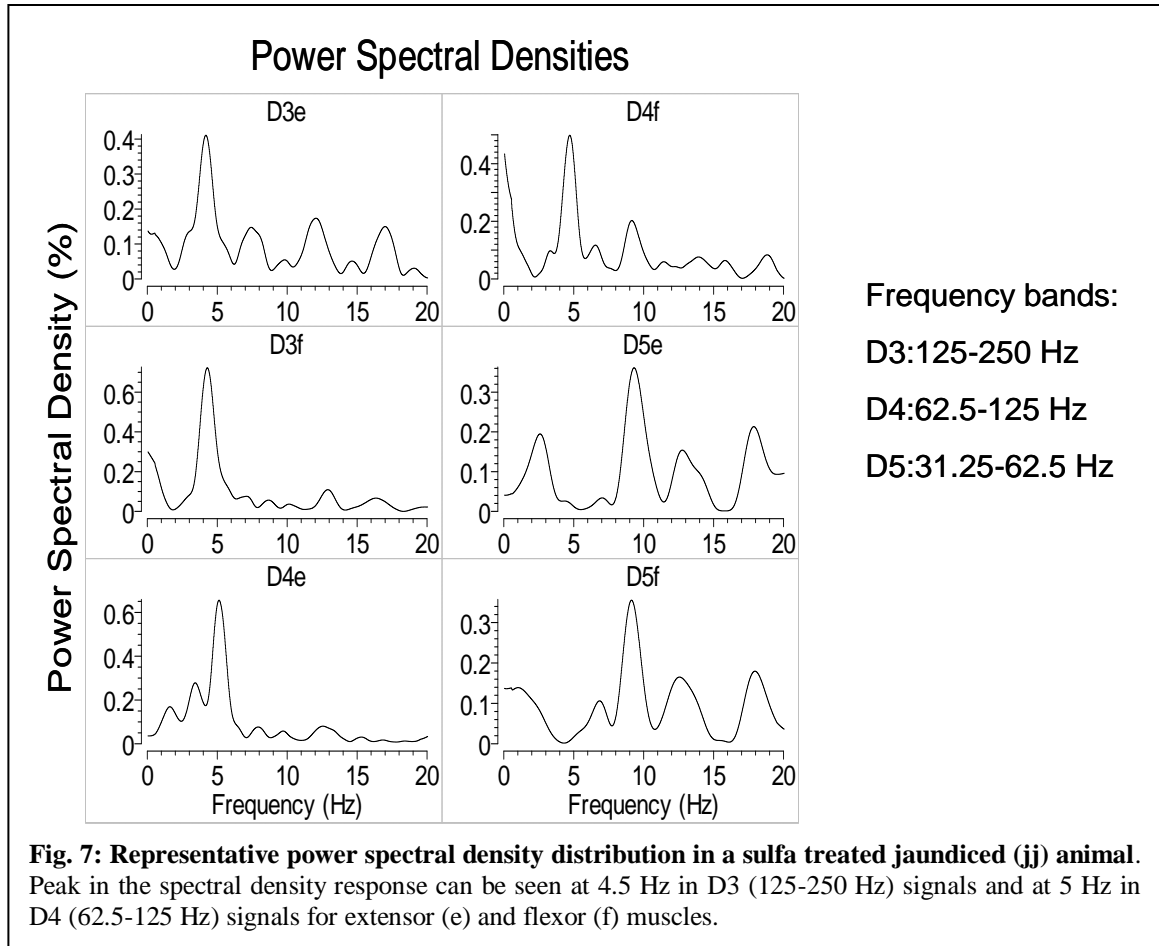
In sulfa treated jj animals, EMG activity showed a prominent peak in the power spectral density at 4.5 Hz in D3 signals and at 5 Hz in D4 signals (**Fig. 7**). In D5 signals, a peak in power spectral density response is seen at greater than 8 Hz. These frequency ranges however are not relevant to studies of dystonia[2], and hence they have not been considered for further analysis. Of note, the peak response shifted towards higher frequencies with the increasing levels of decomposition (i.e. from D3 to D5).

Fig. 8: Percentage power spectral density in four groups of animals. There is an increase in the power spectra in 4-7 Hz range (highlighted area) in jaundiced (jj) sulfa treated animals in D3 (125-250 Hz) and D4 (62.5-125 Hz) signals for extensor (e) and flexor (f) muscles.
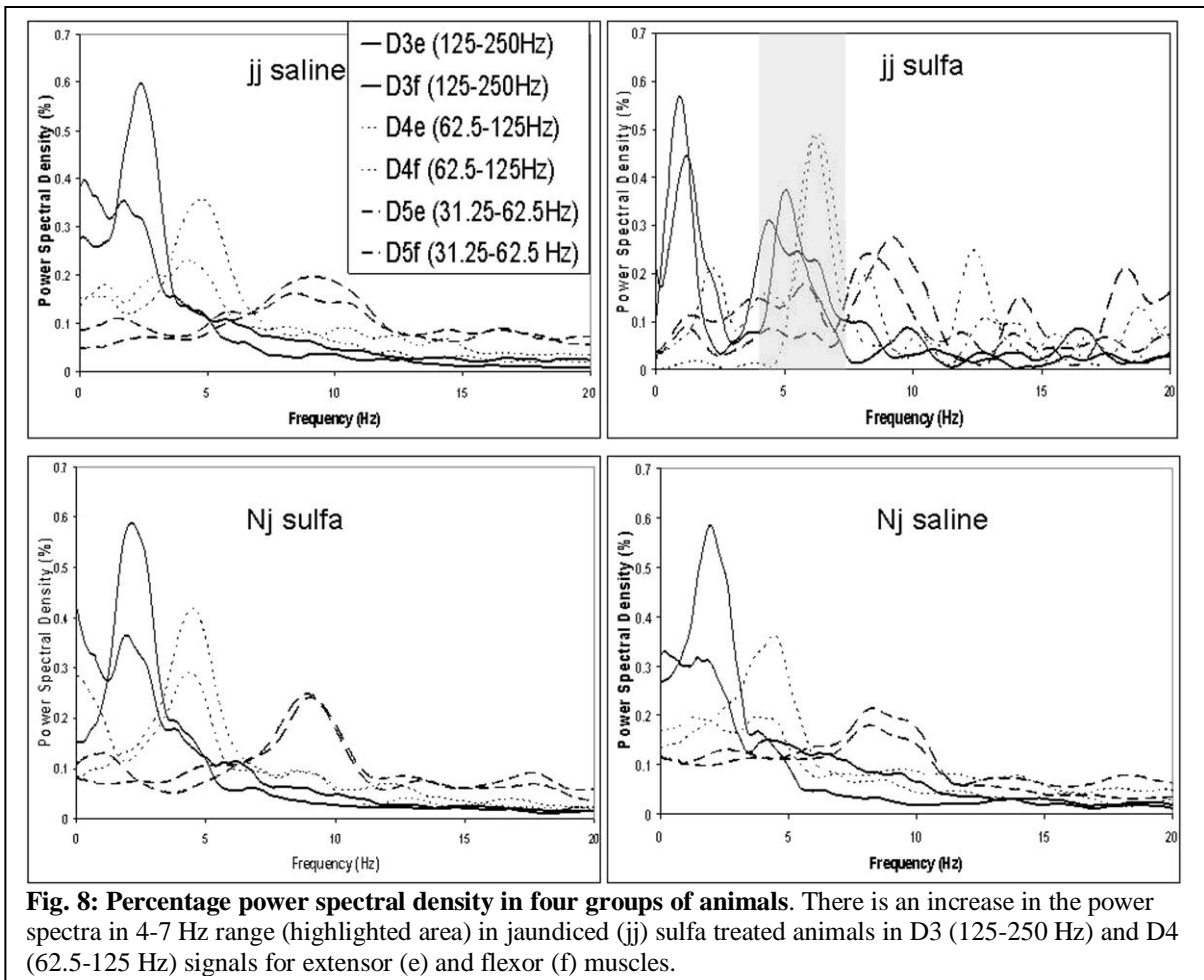
To compare groups, the average power spectra obtained in the four different groups of animals was calculated. The 4-7 Hz peak in power spectra was significantly prominent in D3 and D4 signals among the sulfa treated jj animals as compared to the other three groups (**Fig. 8**). To compare the PSD's in the 4-7 Hz range in the four different groups of animals the unequal variance F test was used. The F value for signals D3e, D3f, D4e, and D4f were 161.7, 143.2, 40.25, and 9.5 respectively among the four groups of animals (all p values < 0.001). Post hoc tests revealed that in all the 4 signals (i.e D3e, D3f, D4e, D4f) the jj sulfa group was significantly different that the other 3 groups (Tukey's HSD).

Fig. 9: Coherence spectra in the four groups of animals. **A.** Coherence spectra of the D3 (125-250 Hz) and D4 (62.5-125 Hz) signals in the 4 groups of animals. A clear prominent peak in the coherence spectra for antagonistic muscles can be seen in sulfa treated jj animals in the 4-7 Hz range **B.** Summary of coherence in the 4 groups (*P<0.05). Error bars indicate the standard error of the mean.

To quantify the co-activation of muscles in dystonic animals, the coherence spectra was measured. Only sulfa treated jj animals showed an abnormal, prominent peak in the coherence spectra in the 4-7 Hz range (**Fig 9A**). The coherence for the D3 and D4 signals at 4-7 Hz were compared across the four groups using the unequal variance F-test and were found to be different (D3, $F[3, 324.6] = 3049.3$; D4, $F[3, 325.77] = 2802.2$; both p-values < 0.0001) (**Fig 9B**). Using Tukey's HSD, sulfa treated jj animals (D3 mean=0.796, D4=0.789) were significantly different from the other three groups. There were no significant differences in coherence between the other three groups (D3 combined mean=0.433, D4=0.461), and there was no significant correlation between the power spectral density of the D3 and D4 signals and the dystonia rating of the rat.

2.5. DISCUSSION:

In this study, EMG recordings from antagonistic hip muscle pairs revealed prominent co-contractions in impaired, but not control rats, which supports the clinical impression that jaundiced (jj) Gunn rats with kernicterus develop dystonia. Using the DWT methodology to enhance the separation of burst from background tonic activity, an abnormal 4-7 Hz drive was observed in antagonistic hip muscles in dystonic jj rats. With this methodology, a distinct 4-7 Hz peak in the PSD was shown more prominently in 125-250 Hz and 62.5-125 Hz signals, which encompass the usual EMG burst frequency band ranges. Prior studies in humans with dystonia have demonstrated a comparable 4-7 Hz drive in antagonistic muscle pairs thereby further supporting the validity of the jaundiced Gunn rat as a model for studying human dystonia. Moreover, because similar 4-7 Hz co-contraction drives have been established in primary human dystonias, studies in the Gunn rat model may have direct implications for primary as well as secondary human dystonias.

The present findings, along with findings from human studies of dystonia, suggest that a central 4-7 Hz drive to dystonic muscle pairs underlies the pathophysiology for many common forms of dystonia. Tijssen showed an abnormal synchronizing drive of 5-7 Hz in antagonistic cervical muscle pairs during involuntary contraction in patients with cervical dystonia (69). Grosse examined the differences in EMG discharge patterns in different etiological groups of patients with dystonia, and observed an abnormal synchronizing drive of 4-7 Hz in patients with primary dystonia (66). Wang studied the functional coupling between EMG's and local field potentials (FP) of the internal globus

pallidum (GPi) in a patient with dystonia (71). A strong coherence was reported between the activity in the GPi and the muscles of the upper arm at frequencies of 4-7 Hz in the dystonic patient.

To date, this is the first time that co-contractions have been observed in antagonistic muscles in secondary dystonia. Grosse and his colleagues found an abnormal pattern of synchronizing descending drive of 4-7 Hz only in the distal lower limb of symptomatic patients with DYTI gene mutation (i.e. primary dystonia) and not in patients with secondary dystonias (66). One possibility to explain the discrepancy may be that many secondary dystonias do not have the 4-7 Hz drive in antagonistic muscle pairs. Another possibility could be that the Gunn rat model, despite being a model of secondary dystonia, may have pathophysiological aspects that are more typical of primary dystonias.

The present study has a number of shortcomings. Firstly, due to the limited range of severity of dystonia in the experimental group the present study fails to assess if correlations exist between EMG power spectral density and the severity of dystonia. However, the lack of correlation suggests that wavelet analysis may be relatively more sensitive to dystonia than more traditional approaches. Secondly, the significance of the present findings depends largely on the premise that co-contractions support a clinical impression of dystonia. Yet, co-contractions however can occur naturally in humans, for instance, during isometric exercise (77) and moreover, dystonia may be exhibited with little or no coincident antagonist muscle involvement (78). Despite these caveats, the present demonstration of a 4-7 Hz co-contraction drive, comparable to that established for

human dystonias and limited to animals exhibiting clinical dystonia, is strong evidence in support of the presence of clinically relevant dystonia. Finally, although the animals appeared alert and displayed their naturally dystonic or normal clinical states during the EMG data collection periods, recording conditions used in this study imposed limitations, especially the possible effects of anesthesia on the responses. However a clear difference in findings between experimental (dystonic) and control groups argue that the effect is not due to anesthesia or other experimental conditions, which would have affected all groups equally. Future studies, are necessary to exclude the possibility that alert rats, moving naturally would, for example, exhibit a different pattern of EMG activity or would exhibit a stronger coherence pattern than lightly anesthetized, stimulated animals.

In summary, the present findings suggest that EMG may provide an objective means to verify the presence of dystonia in the Gunn rat model. This approach may provide a convenient and reliable means to objectively quantify dystonia for further experiments in the Gunn rat, as well as in other animal models of dystonia. The jaundiced Gunn rat model of kernicterus should serve as a reliable model to investigate pathophysiological mechanisms for dystonia, and to test novel therapies.

CHAPTER 3 QUANTIFICATION OF GAIT IN DYSTONIC GUNN RATS

3.1. INTRODUCTION:

Abnormal muscle contractions in dystonia cause disorganized, uncontrolled and excessive movements (1, 79). Patients often develop distinct walking patterns and balance disturbances (80). Particularly in generalized forms, the disorder may become so severe as to prevent independent standing and walking (81). The underlying pathophysiology of dystonia is poorly understood and treatments are inadequate (4, 82, 83). Therefore, experimental studies in animal models are critically necessary towards understanding the underlying pathophysiological mechanisms and ultimately developing better therapies (6).

A number of groups have developed other valuable animal models of dystonia (3) and various rating scales have been introduced to assess the dystonia (84, 85) in these models. Deficits in genetically dystonic (dt) rats have been assessed by describing abnormal motor features (falls, twists, clasps, pivots) and motor performance (activity, climbing, righting, homing, hanging) (86). Motor performance of DYT1 knockdown mice has been successfully measured using rotarod, beam-walking and open-field tests (87).

Because the principle clinical features of the dystonia vary between animal models,

different techniques may be preferable for characterizing the different dystonias.

Regardless, novel objective techniques are needed to quantify the dystonias and provide

sensitive measures to detect subtle forms of the movement disorder (6). Gait analysis has

been used extensively to quantify experimental spinal cord injuries (88, 89), peripheral

neuropathy (90) and Parkinson disease (91) in rodent models. In these studies, quantitative

aspects of gait have been assessed from video recordings of freely moving animals. The

purpose of this study was to adapt current gait assessment techniques to be used for

experimental assessment of dystonia in rodents. Based upon visual inspection of dystonic

Gunn rats, assess specific gait parameters have been chosen to highlight the clinical

features of the dystonia, including hindlimb spread, stance to swing ratio, walking speed

and a novel parameter, step length ratio variability.

3.2. CHALLENGES FACED IN THE PROJECT:

Challenge 1. Measurement should be non-invasive:

While designing this study there were several ideas in mind for assessing gait measurements. One of them was to mount positional sensors on the animal's limbs to measure the movements in 3D space. However, after initial trials, it was determined that the animals would not tolerate multiple such sensors mounted on their limbs during walking. Also, these sensors were expensive. Therefore, in this study a simple, cost effective and non-invasive method has been used to assess gait measurements.

Challenge 2. Selection of gait parameters:

There are several parameters of gait than can be quantified for movement analysis in dystonia. The challenge was to select gait parameters that were reproducible and easy to measure in animals with different severities of dystonia. The parameters used in this study have been selected by thorough visual inspection of these animals.

3.3. MATERIALS AND METHODS:

All animals and procedures used for the study were approved by the Institutional Animal Care and Use Committee (IACUC) at Virginia Commonwealth University. A total of 32 animals from six different litters were used for this study. The methods and the treatment have been described previously (36). Briefly, at 16 days of age, 18 jj animals received an intraperitoneal injection of sulfadimethoxine 100 mg/kg. Five of these animals developed mild to moderate motor disability and comprised the experimental group. Of the remaining animals, six were severely affected and did not survive the acute bilirubin encephalopathy, and seven were not affected and were not studied further. The experimental group (n=5) was compared with jj controls given saline (n=5) and Nj controls given either sulfa (n=4) or saline (n=4). Body weights were regularly monitored as an indicator of the general condition of the animal.

3.3.1. Clinical scores

On postnatal day 15 (baseline) and again on postnatal day 31, dystonia was rated subjectively using a Kernicterus Clinical Rating Scale based on Schutta et al. (1969) and Rose et al. (1979) (24, 28) as follows: 0) normal, 1) slight limb dystonia and gait abnormality, 2) mild limb dystonia and gait abnormality, and impaired righting reflex, 3) moderate limb dystonia and gait abnormality with prolonged righting reflex, 4) severe failure of ambulation, general lack of spontaneous movement with occasional bursts of hyperactivity, and no righting reflex, and 5) moribund, including seizures and agonal

respiration. An additional 0.5 was added to the score of animals appearing to be midway between one category and the next higher one.

3.3.2. Gait analysis

The experimental setup was adapted from the design by Yu et al. (2001) (90) (Appendix B, Page 161) **(Fig. 10**). Animals were videotaped while spontaneously walking inside a Plexiglas chamber towards a darkened goal box. The rats were trained initially and quickly acclimatized to the experimental conditions. The magnification of the camera was calibrated so as to accommodate a 25 cm reflected ventral view of the chamber. The

Fig. 10: **Design of experimental set up for gait analysis** (adapted from Yu et al. (2001)). The walking apparatus consists of a Plexiglas chamber. A mirror was placed at 45^0 angle to the bottom panel. The video camera was positioned to record the reflected under view of the chamber.
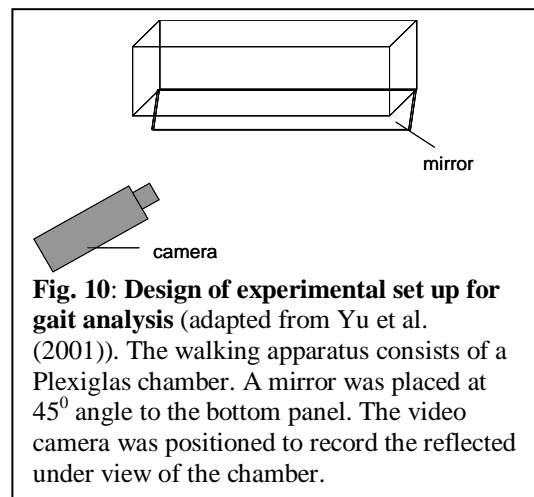
bottom panel of the chamber was marked with horizontal and vertical grid lines one cm apart. In order to determine the orientation of the body relative to the grid, the sagittal plane of the body on the ventral side was marked with a red marker. This line acted as a body reference marker that was taken into consideration while calculating the gait parameters. In each rat, three satisfactory runs without pauses were recorded for analyses. Digital video images were collected at a rate of 30 frames per second. Video recordings were obtained on postnatal day 15 (baseline) and again on postnatal day 31, two weeks

after sulfa treatment. To study the locomotor deficits, the following gait parameters were analyzed:

1. **Walking speed**: The walking speed during each trial (distance/time) was determined based on the time (number of frames) required to travel a 25 cm track.

2. **Hindlimb spread**: During each foot placement along the grid, parallel lines were drawn to the body reference marker from the middle phalange of hind feet and the perpendicular distance between them was measured as the hindlimb spread. Representative measure of the hindlimb spread is shown in **Fig. 11**.

3. **Step length ratio (SLR) variability**: The SLR variability assessed the inconsistency of foot placement over repeated steps. For calculating variability, first the step length was calculated as the anterior-to-posterior distance from the middle phalange of one hindfoot to the other. The SLR was then obtained by dividing the right to the left step length by the left to the right step length. Measures of SLR variability in each group were determined as the coefficient of variation (CV) which was calculated by using the equation: ((*Standard deviation/mean*) x 100).

4. Stance to Swing ratio (SSR): Duration of the stance and the swing phases were determined by analyzing the videos on a frame by frame basis. The stance to swing ratio (SSR) was obtained by dividing the right stance/swing ratio with that of the left (90).

The video recorded was digitized on a computer and individual frames of the video were captured using Studio Quickstart (Pinnacle Systems Inc., Mountain View, CA). Further image analysis was carried out using the image analysis software Image J (NIH).

3.3.3. Statistics

Statistical analysis was performed by using the JMP® and SAS® software packages (SAS Institute Inc., 2007). Since each animal is repeated in three trials and over time these observations are correlated. To account for these correlations the repeated measures mixed effects model was used. The mean $\pm$ SE reported are the least square means estimated from this model. The standard deviation and the coefficient of variation were calculated for each group to determine the dispersion from the mean. Measures including the weight, the baseline gait measurements, gender and the interlitter variability were used as covariates. Post-hoc comparisons were made using the Tukey-Kramer honestly significant different (HSD) test. A probability value of <0.05 was considered to be statistically significant for making comparisons between groups.

3.5. RESULTS:

Fig. 11: Ventral view during gait analysis. **A**. Normal non-jaundiced (Nj) rat. **B**. Abnormal hindlimb spread seen in dystonic rat. Horizontal and vertical grid lines seen in the figure assist with gait measurements. Representative measurement of hindlimb spread in normal and dystonic rat is highlighted in the figure.
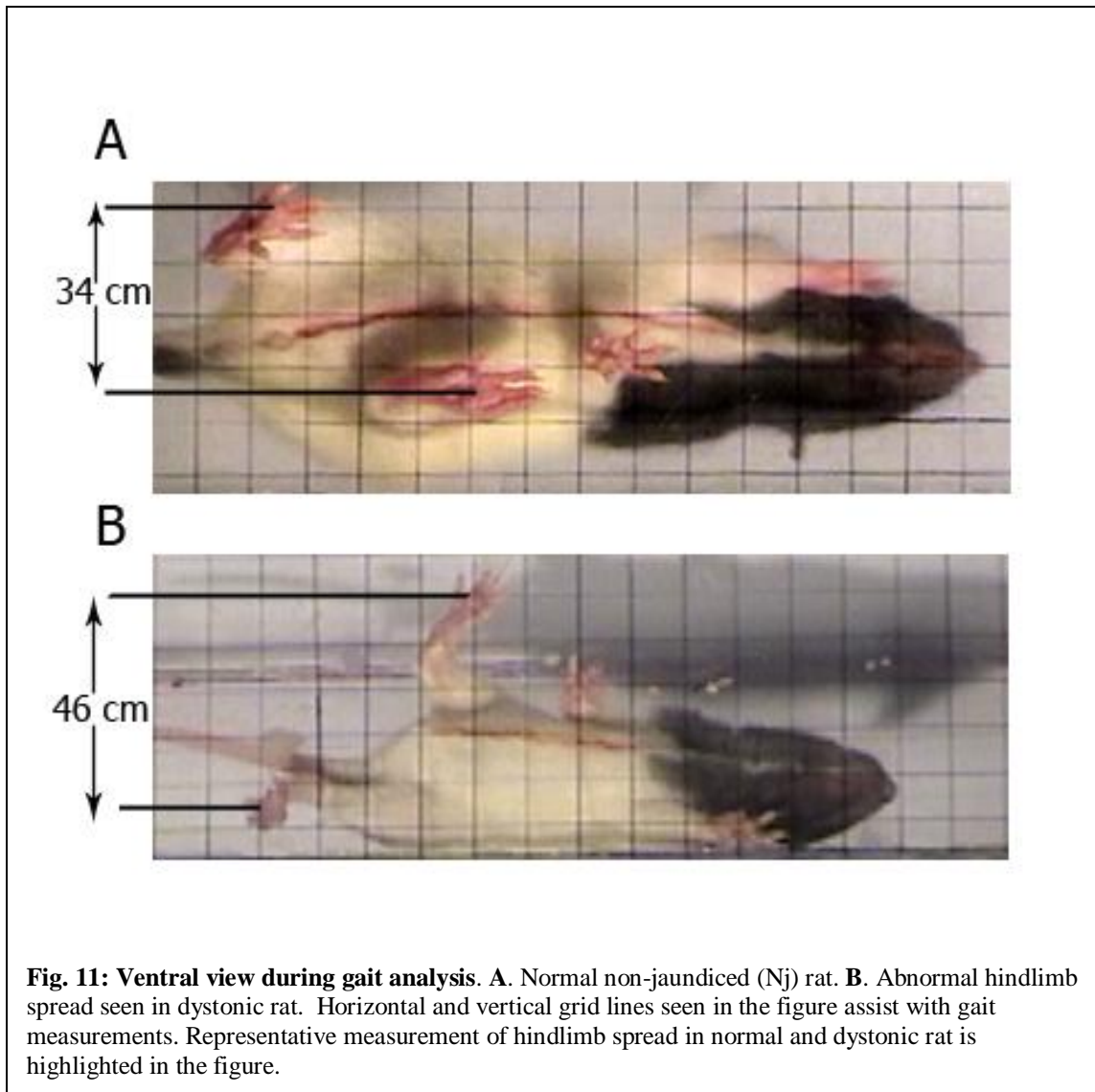
3.4.1. Physiological parameters

Fig. 11 shows the ventral view of a normal and a dystonic animal walking inside

the Plexiglas chamber. Within 24 hours after sulfa injection, sulfa treated jaundiced

animals developed abnormal axial and appendicular posturing. The gait in dystonic animals was marked by an uncoordinated walk with twisting of the trunk and disruptive, prolonged hindlimb extensions with less forelimb involvement. **Table 3** provides a summary of the weights and clinical scores of all the animals used for gait analysis. The jj animals (27.7 ± 0.18 g) weighed significantly less than Nj animals (32.3 ± 0.19 g) (**p-**value < 0.0001) at 15 days of age, which is commonly seen at this age in this model. At 31 days of age, body weights in all four groups of animals were found to be significantly different from each other ($p < 0.0001$). Nj sulfa animals had more females (n=3), and as a result, they weighed significantly less than the Nj saline animals (n=1 female). In sulfa treated jaundiced animals, body weight dropped in the first few days after treatment due to the acute bilirubin encephalopathy, whereafter the weights gradually increased. At 31 days of age, the sulfa treated jaundiced animals weighed significantly less as compared to the three control groups (**p**-value < 0.0001). On postnatal day 31, the five sulfa treated jaundiced animals used in this study received clinical scores between 1.0 and 2.5, whereas jj saline animals all received scores of 0.5 and all Nj animals (sulfa or saline treated) received scores of 0 (**p**-value < 0.0001).

Table 3: Summary of weights and clinical scores (CS) of the animals used for gait analysis

Type, Treatment	Day 15		Day 31	
	Weight (g)	CS	Weight (g)	CS
jj, sulfa (n = 5)	26.0 ± 0.18	0.5 ± 0	57.2 ± 0.48	1.5 ± 0.31
jj, saline (n = 5)	25.8 ± 0.17	0.5 ± 0	77.8 ± 0.45	0.5 ± 0
Nj, sulfa (n = 4)	27.4 ± 0.19	0 ± 0	86.9 ± 0.49	0 ± 0
Nj, saline (n = 4)	28.5 ± 0.29	0 ± 0	107.0 ± 0.44	0 ± 0

mean $\pm$ standard error

3.4.2. Gait Parameters

Table 4 provides a summary of the gait parameters at 15 and 31 days of age.

Gender was evenly distributed between the jj and Nj groups. Step length was unaffected by

the walking speed for both the right (**p**-value = 0.206) and left (**p**-value = 0.624) leg. There

was a negative correlation between the walking speed and the stance phase (**p**-value <

0.0001) and swing phase duration (**p**-value = 0.037) at 15 days of age, with a correlation of

$R^2 = 0.764$ and 0.762 for both the left and right stance phase respectively and $R^2 = 0.209$ for

both the left and right swing phase.

Table 4: Gait parameters in jaundiced (jj) and non-jaundiced (Nj) animals at 15 and 31 days of age. Values are mean $\pm$ standard error

Gait parameters	Day 15		Day 31			
	jj animals	Nj animals	jj sulfa	jj saline	Nj sulfa	Nj saline
	(n=10)	(n=8)	(n=5)	(n=5)	(n=4)	(n=4)
Hindlimb spread (mm)	32.74 $\pm$ 0.27*	31.85 $\pm$ 0.30	47.18 $\pm$ 4.59**	37.30 $\pm$ 1.96	34.25 $\pm$ 2.24	35.44 $\pm$ 3.70
Right step length (mm)	37.22 $\pm$ 0.43*	39.05 $\pm$ 0.49	38.44 $\pm$ 0.50**	49.36 $\pm$ 0.56	52.04 $\pm$ 0.72	50.90 $\pm$ 0.43
Left step length (mm)	38.31 $\pm$ 0.53*	38.77 $\pm$ 0.62	41.27 $\pm$ 0.54**	49.18 $\pm$ 0.55	52.95 $+$ 0.39	49.83 $\pm$ 0.46
Right stance phase (ms)	277.64 $\pm$ 6.67*	288.30 $\pm$ 7.67	302.66 $\pm$ 5.62**	241.64 $\pm$ 7.67	239.31 $\pm$ 7.33	248.30 $\pm$ 5.28
Right swing phase (ms)	185.64 $\pm$ 4.00	177.98 $\pm$ 4.67	168.02 $\pm$ 6.38**	144.98 $\pm$ 5.99	152.30 $\pm$ 4.37	144.22 $\pm$ 6.22
Left stance phase (ms)	280.64 $\pm$ 6.33	285.97 $\pm$ 7.67	300.01 $\pm$ 4.07**	242.43 $\pm$ 4.56	245.31 $\pm$ 5.02	245.63 $\pm$ 4.18
Left swing phase (ms)	179.98 $\pm$ 4.00	181.65 $\pm$ 5.00	171.98 $\pm$ 4.00**	154.98 $\pm$ 5.23	152.73 $+$ 7.32	149.92 $\pm$ 5.80
Walking speed (cm/s)	16.02 $\pm$ 0.10*	16.29 $\pm$ 0.11	14.31 $\pm$ 0.70**	16.94 $\pm$ 0.26	16.99 $\pm$ 0.34	17.84 $\pm$ 0.20

* significant difference between groups , p < 0.05

** significant difference between groups, p < 0.0001

At 31 days of age, step length increased with increased walking speed for both the

right and the left foot, with a correlation of $R^2 = 0.555$ for right foot and $R^2 = 0.527$ for the

left foot. Additionally, stance phase duration was inversely correlated with walking speed

(**p**-value < 0.0001, $R^2 = 0.843$ and 0.845 for both the left and right stance phase

respectively). In contrast, the swing phase duration remained unaffected by walking speed

($R^2 = 0.119$ for left leg and $R^2 = 0.176$ for right leg). Consistent with previous findings (Yu

et. al., 2001), the step length ratio (SLR) found to be independent of the walking speed (*p*-value = 0.25).

3.4.3. Walking Speed

The random effects model showed that walking speeds in the four groups were significantly different at 31 days of age (*p*-value < 0.0001) after covarying out the weight effect (*p*-value = 0.17), walking speed at day 15 (*p*-value = 0.82), interlitter variability (*p*-

Fig. 12: Comparison of walking speed and hindlimb spread in the four groups of animals. A: Least Square means of the walking speed in the four groups of animals at 31 days of age. **B:** Least Square means of hindlimb spread in the four groups of animals, * p < 0.0001. Error bars indicate the standard error of the mean.
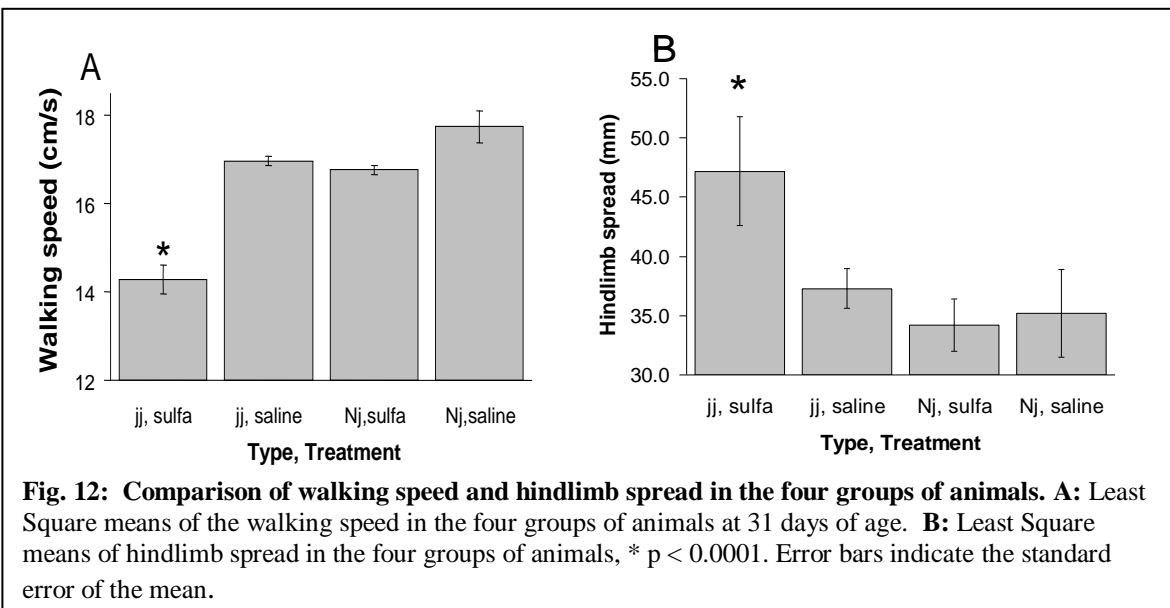
value = 0.03) and the gender effect (*p*-value = 0.42). Post-hoc comparisons revealed that the walking speed in dystonic animals (adjusted mean = 14.31 ± 0.70 cm/sec) was slower as compared to the saline treated jj (adjusted mean = 16.94 ± 0.26 cm/s) and sulfa treated Nj animals (adjusted mean = 16.99 ± 0.34 cm/sec) (**Fig. 12A**).

3.4.4. Hindlimb Spread

The hindlimb spread in the four groups were compared using random effects model and were found to be significantly different (p-value < 0.0001) after covarying out the hindlimb spread on day 15 (p-value $=0.94$), interlitter variability (p-value $= 0.43$), weight effect ($p = 0.58$) and the gender effect (p-value $= 0.71$). Post hoc comparisons revealed that dystonic animals had greater hindlimb spread (adjusted mean $= 47.18 \pm 4.59$ mm) as compared to Nj sulfa and jj saline groups (combined mean $= 35.80 \pm 2.88$ mm). There was not a statistically significant correlation between hindlimb spread and the clinical scores (**Fig. 12B**).

3.4.5. Step Length Ratio Variability

Table 5: Step length ratio (SLR) in the four groups of animals at 31 days of age

Type, Treatment	Least Sq Mean	Std Error	Lower 95%	Upper 95%
jj,sulfa	0.94	0.04	0.86	1.02
jj,saline	0.98	0.01	0.96	1.01
Nj,sulfa	1.01	0.02	0.98	1.04
Nj,saline	1.05	0.05	0.95	1.14

Using random effects model, the step length ratio (SLR) was calculated at 31 days of age (**Table 5**). The SLR was not found to be significantly different between groups after covarying out the SLR at day 15 (p-value $= 0.50$), interlitter variability (p-value $= 0.01$), gender effect (p-value $= 0.04$) and the weight effect (p-value $= 0.14$). The F-test demonstrated that variability in SLR among dystonic animals was significantly greater as compared to the three control groups (p-value < 0.0001). The coefficient of variation of SLR among dystonic animals was five times higher in dystonic animals as compared to

controls. There was not a statistically significant correlation between SLR variability and the clinical scores.

3.4.6. Stance to Swing Ratio

The stance to swing ratios (SSR) in the four groups of animals at 31 days of age are summarized in **Table 6**. Although the prolonged hindlimb extensions in dystonic animals caused increase in the stance phase and swing phase duration of the hindlimbs (**Table 6**), they were similarly affected for both the limbs, and so, analysis of SSR after adjusting for covariates revealed no statistically significant differences between experimental and control groups. Further, the respective covariates of weight, SSR at day 15, interlitter variability, and gender effects were also not statistically significant. Additionally, no statistically significant differences were found in the stance to swing variability between the four groups of animals.

Table 6: Stance to swing ratios (SSR) in the four groups of animals at 31 days of age

Type, Treatment	Least Sq Mean	Std Error	Lower 95%	Upper 95%
jj,sulfa	0.98	0.15	0.67	1.28
jj,saline	1.05	0.05	0.95	1.14
Nj,sulfa	1.04	0.06	0.93	1.15
Nj,saline	1.07	0.17	0.72	1.41

3.5. DISCUSSION:

The purpose of the present study was to test the utility of objective gait measures for assessing dystonia in Gunn rats. The major findings from this investigation were that walking speed, hindlimb spread, and SLR variability differed in dystonic animals compared to controls, while stance to swing ratios did not differ. Parameters like the hindlimb spread and the SLR variability might be especially sensitive for detecting small degrees of dystonia and for distinguishing small differences in severity in Gunn rat model.

Based on visual inspection of dystonic Gunn rats, it was initially hypothesized that that hindlimb spread, SLR variability and SSR ratio would be particularly sensitive for detecting changes in motor behavior resulting from dystonia. Among these parameters, the current findings indicate that the SLR variability is probably the most sensitive parameter to detect dystonia in Gunn rats. Unlike the step length that provides information just over a single step, SLR variability reflects the gait pattern over a relatively long walk. Across all variables tested, the most striking difference between dystonic animals and controls was seen in SLR variability (five times as variable as controls).

Gait analysis is being used as an investigative technique across many areas of research. Traditionally, gait analysis was performed using the footprint method (92, 93) that measured the footprint length and the toe spread from ink foot imprints. This method, however, does not provide information regarding gait kinetics nor does it take into account walking speed. This method also suffers from technical problems of related to the variable foot imprinting with the applied ink. This technique could be particularly a problem in

dystonic animals as they do not always place their feet fully flat while ambulating. Clearly, methods involving reviews of videotape frames without the use of ink imprinting, as done in this study are more ideal. Another technique commonly used is the treadmill method in which gait is assessed while the animal runs on a motorized treadmill (94, 95). This technique provides an accurate assessment of several gait parameters at adjustable speeds and inclinations. This method however would not be useful in dystonia as more affected animals would not be able to comply with the requirement for ambulating on a treadmill. Other behavioral studies like beam walking (96) and beam balance (97) are effective in assessing postural stability; however, cannot adequately differentiate between severities of dystonia. The gait analysis approach using force plates provides information about several dynamic parameters like the ground reaction forces and the weight bearing capacity of the limb during locomotion (98). Some studies integrate electromyography (EMG) measurements to evaluate muscle activity during locomotion (99, 100). In future studies, force and electromyography measures should be incorporated into the current set up to provide a better understanding of the gait deficits seen in dystonic animals.

The present study has some shortcomings. First, the present study failed to show significant correlations between the gait parameters and the clinical scores. One possible reason for this could be the limited range of severity of dystonia within the experimental group (dystonic animals). The subjective clinical scales may be simply too insensitive to accurately differentiate between animals of similar disability. Additional studies, using animals with clearly different clinical severities of dystonia would be necessary to affirm

that the gait parameters investigated here reliably distinguish between different severities of dystonia. Secondly, the utility of the present method depends largely on the premise that inconsistent foot placement in dystonic animals is due to their motor impairment. Inconsistent foot placement can also be attributable, for example, to changes in walking speed or attention (101). However, the assessment of SLR in the present study has been shown to be independent of the walking speed. Furthermore, the huge variability in foot placement shown here in the dystonic animals relative to controls is expected and consistent with their prominent and erratic truncal and limb contractions during ambulation. Thirdly, although abnormal hindlimb spread and SLR variability appear to chiefly reflect marked variable dystonic hindlimb extensions during ambulation in dystonic Gunn rats, these parameters are more traditionally associated with cerebellar ataxia in human patients. However, at this stage, ataxia cannot be excluded as a contributing factor to gait assessments in these animals. Lastly, based on visual inspection of prolonged hindlimb extensions in dystonic animals, stance to swing ratio was selected for assessment of gait. However, neither SSR nor its variability was found helpful for quantification of gait in dystonic animals.

Dystonia is a heterogeneous disorder. As such, although the results suggest that hindlimb spread and SLR variability provide valuable measures for objectively assessing dystonia in Gunn rats, the utility of these parameters for assessing dystonia in other animal models requires affirmation. Additionally, the present findings could potentially extend to human studies. Currently, clinical rating scales are mostly used to assess the severity of

dystonia (e.g. the Unified Dystonia Rating Scale (UDRS) and the Burke-Fahn-Marsden (BFM) Dystonia Rating Scale) but these are highly subjective (102). The current concept can be expanded for systematic measurements of gait parameters in human patients with dystonia, for example with light emitting diodes (LEDs) placed on the limbs of human patients with dystonia to provide more objective measures of gait disability.

In conclusion, gait analysis provides a simple, non-invasive method to quantify the severity of dystonia in jaundiced Gunn rat. Because of the erratic limb and truncal contractions in dystonic Gunn rats, both hindlimb spread and SLR variability are particularly good measures for assessing dystonia in this model. The findings of the present study will have implications for assessing therapeutic responses to treatment for dystonia in Gunn rats, and potentially other rodent models, and may also be useful for designing similar assessments of dystonia in humans.

CHAPTER 4: A NOVEL STEREOTAXIC APPARATUS FOR NEURONAL

RECORDINGS IN AWAKE HEAD-RESTRAINED RATS

4.1. INTRODUCTION:

The detection and measurement of neuronal discharge activity of the brain provides unique insight into the neurophysiological mechanisms of brain function. Despite limitations on the interpretation of neuronal discharge activity in sedated or anesthetized animals, most neurophysiological experiments in rodents continue to be performed using sedation or general anesthesia (103-105). In these studies, neuronal recordings are generally completed under sedation while restraining the animal's head in a stereotaxic frame using ear bars and mouth piece. Although this technique permits stabilized neuronal recordings from specific locations and is relatively easy to perform, the spontaneous neuronal activity is altered by the anesthetic agents (106-108). While a number of investigators have correlated neuronal discharge activity with various behaviors and movements in anesthetized animals, the abolishment of such activities by the anesthesia compromises the interpretation of such studies.

A number of investigators have circumvented the need for general anesthetics by performing neuronal recordings in freely moving animals using implanted electrode arrays (109-112). This technique has an advantage of allowing stabilized recordings from individual nuclei for long periods of time and correlates discharge activity with behavior. However, implementation of this technique is costly and technically difficult. Additionally, multi-electrode arrays used in these systems are permanently implanted within a single nucleus or a group of adjacent nuclei and does not permit advancement of electrodes to more extensively record many neurons over multiple tracks.

Various head-restraining techniques have previously been instituted to permit single-unit extracellular recordings along multiple tracks in unanaesthetized rodents (113-116). Because of perceived limitations posed by currently available devices, this study was focused towards developing a novel stereotaxic apparatus. The design presented in the present study has the following advantages: 1) simplified and strong stabilization of a head fixture with an eight point skull fixation, 2) a light weight design, which permits quick and reliable securing of the head fixture without the added time and weight of traditional epoxy-based techniques 3) adaptability of the head fixture to readily fit various skull sizes, 4) a novel and accurate skull alignment technique which circumvents the initial requirement of ear bars and 5) excellent access to the animal during experimental conditions.

4.2. CHALLENGES FACED IN THE PROJECT:

Challenge 1. To determine the ideal age for neurophysiological recordings:

The following factors were taken into consideration while determining the age for neurophysiological recordings.

Recovery from bilirubin toxicity: Jaundiced Gunn rats were made dystonic by injecting them with sulfadimethoxine (100 mg/kg) at 16 days of age. Within 24 hours after sulfa injection the animals developed abnormal dystonic features. It took 2-3 weeks post sulfa injection for the animals to recover from the acute bilirubin encephalopathy and show stabilized dystonic features. This was taken into consideration while deciding the age for neurophysiological recordings.

Time investment in feeding dystonic animals: Post-sulfa administration, in jaundiced animals the acute bilirubin toxicity causes dystonia and lethargy leading to dehydration and decreased food intake, which may exacerbate hyperbilirubinemia. Because of the dystonia, animals develop abnormal axial and appendicular posturing and are unable to feed themselves. All animals used for neurophysiological recordings were carefully monitored each day for loss of body weight and as necessary, compensated with oral food supplements. Animals were hand fed several times during the day to make sure that they stay hydrated and gain weight. Thus, this involved a considerable investment of time which was taken into account while deciding on the age of neurophysiological recordings.

Growth of skull: The plan was to record from animals for upto a week after mounting the head fixture. Thus, to ensure that the chamber does not dislodge from the skull it was critical to determine the growth of skull at different time points to decide an optimal age for electrophysiological recordings.
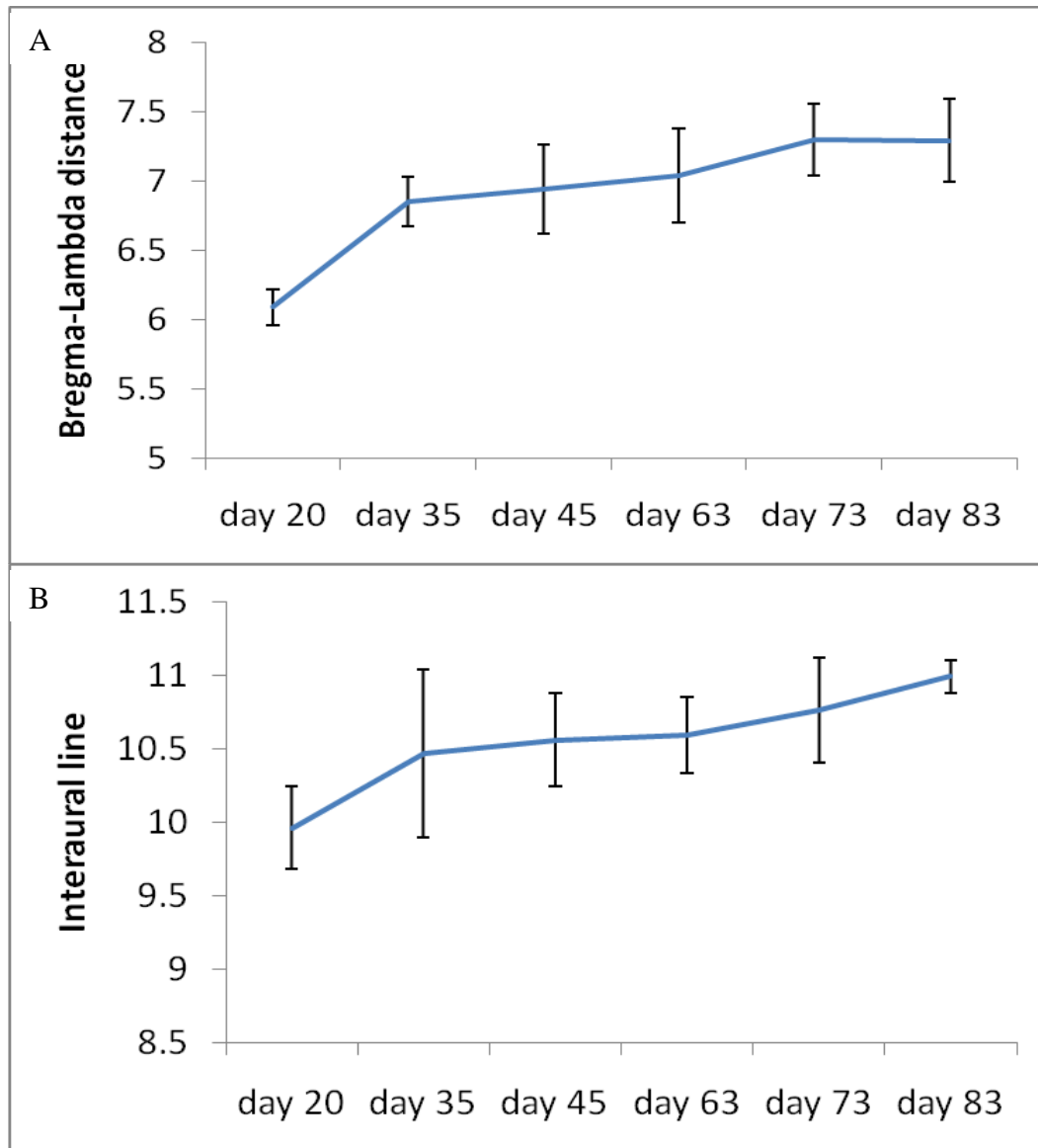
Fig. 13: Growth of skull with increase of age: A Bregma-Lambda distance on skulls of different ages. B. Interaural increase in skulls of different ages. Error bars indicate mean $\pm$ SD

Study: Skulls from animals (both Nj's and jj's) were dissected in 20 (n=5), 35 (n=8), 45 (n=5), 63 (n=4), 73 (n=6) and 83 (n=3) day old rats. Growth of the skull was studied by measuring the bregma-lambda distance, inter-aural distance and skull thickness using vernier caliper.

Results: Overall, the results indicated that as the animal grows older the skull becomes thicker and grows larger in size. Plots in **Fig. 13** highlight growth of skull with increase in age. Skull growth continues to take place till about day 45 after which it plateaus out. There was a rapid increase in bregma-lambda and inter-aural distance till about 45 days of age after which it tapers out. Dura thickness at day 45 is 0.4 mm.

Thus, taking into consideration all these factors day 45 was selected for neurophysiological recording studies.

4.3. MATERIALS AND METHODS:

4.3.1. Stereotaxic Apparatus Design

The stereotaxic apparatus is composed of two principal components: 1) a stainless steel head fixture, which is mounted to the skull (**Fig. 14A**) and 2) a stereotaxic positioner used to accurately achieve the flat skull position for stereotaxic alignment (**Fig. 14B**). The apparatus was designed in collaboration with Custom Design & Fabrication, a mechanical and electronics support facility under the Department of Radiology at Virginia Commonwealth University, Richmond, VA.
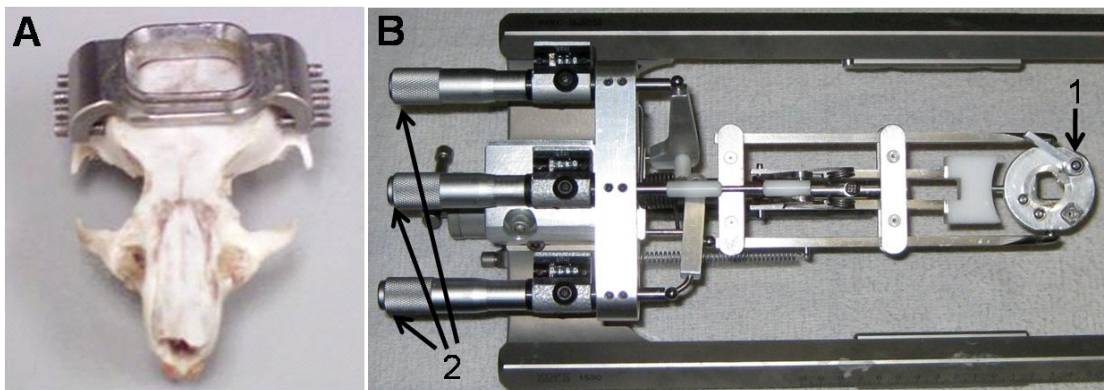
Fig. 14: Head fixture and Stereotaxic Positioner. A. Stainless steel head fixture. **B.** Positioning System. **1**. Cam-lock for securing the head fixture, **2**. Micrometer adjustments for yaw, pitch, and roll.

4.3.1.1. Head fixture:

The head fixture is constructed from stainless steel and weighs 2.8 grams. The skull mounted fixture is designed to remain secure for longer periods than adhesives can provide, to minimize the size and weight of the head fixture so that it could be easily supported by the animal, and to facilitate rapid and precise repositioning for repeat

recording sessions. The fixture has remained secure in studies lasting up to two weeks in rats weighing 45-220 gms. Also, for repeat recording sessions the animal's head position can be precisely reestablished in within minutes.

The fixture is secured to the skull using eight miniature 0-80 stainless steel set screws. The faces of these screws are machined flat with the exception of a 0.3 mm long center spike. The flat surface distributes the clamping pressure over the 1.2 mm diameter face of the screw and the spike prevents the screw from sliding on the bone. The eight point mounting allows the fixture to conform to the skull contour and distribute the clamping forces over a fairly large area. This mounting provides excellent stability of the skull for neuronal recordings.

A 1 x 1 cm (adaptable sized) opening in the center of the fixture (**Fig. 14A and Fig. 16**) provides ample access for passing microelectrodes over a large surface area. This protruding access port serves as the mounting point for securing the fixture to the positioner. A cam forces the fixture into a V shaped corner wedge locking the chamber onto the stereotaxic positioner (**Fig 14B**, #1). A tapered groove on the perimeter of the access port mates with the cam and wedge to ensure precise fixture alignment. Between recording sessions, the access port is sealed with a plastic cap (not shown) which slides into the tapered groove.

4.3.1.2. Stereotaxic positioner

A positioning system (**Fig. 14B**) was designed to be mounted onto a standard sized large animal stereotaxic frame. Three micrometer heads permit head alignment in three directions (yaw, pitch, and roll) to achieve the flat skull position required for accurate regional brain targeting using standard stereotaxic atlases. Once proper alignment is achieved, the values from the digital readouts on the micrometer heads are recorded allowing the position to be quickly and accurately restored later after the skull reference points have been removed.

4.3.2. Implantation of head restraint

All animals and procedures used for the study were approved by the Institutional Animal Care and Use Committee (IACUC) at Virginia Commonwealth University. A total of 18 juvenile Gunn rats (45-220 gms in weight), a strain of Wistar rats, were used for this study. Animals of different weights were selected to test the stability of the head fixture on skulls of different sizes. Extracellular neuronal recordings were performed for 2-3 hrs a day for up to two weeks on 13 of 18 animals used in this study. The five remaining animals were used for post-mortem verification of accuracy of targeting. For these animals, the neuronal recordings were restricted to a single session to ascertain accurate histological reconstruction of the location of recording tracks.

 During surgery, the rats were anesthetized with isofluorane (1-2%) and body temperature was maintained at $37.0 \pm 0.5\,^{\circ}\mathrm{C}$ with a regulated heating pad. Using sterile techniques, an incision was made along the sagittal plane of the head. The exposed area of

the skull was dried thoroughly to assure that no soft tissue or fluid covered the site of

implantation. The head fixture was visually centered on the skull and then firmly attached

using the miniature screws positioned just below the ridges of the parietal bone of the

Fig. 15. Customized tool for measuring skull alignment. 1. Dial test indicator 2. Plexiglas platform that slides along the stereotaxic frame 3. Retractable arms for measuring the leveling of the skull
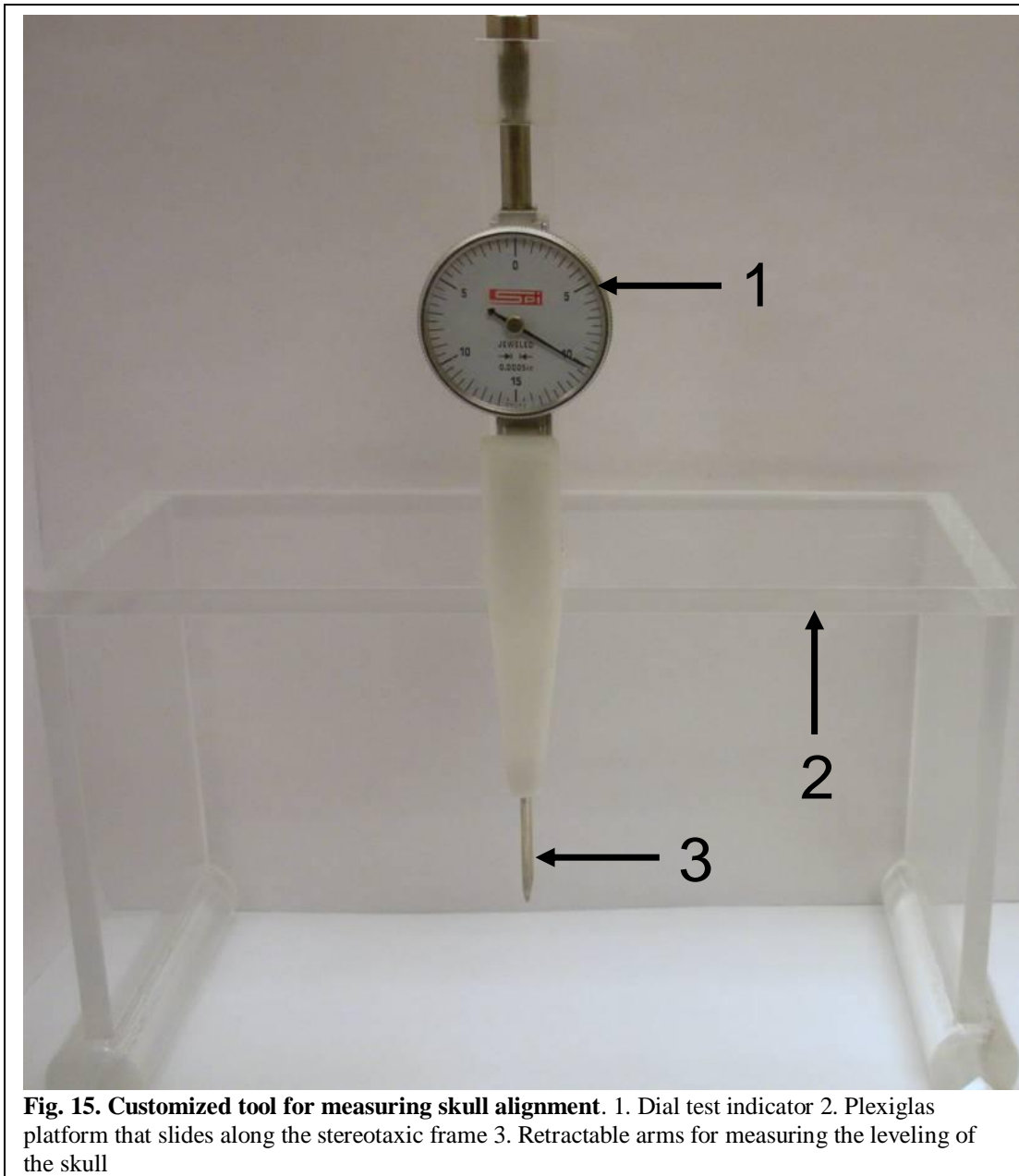
skull. Electromyography (EMG) fine wire electrodes (A-M Systems, Carlsborg, WA) were

implanted into hip muscles and soldered to a micro-circuit board. A slot made in the plastic cap holds the micro-circuit board when the cap is secured on the chamber. Dental acrylic was applied along the inside of the chamber opening to enhance binding of the fixture and prevent leakage of saline placed to prevent drying of the tissues. After the surgery, the animals were returned to their cage and allowed 24 hours for recovery. No overt signs of stress, pain or change in behavior were evident after implantation of the head fixture.

4.3.3. Skull alignment

To precisely target brain regions using a standard stereotaxic atlas, it is necessary to accurately achieve a flat-skull position (117). To achieve this a system was designed to adjust for the movement of the head in space, which follows a three axis coordinate system: yaw, pitch and roll. Yaw refers to the rotation about the Z or vertical axis, pitch about the Y or transverse axis and roll about the X or longitudinal axis. The custom alignment tool (**Fig. 15**) consists of a clear Plexiglas platform that slides along the outer support rail of the stereotaxic frame. The platform is also fitted with a sensitive dial indicator and retractable probe. The retractable probe is connected to a pair of retractable arms that when level on the skull is reflected by a zero reading on the indicator dial.

On the day of recording, the rat's head was immobilized by clamping the head fixture into the stereotaxic positioner. Next, principal landmarks (bregma, lambda and the inter-aural line) were visually identified and the skull aligned as follows:

Yaw alignment (**Fig. 16A**). The midline, connecting the bregma to lambda, was identified on the skull. The yaw alignment was achieved by adjusting the corresponding micrometer on the positioner such that the bregma-lambda line was visually centered within a reticule scribed on the platform.

Pitch alignment (**Fig. 16B**). The dial test assembly was mounted such that the arms of the test indicator gently touch the midline. The corresponding micrometer on the positioner was adjusted until the dial test indicator was zeroed. Several measures were obtained at different points along the bregma-lambda line and their average was used for alignment.

Roll alignment (**Fig. 16C**). The alignment procedure was carried out following a similar process as for the pitch alignment, except the probes of the dial indicator are oriented perpendicular to the midline and a third micrometer is adjusted accordingly.
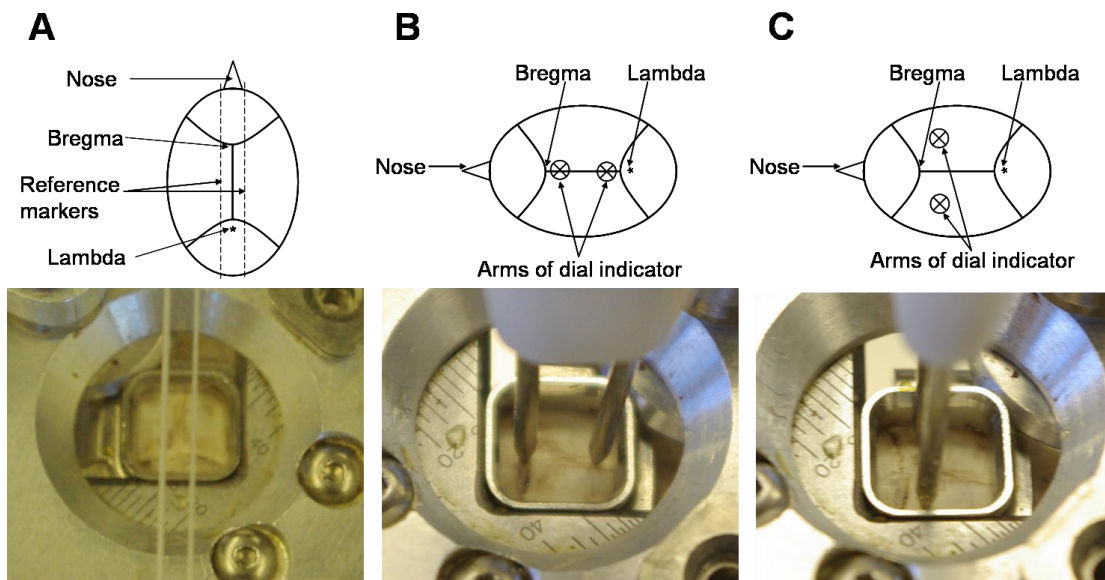
Fig. 16: Adjustments for establishing a flat skull position. **A**. Yaw measurement using reference markers **B**. Pitch measurement using arms of the dial indicator **C**. Roll measurement using arms of the dial indicator.

The skull alignment is painless, non-invasive, and is performed without the use of anesthesia. The skull alignment needs to be done only once and with experience, was quickly performed in about 5 minutes. The values from the digital readouts on micrometers are recorded so that the appropriate skull position can be realigned at the start of each recording session. Thus, the skull can be rapidly realigned without the use of ear and mouth piece, minimizing setup related distress for the animal.

4.3.4. Craniotomy

On the day of the first recording session the animals were anesthetized with isofluorane (1-2%) with the head restrained within the positioning mechanism. A 3.5 mm burr hole centered at 2 mm caudally and 1.5 mm laterally to the bregma reference point targeting the entopeduncular nucleus (EP) or globus pallidus (GP) was drilled into the bone exposing the underlying dura mater. The craniotomy was completed on the side contralateral to EMG electrodes using a drill supported by an adjustable stereotaxic arm. At the start of subsequent recording sessions, scar tissue that accumulated over the exposed dura mater was carefully removed and the chamber opening was thoroughly cleaned.

4.3.5. Microelectrode recordings

After drilling the burr hole, the anesthesia was discontinued and the animals promptly awoke. The animals consistently adapted quickly to the head restraint and no

separate training or habituation period was required. Within about 30 min. of the initial period of head restraining, neuronal recording sessions were initiated. In subsequent daily recording sessions, the head fixture could be easily and quickly restored, was mostly well tolerated, and recordings could be initiated immediately without an adaptation period. During recording sessions, soft gauze was placed on either side of the animal, room noise was minimized and contact with the animals was limited. In-between recording tracks, the animals, were regularly given formula to keep them hydrated.

A mini-XYZ-manipulator (Thomas Recording, Giessen, Germany) was mounted onto a Kopf stereotaxic arm and a concentric micro-drive head with 300 μm intra-electrode spacing was used to simultaneously introduce up to 3 glass coated tungsten microelectrodes (100 μm diameter) into the posterolateral (motor) territory of EP or GP. The following coordinates were used for targeting of the microelectrodes: 1) EP, 1.0-1.5 mm posterior from bregma and 2.9-3.4 mm lateral from midline, 2) GP, 0-1.0 mm anterior from bregma and 2.9-4.6 mm lateral from the midline. Extracellular recordings were collected by independently advancing the microelectrodes (impedance: 1 - 2 MΩ) to the targeted areas. Each nucleus was readily identified by its characteristic neuronal firing pattern. The optic tract, just below the EP, was readily identified by its distinct response to light flashes. During the recordings, this provided confirmation of the location of the microelectrodes. The location and firing patterns of cells and the borders of encountered nuclei along each microelectrode track were plotted and were superimposed on transparencies of parasagittal sections from the Paxinos and Watson atlas to estimate the

precise location in the brain. During the recording sessions, the state of vigilance of the animals was routinely monitored.

The recorded neuronal activity was displayed over two oscilloscope screens (HAMEG Instruments, Mainhausen, Germany) and connected to an audioamplifier for aural monitoring of the signal. EMG activity was monitored continuously on a desktop computer using Sort Client (Plexon Inc., Dallas, TX). Both, neuronal and EMG activity were collected for a minimum of 120 secs at a sampling rate of 40 kHz and were passed into a Plexon pre-amplifier (gain = 50, bandwidth 0.07-8 kHz).

4.3.6. Histology

In five animals, at the end of the recording session, the rats were deeply anesthetized with sodium pentobarbital and perfused transcardially with formalin. The brains were removed and each hemisphere was paraffin embedded in the sagittal plane. The brains were sliced at 20 µm throughout the hemisphere and representative sections were stained with cresyl violet.

4.4. RESULTS:

4.4.1. Neurophysiology

The assembly provided excellent stabilization of the skull during neuronal

recordings, while the large opening at the center of the fixture permitted stereotaxic access

at any desired angle. Based on physiological mapping to a standard atlas in 18 animals, the

initial targeting was within 0.5 ± 0.3 mm, which is comparable to standard ear bar

Fig. 17: Single unit extracellular discharge activity in the entopeduncular nucleus (EP) in head restrained rats during movement. (A) 2 neurons collected on a single microelectrode and **(B)** a third neuron collected simultaneously on an adjacent microelectrode. The distinct clusters and shape of each unit illustrates the excellent quality of recordings obtained using our head restraint system. **C.** Raster displays for these three neurons during periods of rest and active movements. The persistent tonic discharge activity in the EP1 and EP1_1 neurons during movement and the movement-related discharge bursts on a stable tonic background in the EP2 neuron together highlight the excellent stability of the head restraining system.

guidance methods, 0.4 $\pm$ 0.3 mm for juvenile Wistar (Paxinos and Watson, 1998). **Fig. 17** depicts an example of multi-unit recordings collected from the motor portion of EP during active movements in a head-restrained rat. **Fig. 17A** shows two EP units, EP1 and EP1_1, collected on a single microelectrode while **Fig. 17B** shows another EP unit simultaneously collected on an adjacent microelectrode 300 µm apart. These units were readily discriminated into separate clusters using Principal Component Analysis (PCA) based on the size and shape of action potentials. **Fig. 17C** shows a raster display of these three units during periods of rest and active movements. Alternating agonist-antagonist bursts in hip muscles during the voluntary movements were associated with recurrent discharge bursts in the EP2 neuron. On the other hand, simultaneously recorded activity in EP1 and EP1_1 neurons showed regular, stereotypical tonic discharge firing throughout the recording period. These examples highlight that our head-restraint system permits stabilized recordings during active movements.

4.4.2. Anatomical results:

Fig. 18 shows the location of electrode track just below the EP (target nuclei). Reconstruction of microelectrode recording tract from histological sections supports the accuracy of the targeting system.
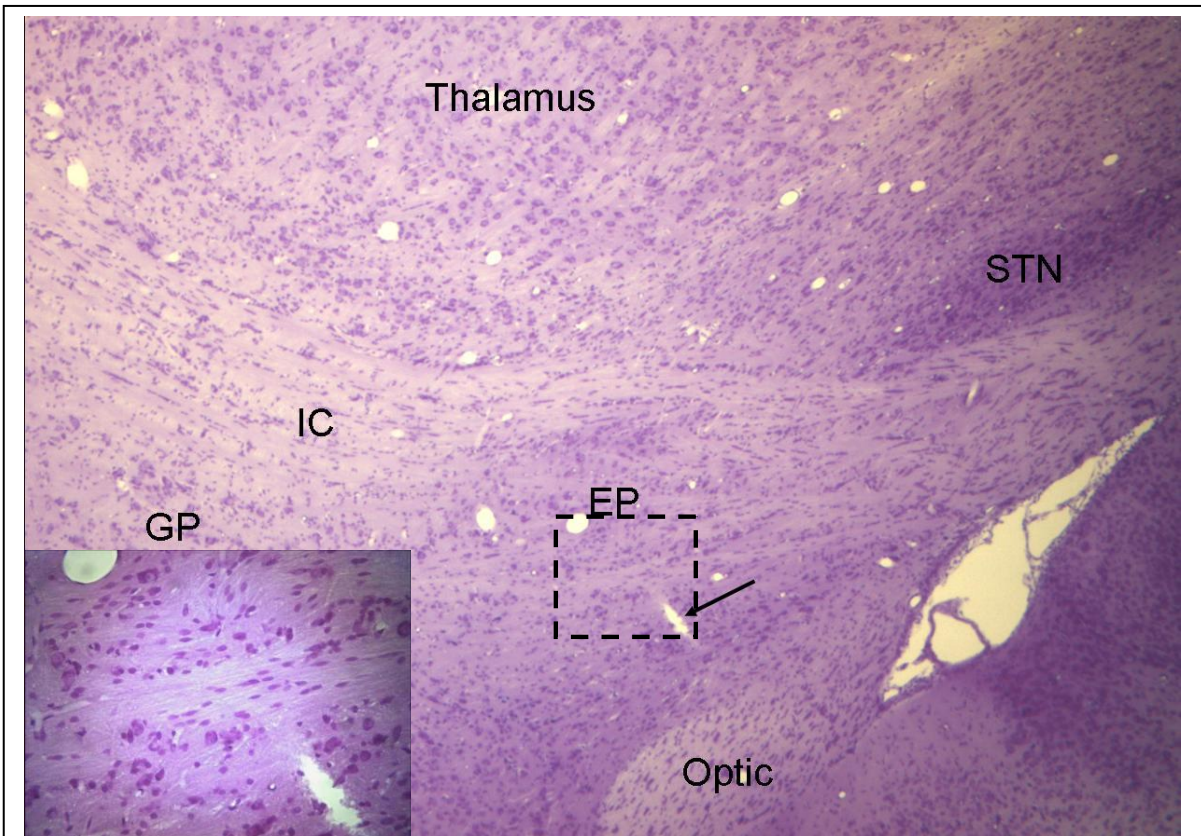
Fig. 18. **Anatomical support for accuracy of the positioning system**. **A**. Nissl stained 10x sagittal section demonstrating the tip of a microelectrode (arrow) just below the lateral motor portion of EP. **B**. The dashed area in figure A. is shown magnified at 40x. STN- subthalamic nucleus, EP- entopeduncular nucleus, GP-globus pallidus, Optic- optic tract.

4.5. DISCUSSION:

In this study, a novel technique has been described to perform neuronal recordings in awake, head-restrained young and juvenile rats. The head fixture and positioning system allow excellent stabilization of the head and accurate stereotaxic localization over multiple sessions of recording. This allows uninterrupted multi-unit recordings in deep brain nuclei in awake head-restrained actively moving animals. The accuracy of targeting using the positioning system compared favorably to our prior experience with standard ear bar guidance methods and with reported accuracy estimates with these standard techniques. This technique allows faster setup time during surgery and during multi-day recording sessions and appreciably reduces the weight of the implant thereby easing the setup process and reducing the stress to the animals.

A number of techniques have previously been introduced to record single unit activity in awake head-restrained rodents, all of which have clear limitations. One of the most utilized techniques involves immobilizing the head using a metallic headpost while recording through a separate recording chamber (108, 113, 115, 118). This method generally requires placing multiple screws into the skull and building up an epoxy base that secures in combination the supporting screws, headpost, and chamber. However, this technique requires considerable surgical time, and the epoxy introduces additional weight on the animal's head. Another technique involves cementing a U-shaped headpiece to the skull which in turn is secured to a stereotaxic restraining frame (114, 119). This system is also substantially heavier than the current design and provides comparatively limited

access to the animal during experimental conditions. Another group developed a head-restraining system using a restraining bridge and dummy ear bars (116). This design is highly complicated and has not been tested for repeat recording sessions.

The recording system described in this study offers a number of additional advantages over current recording systems. The durability of the head fixture was successfully established in animals of different sizes ranging from 45 to 220 gms in weight. Thus, the head fixture can be expected to be reliable for investigating young and adult rats, as well as adult mice. Additionally, the positioning mechanism provides the ability to rapidly and accurately target desired brain regions over multiple days by simply adjusting 3 dials (yaw, pitch and roll) at the start of each session. This provides a huge convenience for studies which involve multiple sessions of recording. Although the focus of this study was to simultaneously record multi-neuronal and EMG activity, the head fixture could, without major design modification, be readily enlarged and adapted to access more lateral portions of the brain or to record, for example, EEG activity. Additionally, this system would readily permit micro dialysis experiments, brain micro-stimulation, lesions and pharmacology studies.

This study has some shortcomings. Although the animals mostly tolerated the 2-3 hour recording sessions very well and habituated quickly to the recording conditions, intense grooming uncommonly caused changes in amplitude or complete loss of neuronal activity. At such times, the recording was stopped and care was taken to make the animal comfortable usually by giving a food reward. Rarely the behavior persisted and the

recording sessions were terminated prematurely. During early experiments the head fixture dislodged from the skull (in 4 animals) within 24-48 hrs of mounting because of improper mounting as a result of lack of experience on part of the investigator. None of the head fixtures dislodged in the last 18 animals used for this study.

In summary, in large part due to limitations of current restraining techniques, many investigators continue to investigate neuronal activity in sedated or anesthetized animals despite major limitations in the interpretation of such data. The novel approach presented here allows high quality stabilized neuronal recordings in awake head-restrained animals during periods of rest and active movements. The system can be very quickly attached to the skull and accurately aligned, is relatively lightweight, and can be quickly resecured for multiple recording sessions. By allowing daily repeat microelectrode studies in rodents without sedation or anesthesia, the use of the novel positioning system could more readily lead to greater advances in the understanding, and ultimately, the treatment of movement disorders and other neurological conditions.

CHAPTER 5: NEUROPHYSIOLOGY IN DYSTONIC GUNN RATS

5.1. INTRODUCTION:

Dystonia is a complex disorder because of its causes, progression, treatment and variability of symptoms. Despite years of research in humans and animal models, neurophysiological findings of dystonia are largely sparse and controversial and the pathophysiological mechanisms still remain largely obscure. The exact mechanisms occurring in either primary or secondary dystonia are unknown. Increasing evidence, however, suggest that dystonia can be associated with altered signaling throughout the basal ganglia thalamocortical "motor" circuitry (120).

Traditional rate-models of basal ganglia suggests that dystonia results from decrease in discharge rate of neurons in the internal segment of globus pallidus (GPi) leading to decreased inhibition of the thalamic activity and consequently to increased excitability of the motor cortex (**Page 13, Fig. 3**) (53, 54).However, these theories fail to account for the sustained improvement in dystonia seen after GPi pallidotomy. Based on the models, one would predict that GPi pallidotomy would remove the inhibitory GPi-thalamic projections and thereby induce excessive movements and worsen dystonia. These

contradictions clearly suggest that in the basal ganglia signaling is more complex than that predicted by the traditional basal ganglia rate models (**Page 13, Fig. 3**)

In the last decade, the understanding of dystonia has improved tremendously with the advent of microelectrode recordings (MER) during deep brain stimulation surgeries. Based on the findings from MER studies in dystonia patients, several researchers have proposed that in addition to discharge rates, the role of phasic discharge activity in basal ganglia and thalamic nuclei is of great importance. In GPi, several studies have reported low discharge rates and irregular grouped discharges with intermittent pauses in patients with dystonia (4, 5, 121-123). In addition to these findings, Starr and colleagues (2005) have reported an increase in the non-oscillatory bursting and oscillatory activity of GPi in human dystonia in patients with dystonic tremor (124). MER studies in GPe (4, 123) and STN (5) have shown low discharge rates and abnormal discharge patterns similar to those found in GPi. In addition to the abnormal patterns, Starr and colleagues have also reported presence of oscillatory discharge in STN neurons (125). Alterations in the pattern of neuronal activity have also been reported at the level of the thalamus (126). Although these findings are important in improving the understanding of dystonia, progress in this field nevertheless has been slow in part due to inherent limits and ethical constraints associated with conducting experiments using innovative techniques during human dystonia surgeries.

A number of animal models have also been introduced to investigate the pathophysiological aspects of dystonia. However, to date, neurophysiologic investigations

in animal models have been primarily limited to the mutant dystonic hamster (dt^{sz}) model which shows a close resemblance to generalized paroxysmal dystonia in humans. (56, 127, 128). Electrophysiological studies in this model have revealed a reduction in neuronal firing rates and discharge patterns in EP, the primary output nucleus of basal ganglia in rodents (58). Despite the usefulness of this model, these studies are limited in that the animals require prolonged periods of stress to express dystonia, attacks of dystonia are age dependant and neuronal recording studies, to date, have been performed under general anesthesia, such that the neuronal signals are altered by the anesthesia and do not reflect actual dystonic movements. In comparison, the Gunn rats develop persistent dystonia that more closely resembles advanced forms of primary and secondary dystonia. Also, in order to systematically investigate dystonia in Gunn rats, previous studies in this project have developed techniques to reliably induce stable dystonic features in Gunn rat pups (Chapter 2, Chaniary 2008(36)), objectively quantify the severity of dystonias (Chapter 3, Chaniary 2009(129)) and perform stable microelectrode recordings in awake head-restrained rats (Chapter 4).

For understanding the pathophysiology of dystonia in Gunn rats, an important first step is to define the role of individual nuclei in dystonia. Since prominent cell loss, primarily confined to the principal motor territories of basal ganglia nuclei, occurs in Gunn rats (**Section 7.2.**), it was critical to establish whether the discharge activity in the surviving neurons in these territories was abnormal, as is hypothesis of this study. In this study, the discharge rates and patterns of neurons in GP, STN and EP were analyzed in

normal and dystonic animals. The intention was to establish if the discharge activity differed significantly between dystonic and control animals in each of these nuclei. The finding of this study are expected to provide a solid basis for understanding the underlying neurophysiology of kernicterus-related dystonia, other forms of dystonia and normal brain functioning.

5.2. CHALLENGES FACED IN THE PROJECT:

Challenge 1: Establish patterns of activity in each nuclei in dystonia

Initial studies in dystonic animals were performed to understand how the patterns of neuronal activity change after dystonia. With experience we found that spontaneously discharging neurons were less frequently encountered in dystonic animals. There were long abnormal regions of silence on recording tracks indicative of neuronal loss in these regions. Additionally, neurons that survived the toxicity fired with abnormal patterns (bursts and prolonged pauses) and had low amplitude with a lot of background activity which affected the quality of isolation. These conditions made neuronal recordings in dystonic animals difficult.

5.3. MATERIALS AND METHODS:

All procedures were approved the Institutional Animal Care and Use Committee. The details of the animal model and techniques for inducing dystonia in Gunn rats has been described previously (36). Briefly, at 16 days of age, jaundiced (jj) and Non-jaundiced (Nj) littermates were treated with an intra-peritoneal injection of sulfadimethoxine and saline respectively. Within hours after sulfa injection jj's develop abnormal prolonged axial and appendicular posturing which clinical resembles dystonia. A total of 27 animals were treated with sulfadimethoxine. Nine of these animals developed mild-to-moderate motor disability and comprised the experimental group. Of the remaining animals, 12 were severely affected and did not survive the acute bilirubin encephalopathy and 6 were unaffected and were not studied further. The experimental group was compared with nine Nj animals treated with equivolume of saline. Body weights were regularly monitored as an indicator of the general condition of the animal.

5.3.1. Surgery

For *in vivo* recording studies, surgical implantation of the head fixture was done on day 45, a month after sulfa injection. Day 45 was targeted for neuronal recordings to allow sufficient time for the animal to recover from acute bilirubin encephalopathy, permit stabilization of the dystonic features and allow sufficient growth of the skulls for supporting the head fixtures. The details of the surgical procedure and technique used for head stabilization have been described in detail in **Chapter 4**. In brief, stainless steel head

fixture was attached to the animal's skull using eight miniature screws. The animals were given 24 hours to recover from the surgery before microelectrode recordings were performed.

5.3.2. Neurophysiological Recordings

On the day of recording, the rat's head was immobilized by clamping the head fixture into the stereotaxic positioner. A burr hole centered at 2mm caudally and 1.5 mm laterally to the bregma reference point was drilled into the bone exposing the underlying dura mater. Within about 30 min. of the initial period of head restraining, neuronal recording sessions were initiated. A Thomas Recording mini-xyz-manipulator (Thomas Recording, Giese, Germany) was mounted onto a Kopf stereotactic arm. Neuronal activity was recorded from the posterolateral (motor) territory of GP, STN and EP. GP was targeted with a 10° medial-to-lateral approach in the coronal plane (for details refer **section 6.3**) while STN and EP were targeted with a 10° anterior-to-posterior approach in the sagittal plane. The following coordinates were used for targeting of the microelectrodes: 1) GP, 0-1.0 mm anterior from bregma and 3.6-4.6 mm lateral from the midline. 3) EP, 1.0-1.5 mm posterior from bregma and 2.9-3.4 mm lateral from midline. Single-unit activity was collected using glass coated tungsten microelectrodes (80 μm base diameter, impedance of 1-2 MΩ) into the brain. Each nucleus was identified by its characteristic neuronal firing patterns. Location of the recording sites were reconstructed by plotting the predicted electrode trajectory, depth from the starting point, firing patterns

of cells, and sensorimotor responses of relevant nuclei along each microelectrode track on scaled drawings. These tracks were superimposed on transparencies of parasagittal sections from the Paxinos and Watson atlas (117), to estimate the precise location in the brain. Also, the optic tract, just below the EP, was identified by its distinct response to light flashes and provided confirmation of the location of the microelectrodes. A concentric micro-drive head with 0.5 mm intra-electrode spacing was used to introduce additional electrodes once a target nucleus (GP, STN or EP) was identified.

The recorded neuronal activity was displayed over two oscilloscope screens (Hameg Instruments, Mainhausen, Germany) and connected to an audioamplifier for aural monitoring of the signal. Neuronal activity was collected for a minimum of 120 secs at a sampling rate of 40 kHz and were amplified and band pass filtered (gain = 50, bandwidth 0.07-8 kHz). Quality of neuronal isolation was continuously monitored online using Sort Client.

5.3.3. Offline analysis

Stored digital data was replayed off-line and individual units were sorted using Offline Spike Sorter (Plexon Inc.) using a combination of manual (k-means clustering, contours and waveform crossing method) and automated sorting techniques (valley-seeking) (130). This enabled separation of waveforms collected from single or multiple electrodes into distinct clusters. Each separated cluster was carefully examined for loss of neuron during recording and for quality for neuronal isolation. Any obvious artifacts in the

signal were removed. Neuronal units were included in the study only if a unit displayed

high quality of separation from background noise, number of recorded potentials > 300 and the activity was recorded for a minimum of 120 secs. Well-isolated clusters could be easily sorted using automated sorting
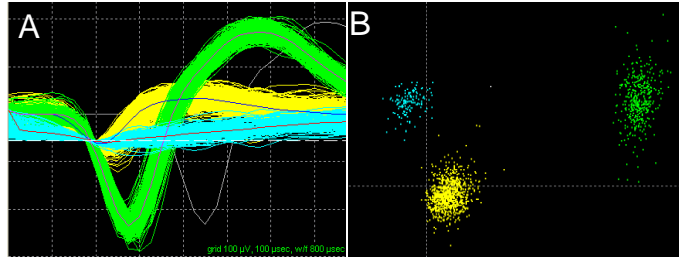
Fig. 19. Single unit isolation using 3-D principal component analysis (PCA) methodology. A. An example showing two neuronal spikes (green, yellow) and background noise (blue) activity collected on the same electrode. **B.** PCA display demonstrating excellent discrimination of neuronal spikes from background noise.

techniques (valley-seeking). An example of single unit isolation using showing two units

as two different clusters is shown in **Fig. 19**.

At times, however, multiple units recorded on a single electrode appeared in close

adjacent clusters. In such cases automated sorting techniques often lead to faulty

classification of the entire cluster as one unit. Isolation of neuronal units in such cases was

achieved via careful selection of clusters (contours or other manual sorting technique).

Also, neuronal units whose location could not be established from the plotted tracks were

excluded from all further analysis. For the present study, the neuronal epics which were

recorded while the animal was at rest.

5.3.4. Data Analysis

Data analysis was carried out by importing the data into NeuroExplorer. The

following parameters were assessed:

1. <u>Discharge rate</u>: The discharge rate provided an idea of how the neuron fired over time. The number of spike occurrences was averaged over the recording time.

2. <u>Discharge patterns</u>: The phasic changes that alter the temporal pattern of firing in dystonic animals were systematically assessed using the following parameters:

    a. <u>Interspike interval histograms</u>: The differences in firing patterns were determined by comparing the interspike interval histograms (ISI). The ISI histograms provide an idea of the stationarity of discharge during firing. The ISI histograms were calculated by dividing the time axis into small bins of 1ms width and intervals upto 200 ms were evaluated to account for long pauses during firing.

    b. <u>Coefficient of variation of ISI</u>: To quantify the variability in discharge activity between normal and dystonic animals, we calculated the coefficient of variation (CV) of ISI's by using the equation (SD of ISI/ mean ISI). This provides an idea of the spike irregularity during firing.

    c. <u>Asymmetry index</u>: To quantify the shape of ISI histogram we measured the asymmetry index using the equation (mode ISI/ mean ISI). The index value will be unity if there is a Gaussian distribution of the ISI. Index value less than 1 is indicative for short ISI intervals i.e. presence of bursting activity in spike train (47).

3. <u>Burst Detection</u>:

Fig. 20: **Comparison of burst detection using Surprise method and interval method**. **A**. Neuronal spike (yellow) superimposed on the background noise (grey) **B**. PCA analysis highlights the neuronal cluster (yellow) from the background (grey). **C**. Raster display shows burst clusters during firing in dystonic animal. Each vertical line represents an action potential **D**. Burst detection using Poisson surprise method at different surprise values (3-15) on a spike train. Burst periods in the spike trains are marked with blue lines. The surprise method wrongly classifies adjacent burst periods as one single burst (dashed boxes). As a result, the non-burst epics separating the burst periods have been wrongly marked as burst. Also, at higher surprise values a number of obvious bursts are rejected by the algorithm (red dashed oval) **E**. Burst detection using the interval method provides greater sensitivity for detecting individual burst periods.

Burst in neuronal signals are transient epics which have much higher discharge rate than other periods in a spike train (131). Over the years, several techniques have been developed for burst analysis in spike trains (131, 132). In this study, burst analysis was

performed using two techniques: 1) Poisson surprise method developed by Legendy and Salcman which uses ISI's to detect burst periods in a spike train and 2) Interval method which is based upon individually defining the burst parameters. Burst and burst related statistics were analyzed initially using the Poisson surprise method as implemented in Neuroexplorer. This method calculates the "unlikeliness" (or surprise) of finding a burst ISI's in a random stream of ISI's, which are assumed to be Poisson-distributed (132). Over the years, several studies have used this method for calculating the burst and burst-related statistics (133-135).

Despite its popularity over the years, this study found that there were two main problems with the Poisson surprise method 1) at low surprise values the algorithm wrongly classifies two adjacent burst epics as one, 2) at higher surprise values obvious burst in the spike train are rejected by the algorithm. To illustrate this point, consider an example GP unit recorded in a dystonic animal (**Fig. 20A, B**). Visual inspection of this unit clearly shows repetitive burst occurring over time (**Fig. 20C**). During burst detection using Poisson surprise method it was seen that at lower surprise values (3 to 14) several burst epics are wrongly grouped as a single burst (dashed box) while at higher surprise values (15) the method fails to detect what seems to be clear patterns of burst activity (red dashed oval) (**Fig. 20D**). These shortcomings of the Poisson surprise method to successfully detect bursting units are overcome by using the interval method defined below. In this method the burst events were identified by the following parameters (**Fig. 21**):

- Maximum interval to start burst = 6ms,

- Maximum interval to end burst = 9ms,

- Min interval between burst = 20ms,

- Minimum duration of burst = 5ms and

- Minimum number of spikes in a burst = 3.

Fig. 21. Explanation of burst parameters used in the interval method. Burst periods are marked with blue lines
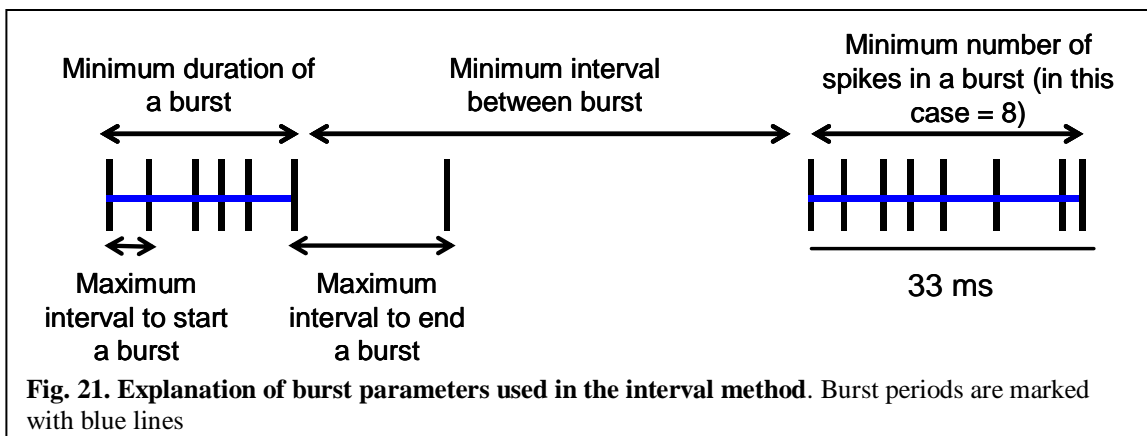
These parameters were determined based on visual inspection of number of spikes having different patterns both in normal and dystonic animals. The burst parameter selected in the interval method provided the highest degree of sensitivity for burst detection (**Fig. 20E**). The detected burst segments were quantified in terms of number of burst/cell, percentage of spikes in burst (burst density), the average and peak intraburst rates and burst index (mean ISI/ mode ISI).

5.3.5. Statistics

Statistical analysis was performed using the JMP software package. Mean $\pm$ standard deviation (SD) of the firing rates were determined for each nucleus. Comparisons between the discharge rates, CV of ISI's, and burst parameters between groups were made using one way ANOVA analysis. Multiple comparisons between groups was made using the Tukey-Kramer honestly significant difference (HSD) test. A probability value of < 0.05 was considered to be statistically significant for making comparisons between groups.

5.4. RESULTS:

Within 24 hrs after sulfa injection, jaundiced animals developed clinical symptoms of dystonia. The dystonic animals weighed significantly less than normal animals at 45 days of age ($p < 0.001$).

5.4.1. Discharge rates

Fig. 22 provides a summary of the discharge rates in all three nuclei. Neuronal discharge rates were significantly reduced in GP (62%, $p < 0.0001$) and EP (67%, $p < 0.0001$) in dystonic animals as compared to controls. In STN, although the rates were reduced in

Fig. 22 Neuronal discharge rates in normal and dystonic animals in key basal ganglia nuclei. Comparison of neuronal discharge rates for normal and dystonic animals reveal reduced discharge rates in all three nuclei * $p < 0.05$. Error bars = standard deviation

dystonics as compared to controls, the difference was not statistically significant (33%, $p = 0.07$).
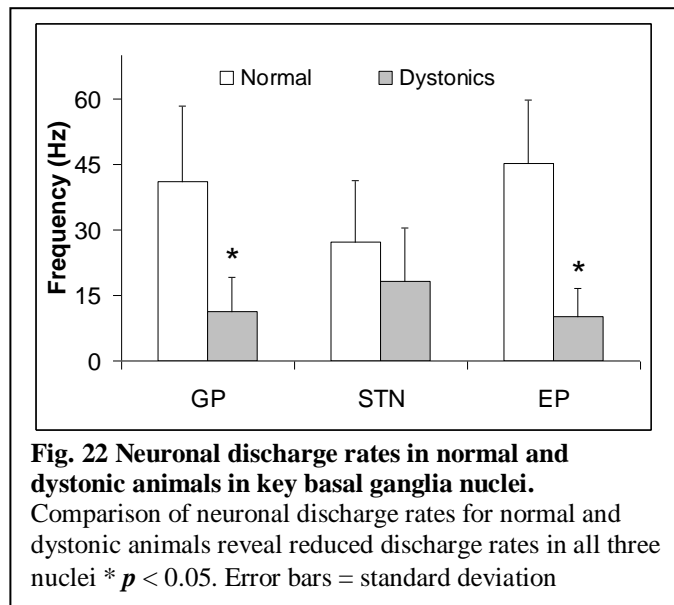
5.4.2. Characteristics GP neurons

Fig. 23: **Discharge patterns of GP neurons in normal and dystonic animals at rest with no sedation.** In each type, spike rasters (three examples) are shown on the left and ISI histograms are displayed on the right **A**. Type 1 neurons in normals showed a regular, tonic discharge reflected by the symmetrical, near-normal distribution of ISI histogram **B**. Type 2 neurons in normals showed irregular, tonic discharge reflected by positively skewed histograms. **C**. Type 1 neurons in dystonics showed burst discharge in grouped clusters reflected by the tall early peak in ISI and long tail. **D**. Type 2 neurons in dystonics showed random discharge reflected by small early peak in ISI and long tail. (ISI histogram bin size = 1ms)

A total of 74 neurons recorded in four normal animals and 46 neurons recorded in four dystonic animals were used for analysis. Most of the GP neurons recorded (83%) in normal animals showed regular tonic discharge firing (Type1, **Fig. 23A**) or slow irregular discharge interrupted by brief pauses (16%) (Type 2, **Fig. 23B**). Only one neuron showed burst discharge during firing. The regular tonic activity is reflected by the symmetrical, near normal distributions of the ISI's, while the irregular discharge is reflected by the positively skewed ISI histograms.

In contrast, the majority of GP neurons (52%) in dystonic animals showed burst discharge in group clusters which occurred irregularly over time (Type 1, **Fig. 23C**) while the remaining neurons (48%) had an irregular firing pattern. The burst activity is reflected by the prominent early peak of the ISI's and long pauses are at times 2-3 sec reflected by the tail lasting beyond the 0.2 sec long scale X-axis shown in the figure (Type 2, **Fig. 23D**). The irregularly firing neurons showed random discharge activity consisting of prominent burst and long pauses. In comparison to normal animals, the ISI histograms of irregularly discharging dystonic GP neurons showed an early peak indicative of burst activity that occurred during firing.

Fig. 24: **Discharge patterns of STN neurons in normal and dystonic animals at rest with no sedation.** In each type, spike rasters (three examples) are shown on the left and ISI histograms are displayed on the right **A**. Type 1 neurons in normals showed a irregular discharge reflected by the positively skewed ISI histogram **B**. Type 2 neurons in normals showed fast, regular, tonic discharge reflected by symmetric distribution of ISI. **C**. Type 1 neurons in dystonics showed random discharge reflected by small early peak in ISI and long tail **D**. Type 2 neurons in dystonics showed slow, irregular discharge reflected by the tall early peak in ISI and long tail. (ISI histogram bin size = 1ms)

5.4.3. Characteristics of STN neurons

A total of 45 neurons recorded in five normal and 34 neurons recorded in four dystonic animals were used for analysis. The majority of STN neurons in normal animals discharged with irregular (49%) or tonic firing patterns (40%) while a small percentage of STN neurons showed burst firing (11%). Irregularly discharging neurons in STN showed slow tonic discharge with occasional burst and short intermittent pauses reflected in the positively skewed ISI histogram (Type 1, **Fig. 24A**). On the other hand, regular tonically discharging neurons in STN showed higher rates and low ISI dispersion of neurons (Type 2, **Fig. 24B**). Clearly different from normal animals, a majority of STN neurons in dystonics (59%) showed a discharge pattern dominated by burst activity as reflected by the prominent early peak in the histogram (Type 1, **Fig. 24C**). The remaining STN neurons (41%) in dystonic animals showed irregular tonic firing interrupted by long pauses (at times 1-2 sec) reflected by the positively skewed ISI histogram (Type 2, **Fig. 24D**).
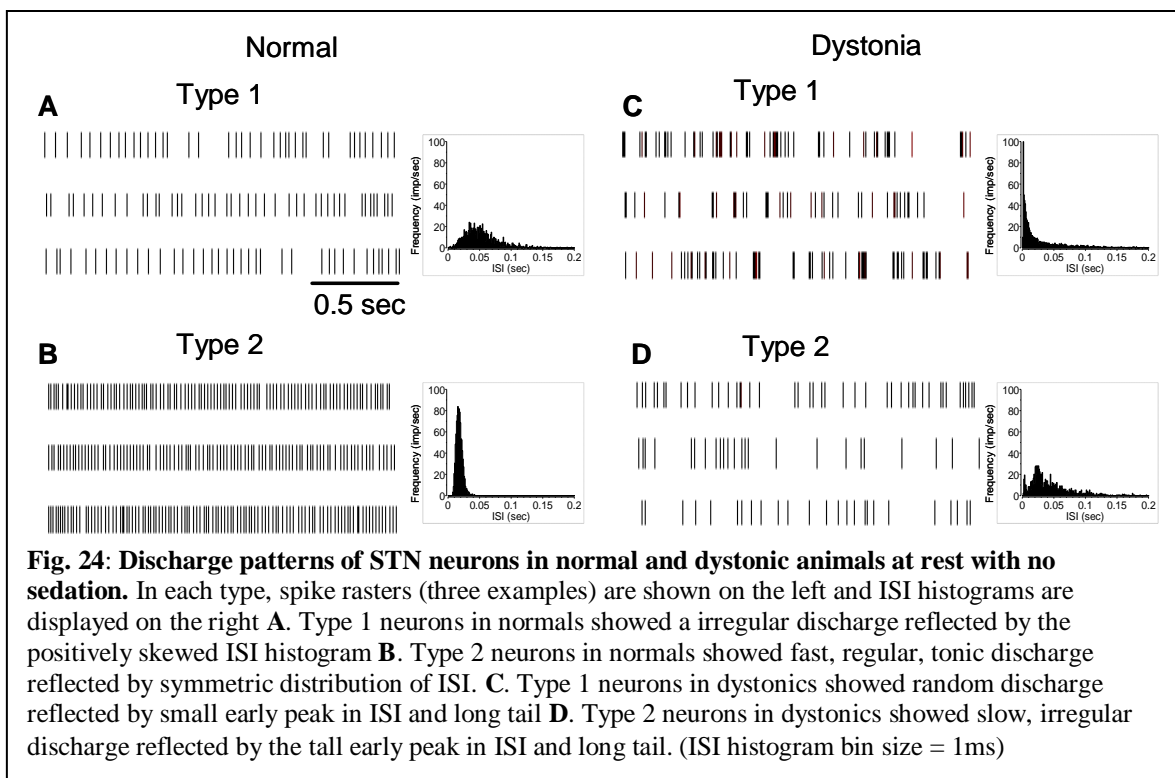
5.4.4. Characteristics of EP neurons

A total of 42 neurons recorded in four normal and 46 neurons recorded in five dystonic animals have been used for analysis. Similar to GP and STN neurons , EP neurons of normal animals showed two main types of firing patterns 1) tonic (60% of neurons) with high discharge rates reflected in the leftward grouped bell shaped ISI histogram (Type 1, **Fig. 25A**), (2) slow irregular firing (40% of neurons) reflected in the positively skewed histograms(Type 2, **Fig. 25B**). In contrast, EP neurons of dystonic animals showed a shift towards burst like multimodal firing and irregular firing patterns. Clearly different from

normals, the majority of EP neurons (57%) in dystonic animals showed irregular firing

patterns characterized by intermittent pauses and occasional bursts reflected in the random

distribution of the ISI's (Type 1, **Fig. 25C**) The remaining. (43%) in dystonics discharged

either in burst mode in group clusters, which occurred at regular intervals or at times

Fig. 25: **Discharge patterns of EP neurons in normal and dystonic animals at rest with no sedation.** In each type, spike rasters (three examples) are shown on the left and ISI histograms are displayed on the right **A**. Type 1 neurons in normals showed a fast tonic discharge reflected by the symmetrical, near-normal distribution of ISI histogram **B**. Type 2 neurons in normals showed irregular, tonic discharge reflected by positively skewed histograms. **C**. Type 1 neurons in dystonics showed random discharge reflected by small early peak in ISI and long tail. **D**. Type 2 neurons in dystonics showed burst discharge in grouped clusters reflected by the tall early peak in ISI and long tail. (ISI histogram bin size = 1ms)

switched to tonic irregular firing reflected in the bimodal distribution of ISI's, consisting of

a large positive peak (reflective of burst) followed by a secondary peak (reflective of

clusters) that was normally distributed and a long tail (reflective of intermittent pauses

during firing) (Type 2, **Fig. 25D**).

5.4.5. Quantitative evaluation of ISI parameters

Normal vs Dystonic animals:

Table 7 provides a summary of ISI parameters between normal and dystonic animals in GP, STN and EP. Quantitative evaluation of ISI parameters confirmed the change in firing patterns of GP, STN and EP neurons after induction of dystonia. The mean ISI in GP (156.6 ± 155.8 vs 31.6 ± 20.0 ms; $p < 0.0001$), STN (111.5 ± 36.4 vs 49.8 ± 26.5 ms; $p < 0.0001$) and EP (149.0 ± 102.6 vs 39.5 ± 18.5 ms; $p < 0.0001$) was significantly higher in dystonic animals as compared to the control group. The coefficient of variation (ISI CV) in dystonic animals was significantly higher than control animals in GP (2.8 ± 1.5 vs 0.7 ± 0.4 ms, $p < 0.0001$), and EP (2.06 ± 1.1 vs 1.06 ± 1.2, $p < 0.0001$) suggestive of tremendous variability in discharge activity among dystonic animals. ISI CV in STN (1.62 ± 0.9 vs 0.80 ± 0.39, $p = 0.03$) among dystonic was higher than control animals however the difference was not significant. Additionally, the asymmetry index was significantly lower in dystonic as compared to control animals in GP (0.07 ± 0.07 vs 0.72 ± 0.22, $p < 0.0001$), STN (0.23 ± 0.16 vs 0.53 ± 0.30, $p = 0.0023$) and EP (0.09 ± 0.18 vs 0.59 ± 0.26, $p < 0.0001$) indicative of an increase in burst activity in basal ganglia nuclei after induction of dystonia.

Dystonic groups:

Among dystonic animals, using Tukey's HSD, it was determined that the CV ISI of bursting neurons in GP (3.6 ± 1.3) was significantly higher ($p = 0.0025$) than in GP and STN (combined mean = 2.8 ± 1.2), reflective of the dominant pattern of burst firing in grouped clustering present in GP neurons.

Table 7: Comparison of ISI parameters in key basal ganglia nuclei between normal and dystonic animals.

Pattern	Mean ISI (ms)	CV ISI	Asymmetry index
GP normals (74)	31.6 ± 20.0	0.7 ± 0.4	0.72 ± 0.22
Irregular (12)	67 ± 23.2	1.1 ± 0.2	0.36 ± 0.15
Tonic (n = 61)	24.9 ± 9.4	0.6 ± 0.4	0.78 ± 0.16
GP Dystonics (46)	156.6 ± 155.8*	2.8 ± 1.5*	0.07 ± 0.07*
Burst clusters (24)	123.2 ± 139.0	3.6 ± 1.3	0.04 ± 0.03
Irregular (22)	193.1 ± 167.8	1.8 ± 1.0	0.10 ± 0.10
STN normals (45)	49.8 ± 26.5	0.9 ± 1.0	0.53 ± 0.30
Irregular (22)	68.0 ± 20.3	1.0 ± 0.3	0.40 ± 0.20
Tonic(18)	25.2 ± 7.9	0.5 ± 0.4	0.80 ± 0.20
STN Dystonics (34)	111.5 ± 36.4*	1.62 ± 0.9	0.23 ± 0.16*
Bursty (20)	147.9 ± 41.7	2.9 ± 1.2	0.09 ± 0.05
Irregular (14)	68.2 ± 34.1	1.1 ± 0.9	0.41 ± 0.20
EP normals (42)	39.5 ± 18.5	1.1 ± 1.2	0.59 ± 0.26
Irregular (17)	55.9 ± 15.5	1.0 ± 0.3	0.36 ± 0.19
Tonic(25)	28.4 ± 10.5	1.1 ± 1.6	0.74 ± 0.17
EP Dystonics (46)	149.0 ± 102.6*	2.1 ± 1.1*	0.09 ± 0.18*
Burst clusters (20)	84.0 ± 43.8	2.6 ± 1.3	0.03 ± 0.01
Irregular (26)	199.0 ± 107.3	1.6 ± 0.6	0.13 + 0.23

* indicates significant difference($p < 0.05$) between normal and dystonic groups
Values are mean ± SD

5.4.6. Burst analysis

Normal vs Dystonic animals:

As compared to non-dystonic control animals, in dystonic animals there was a significant shift towards irregular and rhythmic burst like firing in all three basal ganglia nuclei. Number of burst per minute was significantly higher in dystonic animals as compared to controls in GP (41.26 ± 57.03 vs 8.23 ± 13.8, p <0.0001), STN (38.12 ± 21.23

vs 5.59 $\pm$ 8.0, p < 0.0001) and EP (33.70 $\pm$ 41.66 vs 9.26 $\pm$ 17.9, p = 0.0007). **Table 8**

summarizes the quantitative analysis of burst parameters among normal and dystonic

animals in all three nuclei. Percentage of spikes in burst was significantly higher in

dystonic animals as compared to controls in GP (35.5 $\pm$ 37.8 vs 1.4 $\pm$ 2.5, p < 0.0001),

STN (25.5 $\pm$ 13.1 vs 1.4 $\pm$ 2.0; p < 0.0001) and EP (21.9 $\pm$ 22.2 vs 2.1 $\pm$ 3.6; p < 0.0001)

signifying an increase in burstiness among neurons after induction of dystonia. Also, the

mean frequency in burst was significantly higher in dystonic animals as compared to

controls in GP (220.9 $\pm$ 106.1 vs 139.8 $\pm$ 97.6 Hz; p < 0.0001) and EP (261.4 $\pm$ 70.5 vs

166.0 $\pm$ 95.3 Hz; p < 0.0001) but did not differ significantly in STN (177.3 $\pm$ 81.2 vs 159.0

$\pm$ 98.9 Hz, p = 0.59).

Dystonic groups:

Among dystonic animals, percentage of spikes in burst and mean frequency in burst

were found to be significantly different in the three nuclei using an unequal variance F-test

(F (3, 41) = 27.3, p < 0.0001) Using Tukey's HSD, it was determined that the number of

bursts per minute was significantly lower in STN (37.2 $\pm$ 24.9) as compared to GP and EP

neurons. Within the GP and EP neurons (combined mean = 72.3 $\pm$ 53.6) there was no

significant difference. Additionally, it was determined that mean frequency of burst was

significantly higher in EP (261.4 $\pm$ 70.5 Hz) as compared to GP and STN neurons. Further,

the mean frequency of burst in GP neurons was significantly higher than STN neurons

(159.0 $\pm$ 98.9 Hz).

Table 8: Comparison of burst parameters in key basal ganglia nuclei between normal and dystonic animals.

Pattern	Bursts per minute	% of Spikes in Bursts(%)	Burst Duration (ms)	Mean Freq. in burst (Hz)	Mean Interburst interval (sec)
GP normals (74)	8.2 ± 13.8	1.4 ± 2.5	13.3 ± 15.7	139.8 ± 97.6	5.3 ± 9.5
Irregular (12)	0.5 ± 1.4	0.2 ± 0.4	2.7 ± 4.9	57.8 ± 106.2	1.4 ± 3.6
Tonic (n = 61)	9.0 ± 13.5	1.5 ± 2.4	15.4 ±16.5	154.7 ± 88.7	6.2 ± 10.2
GP Dystonics (46)	41.3 ± 57.0*	35.0 ± 37.8*	14.0 ± 8.1	220.9 ± 106.1*	4.1 ± 6.8
Burst clusters (24)	76.5 ± 60.3	65.1 ± 28.3	19.0 ± 5.6	280.5 ± 45.4	2.3 ± 5.9
Irregular (22)	2.9 ± 4.3	2.1 ± 2.6	8.5 ± 6.8	155.9 ± 115.7	6.0 ± 7.4
STN normals (45)	5.6 ± 8.0	1.4 ± 2.0	9.7 ± 6.2	159.0 ± 98.9	9.2 ± 16.9
Irregular (22)	6.2 ± 9.6	1.9 ± 2.5	8.7 ± 5.5	170.0 ± 108.1	11.5 ± 21.3
Tonic (18)	4.7 ± 5.0	0.7 ± 0.8	11.3 ± 7.0	142.4 ± 83.3	5.8 ± 5.1
STN Dystonics (34)	28.7 ± 21.8*	25.5 ± 13.1*	11.3 ± 5.1	177.3 ± 81.2	4.8 ± 7.5
Bursty (20)	37.2 ± 24.9	32.1 ± 14.9	11.9 ± 4.6	210.2 ± 67.7	4.5 ± 6.5
Irregular (14)	13.2 ± 16.2	14.2 ± 12.0	10.4 ± 6.3	163.0 ± 109.5	5.4 ± 8.1
EP normals (42)	9.3 ± 17.9	2.1 ± 2.6	10.0 ± 6.7	166.0 ± 95.3*	6.8 ± 8.9
Irregular (17)	7.4 ± 13.9	2.1 ± 3.7	8.7 ± 5.5	173.5 ± 106.5	6.4 ± 7.3
Tonic (25)	10.6 ± 20.3	2.0 ± 4.2	10.8 ± 7.5	160.1 ± 88.9	7.1 ± 10.0
EP Dystonics (46)	33.7 ± 41.7*	21.9 ± 22.2*	11.5 ± 3.8	261.4 ± 70.5	10.3 ± 19.9
Burst clusters (20)	68.1 ± 42.4	40.4 ± 20.8	13.2 ± 2.1	283.5 ± 44.7	1.9 ± 2.6
Irregular (26)	7.2 ± 8.7	7.7 ± 8.3	10.1 ± 4.3	244.4 ± 82.1	16.8 ± 24.6

* indicates significant difference($p < 0.05$) between normal and dystonic groups
Values are mean ± SD

5.5. DISCUSSION:

The aim of the present study was to compare and contrast the discharge rates and firing patterns of basal ganglia neurons in normal and dystonic animals. The findings suggest that after induction of dystonia in these animals the discharge activity in all three nuclei (GP, STN and EP) changes from the fairly regular tonic firing to a pattern dominated by bursts and long abnormal pauses. The significant differences in ISI and burst parameters between normal and dystonic animals are reflective of these changes. These findings suggest that abnormally patterned signaling in surviving basal ganglia neurons plays a major role in the development of dystonia in Gunn rats. In addition to having major implications for studies in rodent models of dystonia, these findings could potentially extend to human studies

The present findings of abnormal discharge activity in dystonia are similar to several previously reported studies in dystonia patients undergoing deep brain stimulation surgeries. Several groups have previously (4, 5, 121, 136) reported the presence of low discharge rates and irregularly grouped discharges with intermittent pauses in GPi in dystonic patients and supported the contention that abnormal patterns play a critical role in manifestation of dystonia. However, these studies provided only discharge rate and pattern information in dystonic neurons and fail to quantify the discharge properties (ISI's, burst) in these neurons. Recently, in addition to characterizing abnormal rates and patterns in dystonia, Starr and colleagues (124, 125) have reported presence of non-oscillatory bursting and oscillatory activity range in GPi and STN among dystonic patients. Only one

human study (123), to date, has systematically characterized different types of patterns (irregular, regular, clustering and bursting) among GPe and GPi neurons in different types of dystonia. In comparison, this study for the very first time provides a comprehensive classification of the discharge rates, patterns and neuronal properties (ISI and burst parameters) in key basal ganglia nuclei in non-anesthetized normal and dystonic animals.

In addition to dystonics, this study contributes to the understanding of basal ganglia signaling in normal condition. The findings in the present study suggest that there are two types of neurons (tonic and irregular) in each of the key basal ganglia nuclei (GP, STN and EP). It is conceivable each type of neuron may have different projection in the basal ganglia. Future studies using a combination of *in vivo* and *in vitro* methods are needed to explore this possibility. These findings could have major implications towards understanding of the current models of basal ganglia.

The present study has some limitations. Firstly, based on histological findings of selective cell loss in the motor territories of STN (**section 7.2**.,page 128) it was decided to target the motor territories of key basal ganglia nuclei for neuronal recording investigations. This study, however, fails to explore whether abnormal patterns of activity exist in non-motor territories of these nuclei. Such findings could have major implications towards the current understanding of physiology of kernicterus-induced dystonia. Secondly, in the present study neuronal activity was collected on an average for 120 secs. Neuronal recordings collected over such small periods fail to answer if the activity of these neurons changes due to behavior or state of alertness of the animal. Future studies should

be designed to determine if firing patterns change over longer periods of recording (10-15 min).

In summary, the present findings suggest that there are striking differences in patterned discharge activity and discharge rates in GP, STN and EP between dystonic and control rats. The demonstration of neuronal discharges closely resembling that reported in secondary and primary human dystonias strongly supports the value of the Gunn rat as a model of dystonia. These studies are expected to lead to significant advances in understanding of the pathophysiological contribution of basal ganglia nuclei to kernicterus-related dystonia.

CHAPTER 6 BASAL GANGLIA INFLUENCE ON MOVEMENTS AS STUDIED IN

NORMAL AND DYSTONIC RATS

6.1. INTRODUCTION:

The role of the basal ganglia in normal and pathological motor control remains poorly understood. Although movement related discharge of basal ganglia neurons has been extensively investigated, the results of these studies has produced conflicting results. Previously it has been reported that neurons in the lateral part of the globus pallidus externa (GPe) and interna (GPi), segments of the pallidum, and the subthalamic nucleus (STN) (motor region) phasically alter their discharge during active and passive movements (137, 138). The phasic changes in basal ganglia neurons during movements are of great interest to researchers for understanding the current models for basal ganglia function. Traditional basal ganglia rate models predict that scaling of movements occur through modulation of GPi activity via the direct and indirect pathways (53, 54, 139). According to these models reduced activity in GPi is thought to facilitate movements by disinhibiting the thalamocortical neurons. In contrast, activation of GPi neurons is thought to lead to

inhibition of movements by inhibiting the thalamocortical projections. However, these models fail to explain improvements from surgical lesioning, as well as DBS procedures in movement disorders and have been highly criticized.

Over the years, multiple studies have documented relations between basal ganglia discharge activity and kinematics of movement including direction, velocity, and amplitude as well as the force exerted (48, 140-142). In contrast, others have suggested that there is no systematic or consistent relation of pallidal discharge to specific movement parameters, but rather that they vary under different task conditions (143-145). Overall, some studies have suggested that the basal ganglia plays a principal role in self-initiated and not stimulus triggered movements (146, 147), although these findings are highly controversial (143, 148).

Much of the current knowledge, about neuronal discharge during dystonic movements is based upon a limited number of reports from patients undergoing DBS surgical implantations. Zhuang and colleagues have reported that in dystonic patients all neuronal bursts have the same average frequency (0.4-0.5 Hz) as dystonic movement and the individual values are correlated (5). Starr and colleagues also reported oscillatory activity but at 3-8 Hz and with only infrequent correlations with EMG activity and mostly confined to patients with dystonic tremor (124). Vitek and colleagues have reported that in dystonia, GPi cells respond to movements in multiple directions and across multiple joints and limbs (4). However, none of these studies could identify clear differences between primary and secondary dystonias with respect to phasic changes during movement.

In the previous chapter it has been shown that abnormal patterned discharge activity exist in motor regions of GP, STN and EP in dystonic animals at rest. These findings suggest that alterations in discharge activity in these basal ganglia nuclei certainly play a major role in the development of dystonia in Gunn rats. The next step is to understand how neurons in individual basal ganglia nuclei communicate during normal and dystonic motor activity. The main hypothesis of this study was that abnormal signaling that originates in individual neurons of basal ganglia nuclei in turn affects the discharge properties of the neurons to which they project. This cascade effect in turn leads to disruption in signal transmission throughout the basal ganglia circuitry thereby leading to errors in cortical output and distorted motor control in dystonia.

To better understand the role of basal ganglia in the execution of externally triggered vs. self-initiated movements, the present study investigated neuronal discharge change activity in the globus pallidus (GP, rodent-equivalent of GPe), entopeduncular nucleus (EP, rodent-equivalent of GPi), and STN in normal and dystonic rats during spontaneous, self-initiated and stimulus driven movements. Under awake head-restrained conditions, neuronal activity was collected from up to three microelectrodes inserted in the principal motor regions of the globus pallidus (GP, equivalent to GPe) and entopeduncular nucleus (EP, equivalent to GPi) during active movements.

6.2. CHALLENGES FACED IN THE PROJECT:

1. Surgery:

Surgeries in this study involved implantation of the head-restraint and suturing of EMG electrodes into desired muscle groups. The original plan was to record muscle activity from multiple pairs of antagonistic muscles in the forelimb and hindlimb (contralateral side) to understand how brain signaling alters muscle activity in dystonia. These surgeries lasted for over 3h since they required multiple incisions in the body and subcutaneous tunneling of several EMG electrodes. With experience it was realized that in dystonic animals, survival rates dropped markedly if the surgeries lasted significantly longer than two hrs. Thus, in order to reduce the surgical intervention time the plan was revised and instead muscle activity was recorded only from a single pair of antagonistic hip muscles (gluteus superficialis and gluteus medius).

2. Soldering of EMG electrodes:

The surgical procedure requires soldering of thin wire EMG electrodes to a micro-circuit board. Soldering thin EMG wires using a surgical microscope besides an anesthetized animal was extremely challenging and time consuming. It required weeks of practice to master this technique.

6.3. MATERIALS AND METHODS:

All procedures were approved the Institutional Animal Care and Use Committee. The details of the animal model and techniques for inducing dystonia in Gunn rats has been described previously (36). Briefly, at 16 days of age, jaundiced (jj) and Non-jaundiced (Nj) littermates were treated with an intraperitoneal injection of sulfadimethoxine and saline respectively. Within hours after sulfa injection develop abnormal prolonged axial and appendicular posturing which clinical resembles dystonia.

6.3.1. Neurophysiological Recordings

6.3.1.1. Surgical procedure and set up

The detailed procedure of surgical details and the recording set up is described in detail in **Chapter 4**. Briefly, at 45 days, under isofluorane anesthesia, stainless steel head restraints were secured to the skull of these animals with screws (dystonic, n = 7; control (Nj-saline), n = 7). The contralateral leg was surgically exposed and fine wires were inserted into hip flexor and extensor muscles. Beginning the following day, the animals' heads were immobilized by securing the head restraint to a custom-designed stereotaxic guidance system for daily recordings without the use of sedation.

6.3.1.2. Head configuration for multi-unit recordings

GP, STN and EP were individually targeted with up to three microelectrodes (80 µm diameter) using a concentric microelectrode arrangement (300 µm separation) shown in **Fig. 26**. The system allows the passage of up to five thin (80 µm base diameter) quartz-platinum/tungsten glass coated microelectrodes in a concentric configuration with 305 µm intra-electrode spacing. Flexible microelectrodes (80 µm diameter) used in this study minimize the degree of tissue damage, are superior to stiffer electrodes for maintaining prolonged single-unit recordings in active animals, and permit excellent isolation. Taking into consideration the size of the nuclei and the angle of targeting (**section 6.3.1.3.**) a maximum of three microelectrodes were introduced into the motor territories of these nuclei at a time.
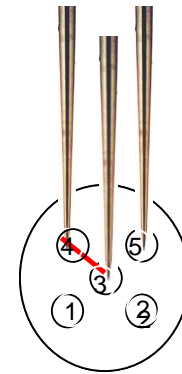
Fig 26: Concentric electrode configuration used for multi-unit recording studies

6.3.1.3. Determination of coordinates

The co-ordinates for recording from motor territories of these nuclei were calculated using the Paxinos and Watson atlas (117). Both, STN and EP were targeted unilaterally via a 10° anterior-to-posterior approach using the following co-ordinates 1) STN, 1.6-2.1 mm posterior from bregma and 2.6-2.9 mm lateral from the midline, 2) EP, 1.0-1.5 mm posterior from bregma and 2.9-3.4 mm lateral from midline. However, compared to the STN and EP, the motor region of GP was more lateral (~3.6-4.6 mm). The chamber design prevented access to the lateral edge (4.2-4.6 mm) of GP using the anterior

to posterior approach. To overcome this, recordings in GP were performed via a 10°

medial-to-lateral approach (coronal plane). Co-ordinates for targeting the motor region of

GP in this plane are described in the **Fig. 27**. This approach was standardized for GP

recordings in all animals used in this study.

Fig. 27: **GP electrode trajectory calculation: A.** An example where recordings are performed in the right hemisphere of the brain with a 10° medial-to-lateral approach and target is the motor region of GP at Lateral 3.8. **B.** Based on our trigonometric calculations we need to enter the dura 1.2 mm medial to our target
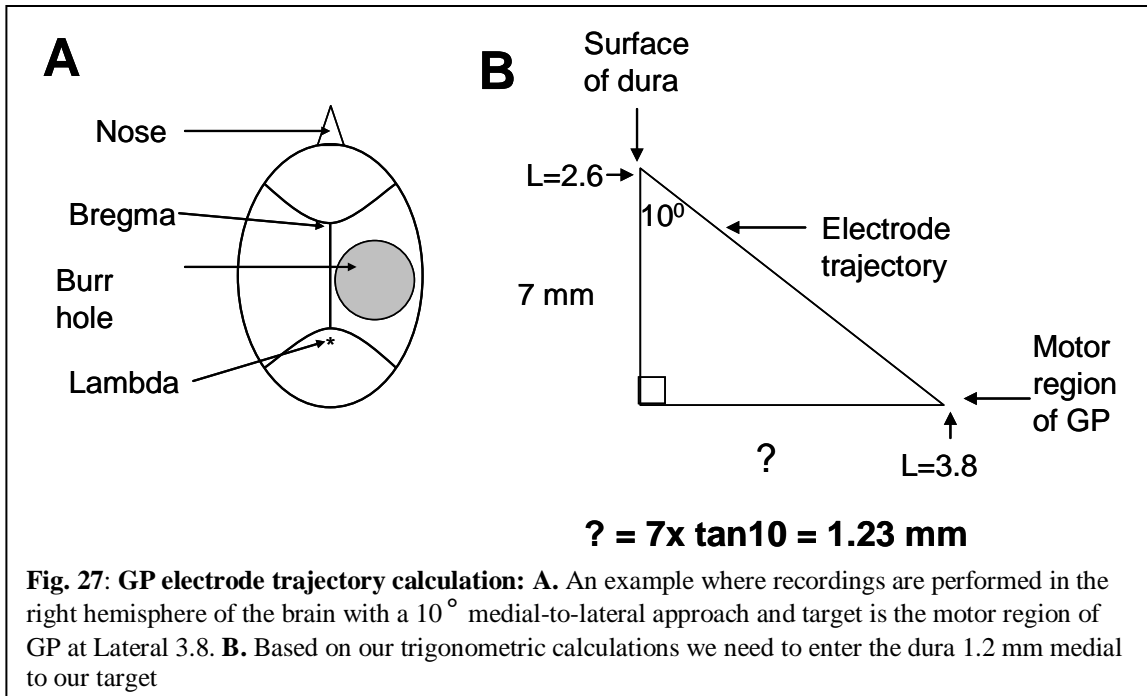
6.3.1.4. Recording strategy:

Initially, only one electrode was lowered into the brain. On each recording track,

the boundaries of the encountered nuclei were delineated and plotted on a graph paper. The

targeted nuclei (GP, STN or EP) were identified by the characteristic neuronal firing

patterns and by their relation to easily identifiable nearby landmarks, including the internal

capsule and optic track. Additional electrodes were lowered to record multi-unit activity

once the target nucleus was identified. Each well isolated unit in the motor region of GP,

STN and EP was recorded for at least 60-120 sec during active hip movements. Neuronal response was assessed during voluntary as well as externally triggered movements.

6.3.2. Data Analysis:

Stored digital data was replayed off-line and individual units will be sorted using Offline Spike Sorter (Plexon Inc.) using a combination of manual (k-means clustering, contours and waveform crossing method) and automated sorting techniques (valley-seeking) (130). This enabled to separate waveforms collected from single or multiple electrodes into distinct clusters. Each separated cluster was carefully examined for loss of neuron during recording and for quality for neuronal isolation. Any obvious artifacts in the signal were removed. Also, neuronal units whose location could be established from the plotted tracks were excluded from all further analysis.

6.3.2.1. Perievent time histogram

Fig. 28: Schematic representation of Perievent Time Histogram.
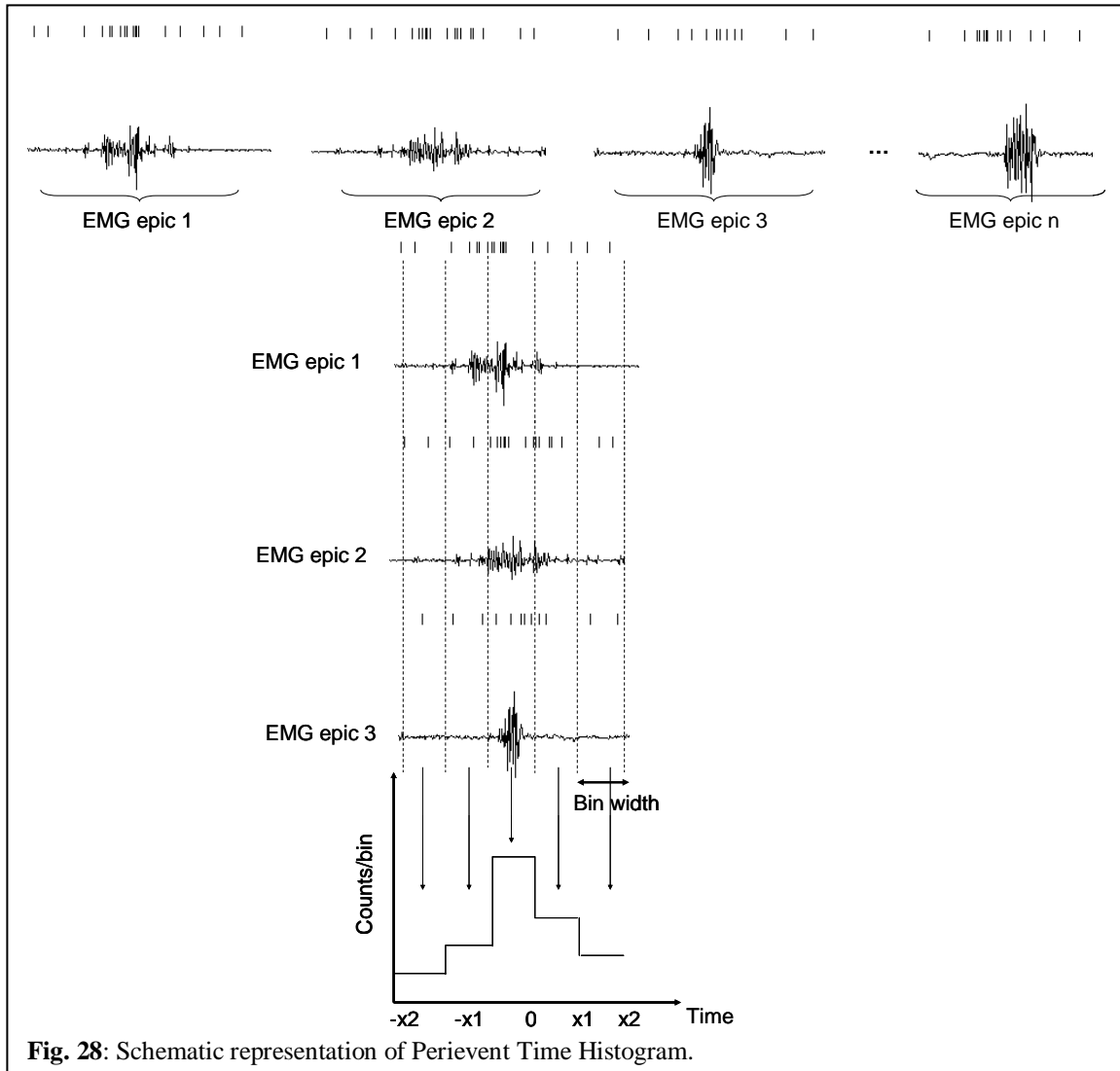
Statistically significant changes in discharge rates during EMG epics (movement) were detected in perievent time histogram calculations. A perievent time histogram (PETH) provides information of the times at which neuron fires in relation to an external stimulus. It gives an overall idea of whether the "movement response" occurred before or

after the EMG epics. **Fig. 28** shows an example of the procedure. To construct a PETH, the segment of spike train corresponding to each EMG epic was cut and then lined up based on the onset of the EMG epics. The lined up spike-EMG epics were then broken into small time segments, which are called bins and the total value in each bin is then plotted in the PETH histogram. With the onset of EMG in each epic defined as time =0, the histograms were plotted for a 400 ms time period i.e. 200 ms before and 200 ms after the movement onset for EMG epics.

6.3.3. Statistics

The spike was considered to have "significant movement response" if four consecutive 5-ms bins were above 95% confidence limits (calculated from the mean firing rate) during the search period ($p < 0.001$).

6.4. RESULTS:

Table 9 provides a breakdown of responses in basal ganglia neurons during hip movements in normal and dystonia animals. Overall, there were a greater number of "movement responsive" cells in normals as compared to dystonic animals. This was because it was difficult to isolate neurons in dystonic animals in all three nuclei. Recordings in dystonic animals at times consisted of small amplitude units with a lot of background activity which affected the quality of isolation. Also, neuronal units in dystonic animals were fragile i.e. at times they were lost during active movements

Table 9: Neuronal responses during hip movement (n = 7 dystonic, 7 controls)

Nuclei	No. of neurons		Type of response of neurons during hip movement					
	Normal	Dystonics	Normals			Dystonics		
			Increase	Decrease	Biphasic	Increase	Decrease	Biphasic
GP	28	25	18	7	3	10	14	1
STN	32	18	27	3	2	13	3	2
EP	36	29	22	12	2	17	11	1

6.4.1. Globus Pallidus (GP)

Activity from 3 normals and 4 dystonic animals was recorded for this study. Two of dystonic animals had severe dystonia (CS~3.5) and the other two had moderate dystonic symptoms (CS~2.5). The patterns and neurophysiological properties of these neurons have been previously discussed in detail in **chapter 5**.

6.4.1.1. Proportion of movement related cells in GP

In GP, increases in discharge during active movements were found in 64% of neurons in normals and 40% of neurons in dystonics. Decreases in discharge activity were found in 25% of neurons in normals and 56% of neurons in dystonics. Biphasic changes (both increase and decrease during movement) were found in 11% of neurons in normals and 4% of neurons in dystonic animals.

Fig. 29. Multi-unit discharge activity in GP during stimulus-induced movements (light strokes to the ipsilateral chest or hindlimb) and voluntary movements in normal rats. (**A**) Normal alternating agonist-antagonists EMG bursts during voluntary movement are associated with recurrent discharge bursts in a select (GP2) neuron ($p < 0.001$). (**B**) Decrease in discharge activity in a select (GP2) neuron occurs throughout epics of voluntary hip extensor activity ($p < 0.001$)

6.4.1.2. Patterns

Fig. 30. Multi-unit discharge activity in GP during stimulus-induced movements (light strokes to the ipsilateral chest or hindlimb) and voluntary movements in dystonic rats. (A) Co-contraction epics associated with abnormal prolonged bursts in (GP1) neuron ($p < 0.001$). **(B)** Decrease in discharge activity in a select (GP2) neuron occurs throughout co-contraction epics ($p < 0.001$)

In normal animals, 12 of 18 GP units that had an increase response to hip movement showed recurrent discharge bursts that were associated with individual EMG epics (**Fig. 29A**) ($p < 0.001$). The remaining 6 units showed either an initial or late phasic

increase during repetitive EMG burst but failed to generate significant change in response*. Four of 7 units that had decrease response to hip movement showed decrease in discharge activity that appeared to correlate throughout EMG epics of voluntary muscle activity (**Fig. 29B**) ($p < 0.001$). Decrease in response in other units (3 of 7) was not significant*. Contrastingly, in dystonic animals, 7 of 10 GP units that had an increase response to hip movement showed abnormal prolonged bursts (**Fig. 30A**) during co-contractions epics suggestive of loss of focused signaling in dystonia ($p < 0.001$). Pattern of movement related decrease in GP units of dystonic animals was similar to that described in normals (**Fig. 30B**).

(* For simplicity, while describing patterns in subsequent nuclei, I have only discussed units that had significant response ($p < 0.001$))

Synchronization: In severely dystonic animals (CS=3.5), simultaneously recorded neurons (4 pairs) showed an abnormal pattern of pause synchronization (**Fig. 31**). Relation of the decrease in neuronal activity to the duration of EMG activity was found to be statistically significant ($p < 0.001$).
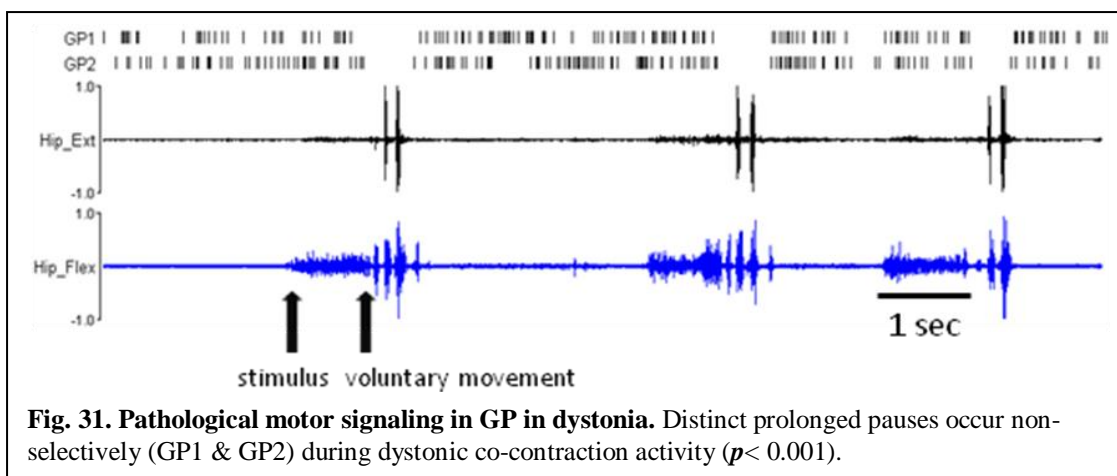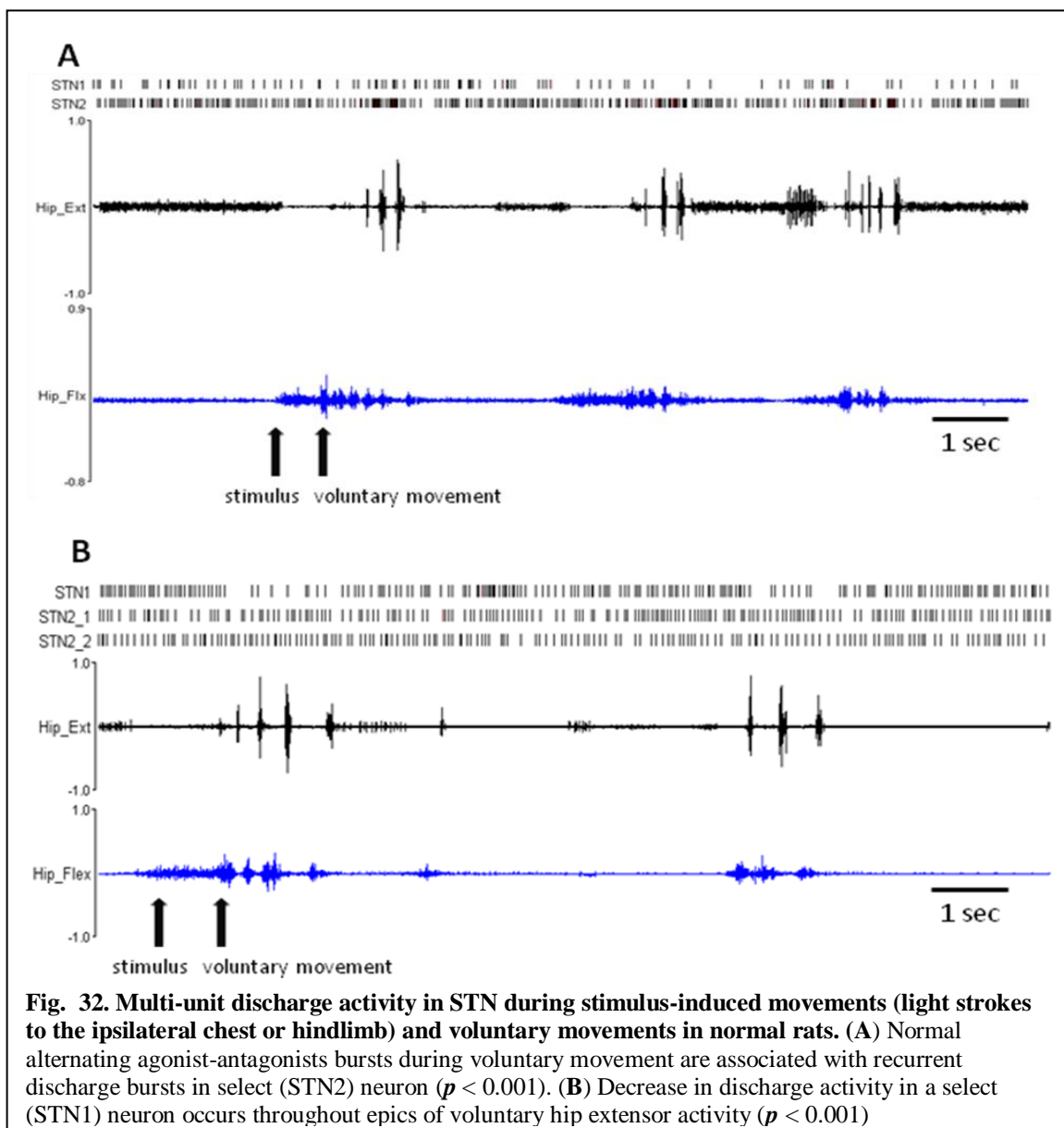

Fig. 31. Pathological motor signaling in GP in dystonia. Distinct prolonged pauses occur non-selectively (GP1 & GP2) during dystonic co-contraction activity ($p < 0.001$).

6.4.2. Subthalamic Nucleus (STN)

Activity from 3 normal and 3 dystonic animals in the subthalamic nucleus was recorded in this study. Compared to GP and EP, neurons in the subthalamic nucleus were particularly difficult to isolate and were highly fragile (sounded injured while recording) in

Fig. 32. Multi-unit discharge activity in STN during stimulus-induced movements (light strokes to the ipsilateral chest or hindlimb) and voluntary movements in normal rats. (A) Normal alternating agonist-antagonists bursts during voluntary movement are associated with recurrent discharge bursts in select (STN2) neuron ($p < 0.001$). **(B)** Decrease in discharge activity in a select (STN1) neuron occurs throughout epics of voluntary hip extensor activity ($p < 0.001$)

dystonic animals. Of the 3 dystonic animals, one animal had severe dystonia (CS = 3.5) while other two had moderate dystonia (CS = 2.5).

6.4.2.1. Proportion of movement related cells in STN

Significant increases in discharge during active hip movements were detected in 85% of cells in normals and 72 % cells in dystonics. In contrast, decreases in discharge during hip movements were less common in STN and were observed in 9 % cells in normals and 17% cells in dystonics. Biphasic changes were observed in 6% of cells in normals and 11% of cells in dystonics.

6.4.2.2. Patterns

In normal animals, 20 of 27 STN units that had an increase response to hip movements showed recurrent discharge burst that were associated with individual EMG
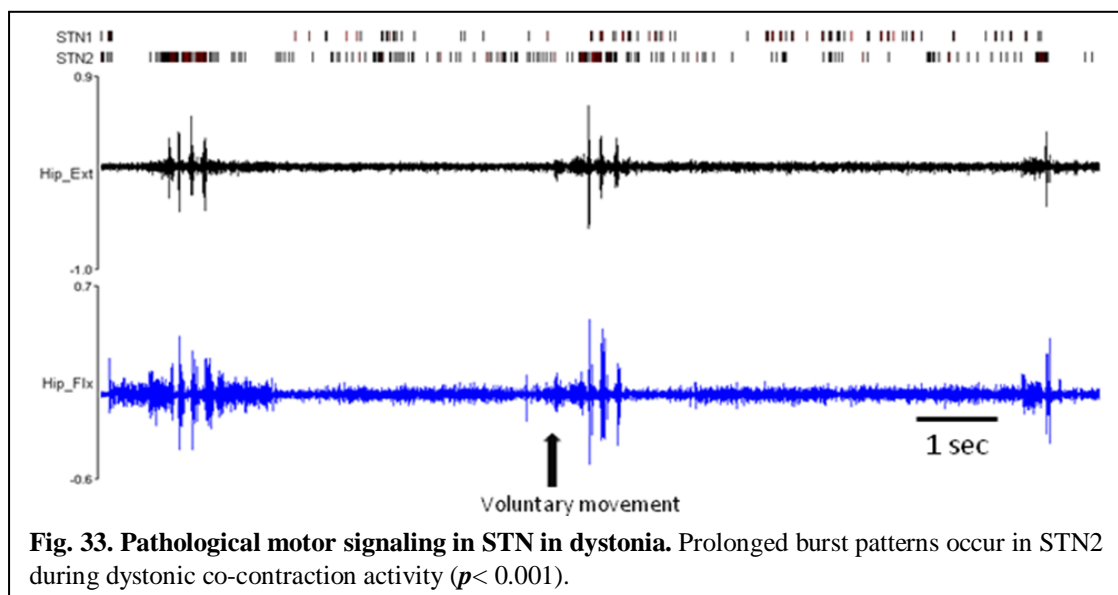

Fig. 33. Pathological motor signaling in STN in dystonia. Prolonged burst patterns occur in STN2 during dystonic co-contraction activity (*p*< 0.001).

epics ($p < 0.001$) (**Fig. 32A**). Two of 3 units that had decrease response to hip movement showed decrease in discharge activity that appeared to correlate throughout EMG epics of voluntary muscle activity ($p < 0.001$) (**Fig. 32B**). In contrast, in dystonic animals, 7 of 13 units that had an increase response to hip movements showed abnormal prolonged burst patterns that were associated with entire EMG epic (**Fig. 33**) ($p < 0.001$). **Among the collected units there wasn't any synchronization of neuronal discharges in STN during co-contraction epics in dystonics animals.**

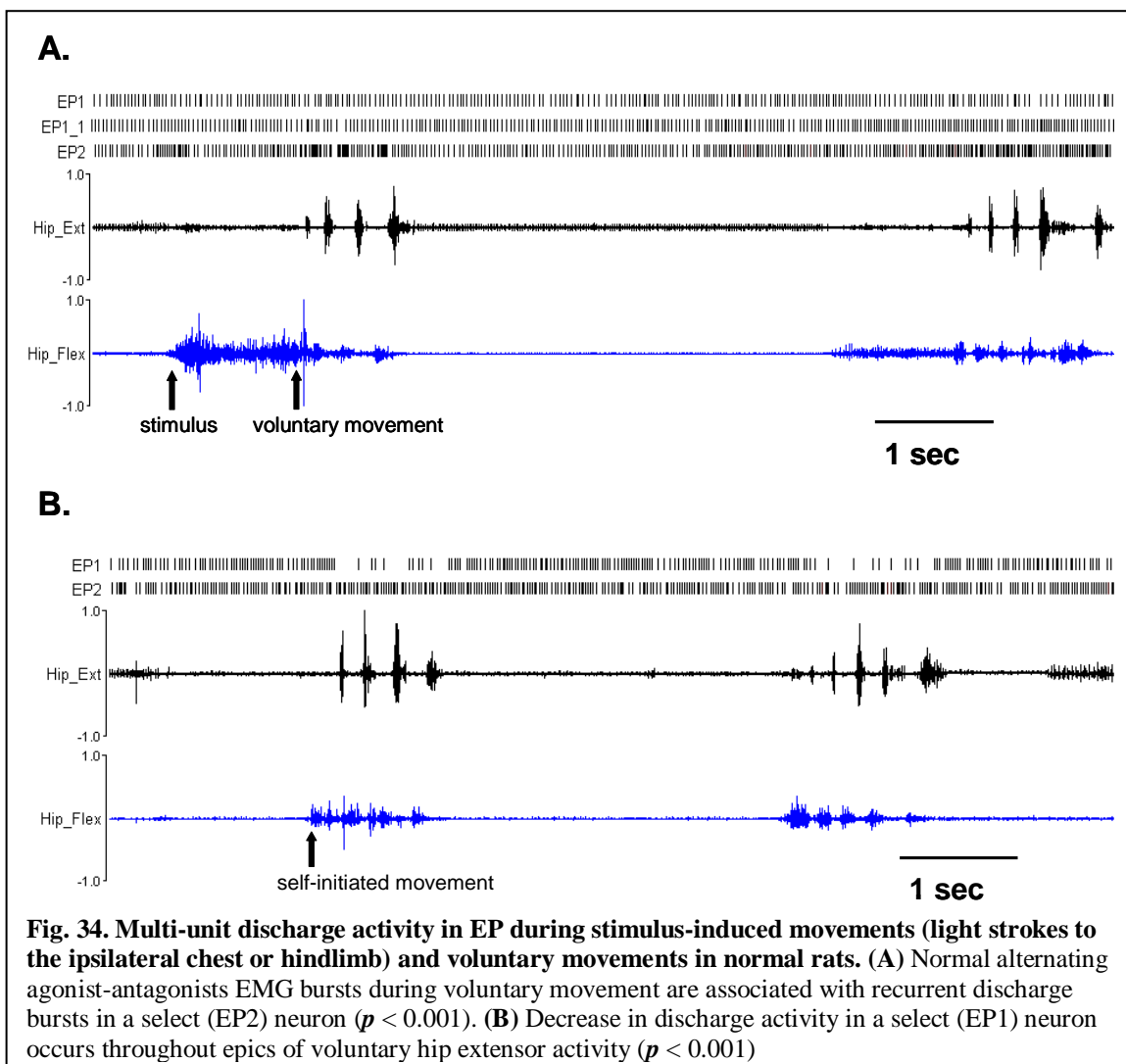### 6.4.3. Entopeduncular nucleus

Activity from 4 normal and 4 dystonic animals in the entopeduncular nucleus was recorded in this study. Of the 4 dystonic animals used in this study, two had a severe dystonia (CS=3.5) while two others had moderate dystonia (C.S=2.5). The patterns and neurophysiological properties of neurons in the entopeduncular nucleus are discussed in detail in **chapter 5**.

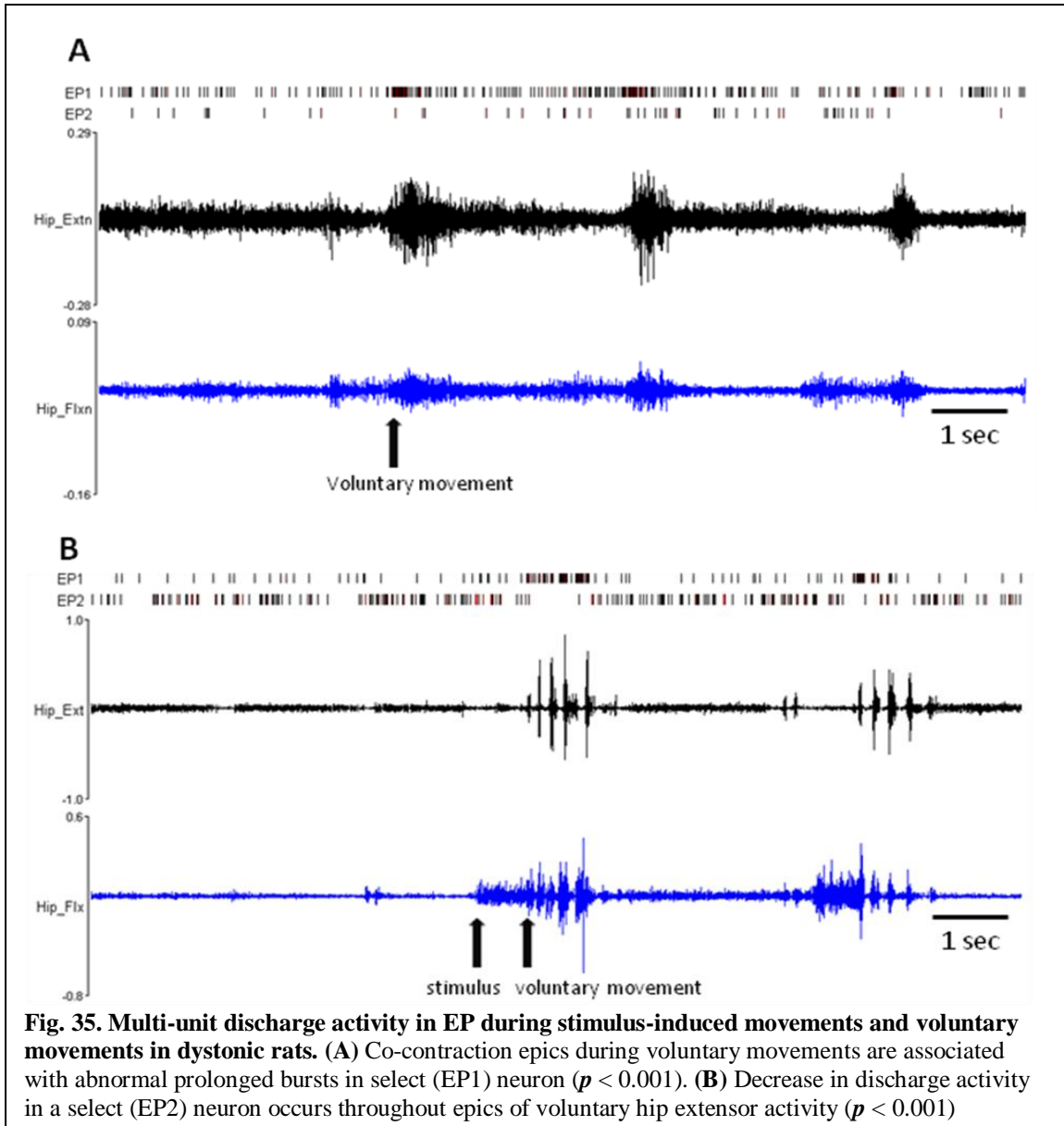### 6.4.3.1. Proportion of movement related cells in EP

The mean firing frequency showed a significant phasic increase during active hip movements in 61% of cells in normals and 59% of cells in dystonics. Phasic decreases during active hip movements were seen in 33% of cells in normals and 37% cells in dystonics. Biphasic responses were found only in 6% of cells in normals and 4% of cells in dystonics.

6.4.3.2. Pattern

In normal animals, 15 of 22 EP units that had an increase response during hip movements showed recurrent discharge burst in EP (**Fig. 34A**) associated with individual EMG epics Seven of 12 units that had decrease response to hip movement showed decrease in discharge activity that appeared to correlate throughout EMG epics of voluntary muscle activity ($p < 0.001$) (**Fig. 34B**). Contrastingly, in dystonic animals, 15 of 17 EP units that had increase response to hip movements showed abnormal prolonged bursting during co-

Fig. 34. Multi-unit discharge activity in EP during stimulus-induced movements (light strokes to the ipsilateral chest or hindlimb) and voluntary movements in normal rats. (**A**) Normal alternating agonist-antagonists EMG bursts during voluntary movement are associated with recurrent discharge bursts in a select (EP2) neuron ($p < 0.001$). (**B**) Decrease in discharge activity in a select (EP1) neuron occurs throughout epics of voluntary hip extensor activity ($p < 0.001$)

Fig. 35. Multi-unit discharge activity in EP during stimulus-induced movements and voluntary movements in dystonic rats. (A) Co-contraction epics during voluntary movements are associated with abnormal prolonged bursts in select (EP1) neuron ($p < 0.001$). (B) Decrease in discharge activity in a select (EP2) neuron occurs throughout epics of voluntary hip extensor activity ($p < 0.001$)
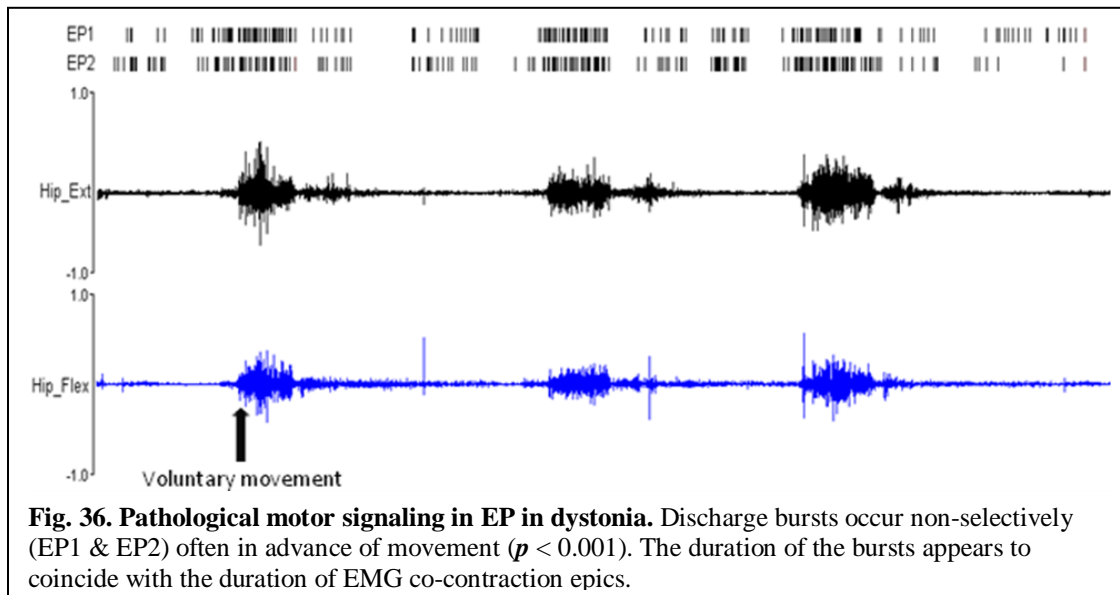
contraction epics suggestive of loss of focused signaling in dystonia (**Fig. 35A**). The

pattern of decrease in EP units during movement epics was similar to that described in

normals (**Fig. 35B**).

Synchronization: In severely dystonic animals (CS=3.5), simultaneously recorded units (4

pairs) showed an abnormal pattern of burst synchronization. (**Fig. 36**). Correlation of

synchronous burst discharge to active dystonic movements was found to be statistically

significant ($p < 0.001$).

Fig. 36. Pathological motor signaling in EP in dystonia. Discharge bursts occur non-selectively (EP1 & EP2) often in advance of movement ($p < 0.001$). The duration of the bursts appears to coincide with the duration of EMG co-contraction epics.

6.4.4. Voluntary vs. externally triggered movements

Fig. 37. **Examples showing differences in movement related neuronal activity during voluntary (A,B) and externally triggered movements (C): A**. Perievent histograms showing significant increase in discharge rate during voluntary movement **B**. Perievent histogram showing significant decrease in discharge rate during voluntary movement **C**. Perievent histogram shows no appreciable change in discharge rate during externally triggered movements in EP. Perievent histograms show the change in neuronal response 0.2 sec before and after the movement across repeated trials (minimum 15). Red line indicates the mean firing rate and yellow lines indicate the 95% confidence intervals. Bin size is 5 ms.
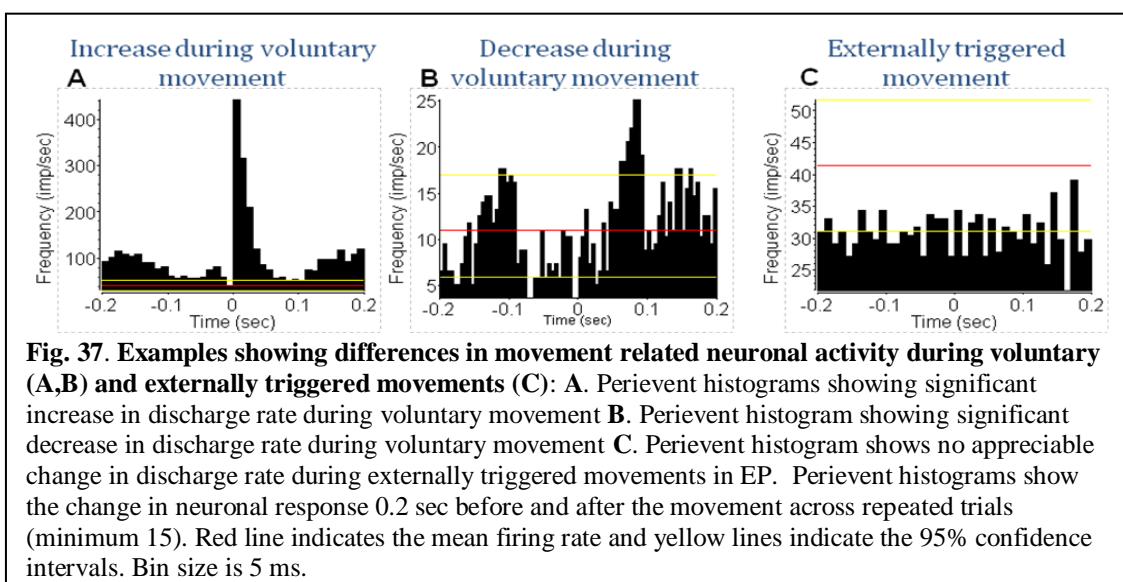
Fig. 37 shows the difference in neuronal responsiveness during voluntary vs externally triggered movements. During voluntary movement epics, hip responsive units showed phasic increases (**Fig. 37A**) or decreases in discharge (**Fig. 37B**) (both $p < 0.001$). In contrast, there was no significant change in the firing rate during externally triggered movements (**Fig. 37C**). These patterns were found in all three nuclei (i.e. GP, STN and EP).

6.5. DISCUSSION:

The aim of the current study was to understand how the brain circuitry controls movements in dystonia. Under awake head-restrained conditions, neuronal activity was collected from up to three microelectrodes inserted in the principal motor regions of the globus pallidus (GP, equivalent to GPe) and entopeduncular nucleus (EP, equivalent to GPi) during voluntary and externally triggered movements in normal and dystonic animals. The key findings were:

- The findings of prolonged burst epics during dystonic movements suggest a mechanism whereby abnormal signaling at the level of individual basal ganglia neurons contributes to the co-contractions in dystonia. Additionally, the preliminary findings of prominent synchronized activity between neurons in GP and EP during movement in dystonic rats suggest that a loss of independent neuronal firing is a fundamental problem in dystonia and likely contributes to the hallmark problems of co-activation and overflow contractions.

- The findings of strong neuronal/EMG correlations selective for non-directed, spontaneous movements in rodents support the contention that the basal ganglia plays a role in voluntary movements, but not in movements directed away from an undesirable stimulus.

- In addition, the novel findings from recording in animals during prolonged, spontaneous movements suggest that during voluntary repetitive movements, discharge bursts in basal ganglia neurons correlate with individual EMG epics

while marked reductions in discharge activity continue throughout entire movement

periods (across multiple EMG epics).

Thus, the present results provide novel insights into the underlying functions of motor

control in basal ganglia and how alterations in basal ganglia neuronal activity produce

dystonia.

6.5.1. Comparison with other studies:

Normals:

In normal animals, the movement related increase in discharge rate in GP (64%) and EP

(61%) were twice as common as movement related decreases. These findings are

consistent with previous studies that have looked upon pallidal influence on movements

(137, 141, 149, 150). In STN, the majority of cells (86%) showed increased discharge

during movement epics. This is consistent with studies in non-human primates (138).

Additionally, the findings that basal ganglia plays a role in self-initiated movements but

not in movements directed away from the undesirable stimulus (pinch) are consistent with

previous reports that suggest a selective involvement of basal ganglia in self-initiated

movements (146, 147).

Dystonics:

The finding that a majority of cells in EP (59%) increase in response to dystonic

movements is contradictory to previous studies which have shown that decreased rates in

GPi are correlated with active dystonic movements (4, 5, 54, 124, 151). One possible

reason for this discrepancy could be that the physiology of kernicterus-induced dystonia

(cell loss, bilirubin toxicity) is different then other types of dystonia. Additionally, the current findings are the first to report synchronization among neurons during co-contraction epics in dystonia. The present findings suggest that a loss of independent basal ganglia neuronal signaling could be fundamental to kernicterus-induced dystonias and contribute to the hallmark problems of co-activation and overflow contractions.

6.5.2. Role of GP and EP in dystonia:

Evidence for increased synchronization during active dystonic movements was found in 5 pairs (n=2 animals) of GP neurons and in 4 pairs (n=2 animals) of EP neurons in animals exhibiting severe dystonia (CS=3.5). The present findings of increased pause synchronization (strong inhibitory drive) in GP and increased burst synchronization (strong excitatory drive) in EP suggest that in dystonia, GP and EP neurons loose their normal ability to discharge independently. It is highly likely that such synchronous discharge within specific population of neurons may critically influence the discharge properties of neurons to which they project. This unwanted pathological synchronization that originates in the GP could trigger similar synchronous activities throughout the thalamocortical circuit (VL thalamus and MC) resulting in involuntary movements and distorted voluntary movements observed in this disorder. This suggests that increased synchronization which has been proposed as a pathological feature in Parkinson disease (152-156) may be important in kernicterus-induced dystonia as well. The present results support a key role in GABAergic GPe-GPi interactions in the pathophysiology of dystonia.

6.5.3 Role of STN in dystonia:

In the current *in vivo* studies, although there were abnormal burst patterns in STN during dystonic epics we failed to observe any synchronization as seen in GP and EP. Thus, based on the current findings the role of STN in dystonia is not clear. In future studies the role of STN in dystonia needs to be further investigated by simultaneously recording in GP, STN and EP *in vivo* to study the influence of STN on EP (**section 7.2**).

6.5.4. Pitfalls in interpretation of results:

Current results have shown evidence for abnormal synchronization during movements only in animals that had severe dystonia (only in few pairs of neurons in both GP and EP). There are two possible theories to explain this. 1) The current understanding of effects of bilirubin toxicity on basal ganglia neurons is poor. It is possible that animals with different clinical severities of dystonia may have different levels of brain damage which inturn could affect the patterned discharge activity in these animals. For example, basal ganglia circuitry in animals with severe dystonia could possibly reorganize by 45 days of age (4 weeks post sulfa injection) with new connections between surviving neurons which could cause abnormal synchronizations (**Section 7.2., page 129**) 2) Alternatively, it is possible that out of the pair of synchronizing units, one unit is related to the proximal joint and other unit is related to the distal joint in the same limb. The reason their firings synchronize is because both the joints are activated at the same time in dystonia.

Additional studies, using animals with clinically different severities of dystonia are required to validate these findings. Also, a non-continuous pattern of burst discharge during movements was observed in GP (6 of 18 units), STN (7 of 27 units) and EP (7 of 22 units) in normal animals. At this stage it is unclear whether the non-continuous bursting patterns in these neurons, occur in response to hip movements or are related to movements of a distal joint in same limb. Future studies, need to record EMG activity from multiple muscles in the same joint to rule out involvement of the distal muscles.

In summary, the preliminary findings of abnormal prolonged bursts and synchronization in key basal ganglia nuclei during active dystonic movements in this study support a critical role for focused motor signaling in the basal ganglia during normal movements. A loss of specificity and abnormal temporal coding of movement-related basal ganglia signaling could be the principal basis for most forms of secondary and potentially primary dystonias.

CHAPTER 7 CONCLUSIONS AND FUTURE WORK

7.1. CONCLUSIONS:

The current project has contributed towards the following:

- Demonstrating the ability to reliably induce stable dystonic features in jaundiced Gunn rats. In future, these techniques will be helpful in developing a chronic model of dystonia (Chapter 2).

- Developing an objective technique using EMG recordings to verify the presence of dystonia in Gunn rats. This study will help to characterize and quantify the abnormal pattern of muscle activation in dystonic animals (Chapter 2).

- Developing a simple, non-invasive measure using gait analysis technique to objectively quantify the severity of dystonia in jaundiced Gunn rats. This study will help provide a sensitive measure of the severity of movement disorder and monitor the improvement post-treatment (Chapter 3).

- Designing and testing a device that allows daily repeat microelectrode studies to be carried out in rodents without the use of anesthesia (Chapter 4).

- Establishing patterns of abnormal neuronal activity that exist in key basal ganglia nuclei in dystonic animals. Knowledge of these patterns will aid future studies while exploring basal ganglia nuclei in dystonic animals. (Chapter 5)

- Providing evidence for abnormal phasic discharge activity during active dystonic movements. Knowledge of these patterns will aid future studies in investigating the role of basal ganglia during normal and pathological motor control (Chapter 6).

Thus, the current project has yielded remarkable findings that can be expected to greatly advance our knowledge about basal ganglia contributions to normal and abnormal pathophysiology and to provide a sound basis for ultimately advancing the treatment of dystonia.

7.2. FUTURE STUDIES:

Based on the current findings the following studies are propose:

Study 1: To understand how abnormal signaling within basal ganglia nuclei triggers dystonia

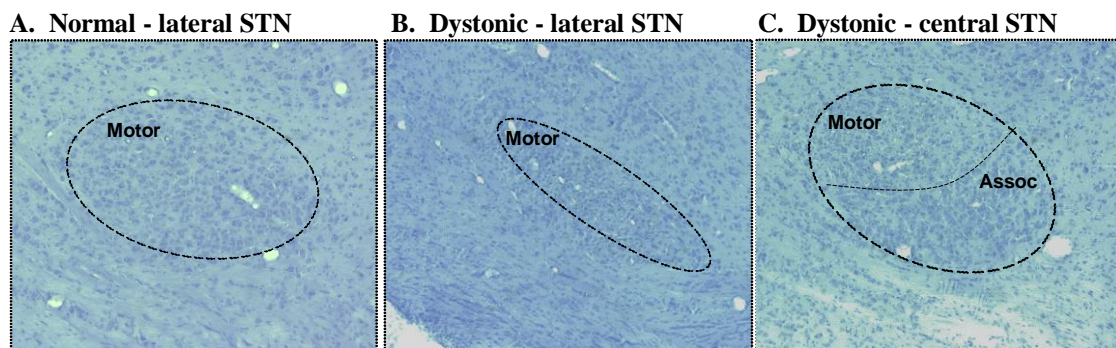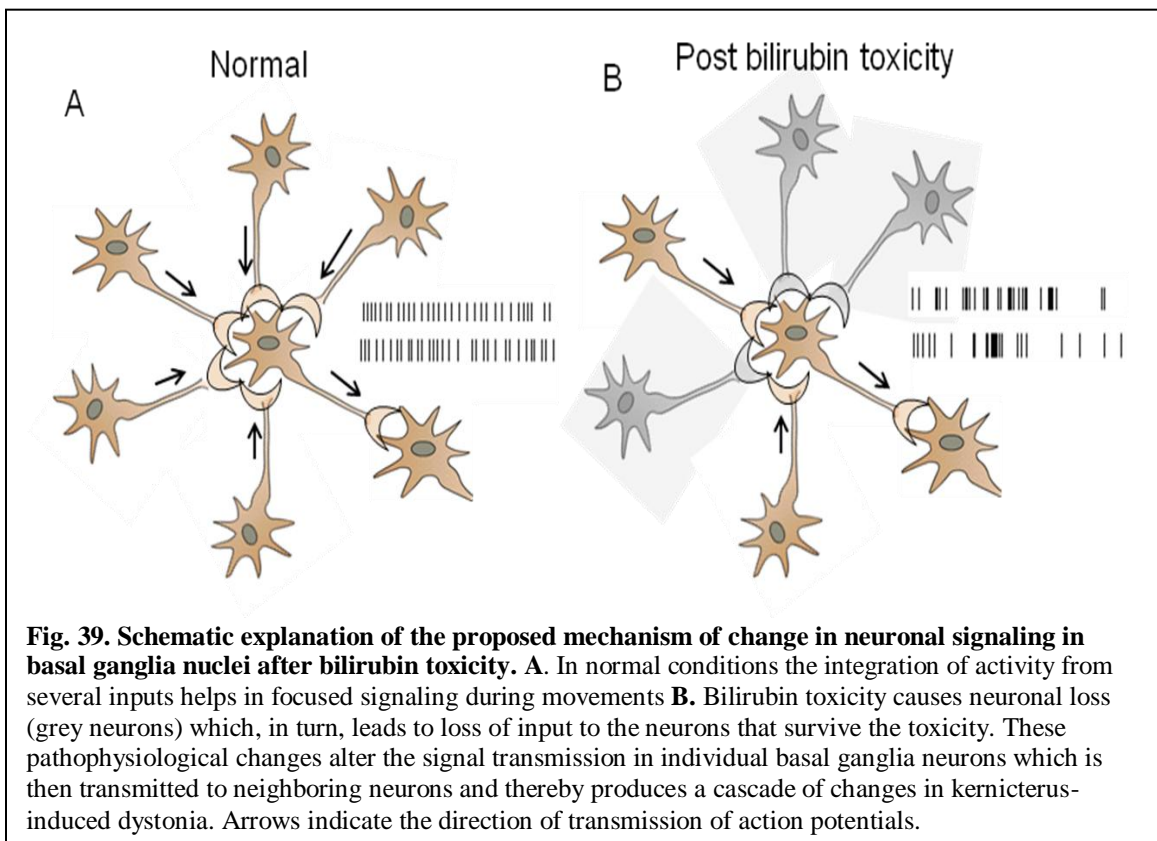Rationale: Injection of sulfadimethoxine in jaundiced Gunn rats results in increase in

Fig. 38. Nissl stained sagittal sections in the STN in a normal (A) and a severely dystonic Gunn rat (B,C). Compared to **A,** a representative section from the lateral motor region in a control Gunn rat, **B,** the lateral region of STN shows marked neuronal loss in the dystonic animal. **C.** A central section in the same dystonic animal shows marked loss in the dorsal motor region **(Motor)** with relatively preserved cells in the ventral associative region **(Assoc).**

concentration of a neurotoxin in the blood, called bilirubin. This bilirubin at high levels enters the brain through the blood-brain barrier and causes cell loss or gliosis most prominently in the basal ganglia and auditory nuclei of the brainstem. Preliminary histological investigations in STN have revealed that neuronal loss was predominantly confined to the dorsolateral (sensorimotor) portion of the nucleus, with approximately 80% loss in this region (**Fig. 38**). The author proposes that this loss of neurons in key basal ganglia nuclei leads to a major disruption in signaling among remaining neurons. A schematic representation of this phenomenon is shown in **Fig. 39**.

In normal animals, individual nuclei consist of a large network of interconnected neurons which acquire and co-ordinate information via transmission of action potentials which allows focused signaling during voluntary movements (**Fig. 39A**). On the other

Fig. 39. Schematic explanation of the proposed mechanism of change in neuronal signaling in basal ganglia nuclei after bilirubin toxicity. A. In normal conditions the integration of activity from several inputs helps in focused signaling during movements **B.** Bilirubin toxicity causes neuronal loss (grey neurons) which, in turn, leads to loss of input to the neurons that survive the toxicity. These pathophysiological changes alter the signal transmission in individual basal ganglia neurons which is then transmitted to neighboring neurons and thereby produces a cascade of changes in kernicterus-induced dystonia. Arrows indicate the direction of transmission of action potentials.

hand, in dystonic animals, bilirubin induced apoptosis causes widespread damage in the motor territories of these nuclei thereby resulting in a loss of input to neurons that survived the toxicity (**Fig. 39B**). These pathophysiological changes lead to a major disruption in normal signaling among remaining neurons. **Thus, a combination of cell loss and abnormal signaling in key basal ganglia nuclei is the principle cause of dystonia in kernicterus.**

Idea behind synchronization

Studies in Chapter 6 have shown evidence for excessively synchronized neuronal discharge activity in severely dystonic animals during active dystonic movements. These findings suggest that abnormally patterned and excessively synchronized neuronal activity could play a crucial role in contributing to the hallmark co-contractions and spread of EMG activation in dystonia. It is conceivable that in dystonic Gunn rats the neuronal loss in key basal ganglia nuclei over time is compensated by reorganization of the neuronal circuitry which, in turn, could lead to new connections between the surviving neurons. This could possibly contribute to uncontrolled increased synchronization during active movements seen in severely dystonic Gunn rats (CS=3.5).

Dellar and colleagues (2006) previously shown that reorganization can occur at any point in time even in the fully developed brain and that the ability to remodel synaptic connections appears to be one of the physiological properties of neurons (157). Similar

phenomena have been observed in the visual cortex of animals who recover neuronal responsiveness after retinal lesions (158-161).

Future studies need to look upon:

- Cellular mechanisms responsible for generation of abnormal discharge patterns within neurons after induction of dystonia.

- Phasic changes in patterned activity in basal ganglia and thalamic nuclei during periods of rest and active dystonic movements using animals with different severities of dystonia.

Study 2: To assess the role of abnormal signaling between nuclei in dystonia

Rationale: Current basal ganglia models predict that alterations in discharge rates within individual basal ganglia and thalamic nuclei play a crucial role in the development of abnormal movements ((53, 54) (**Fig. 3, page 13**). Neurophysiological findings in this project suggest that investigating the phasic alterations in individual nuclei is the key to understanding the brain signaling in dystonia. These unique abnormal discharge patterns within individual neurons in dystonia are likely to have more subtle effects on motor circuitry rather than merely altering the discharge rates. Based on the findings in Chapter 5 and 6 it is hypothesized that the abnormal signaling that originates within individual basal ganglia nuclei causes temporal fluctuations in signal transmission throughout the motor circuitry. Future studies need to be performed by:

- Simultaneously recording from GP, STN and EP to determine how the signal is transmitted within basal ganglia nuclei in dystonia.

- Simultaneously recording in EP, VL thalamus and MC to determine how abnormal signaling within the basal ganglia interferes with signal transmission along the pallidothalamocortical circuitry.

Study 3: To study the acute effects of bilirubin toxicity:

Within hours after sulfa injection (17 days of age) jaundiced animals develop abnormal axial and appendicular posturing. In future studies, neurophysiological experiments outlined in Chapter 5, 6 should be performed in animals at 17 days of age to understand the acute effects of bilirubin toxicity on signaling within basal ganglia neurons. These findings will directly relate to changes occurring in preterm infants immediately following bilirubin toxicity. It is possible that at an early time point (17 days of age) neurons may be affected by the bilirubin toxicity but not be dead. Based on the findings of this study, future experiments could be planned to reverse the effects of bilirubin toxicity to save the 'sick' cells and recover motor function.

7.3. PITFALLS IN INTERPRETATIONS OF RESULTS:

1. Animal recovery from dystonia:

In this project, there were several animals (~20-25%) that initially showed dystonic symptoms (abnormal posturing, jerky limb movements etc) but then later recovered and were completely normal by 45 days of age. The neuronal firing patterns and their EMG features in these animals (n=2) showed no physiological abnormalities. It is conceivable that basal ganglia neurons after bilirubin toxicity don't always die right away and instead become 'sick' and then completely recover after a few weeks. Whether or not animals remain dystonic could depend on the susceptibility of the brain cells to the bilirubin toxicity.

2. Additional symptoms from bilirubin toxicity:

In addition to the abnormal muscle contractions, the bilirubin toxicity in jaundiced Gunn rats also causes balance difficulties, slowness in gait, rigidity, body tremors and periods of hyper excitability. At this stage, it is unclear whether alterations in basal ganglia activity reported in this project are purely due to dystonia or a combination of these symptoms.

3. Failure to see co-contractions in animals with mild dystonia:

We failed to see co-contractions in animals that exhibited mild dystonic symptoms. Prominent co-contractions features in EMG's were only seen in animals had exhibited

moderate to severe symptoms of dystonia (i.e. animals that developed abnormal postures while initiating movements).

Literature Cited

1. Volkmann J, Benecke R. Deep brain stimulation for dystonia: Patient selection and evaluation. Mov Disord. 2002;17 Suppl 3:S112-5.

2. Yanagisawa N, Goto A. Dystonia musculorum deformans. analysis with electromyography. J Neurol Sci. 1971;13(1):39-65.

3. Raike R, Jinnah HA, Hess E. Animal models of generalized dystonia. NeuroRx. 2005;2(3):504-12.

4. Vitek JL, Chockkan V, Zhang JY, Kaneoke Y, Evatt M, DeLong MR, et al. Neuronal activity in the basal ganglia in patients with generalized dystonia and hemiballismus. Ann Neurol. 1999 Jul;46(1):22-35.

5. Zhuang P, Li Y, Hallett M. Neuronal activity in the basal ganglia and thalamus in patients with dystonia. Clin Neurophysiol. 2004;115(11):2542.

6. Jinnah HA, Hess E, Ledoux M, Sharma N, Baxter M, Delong M. Rodent models for dystonia research: Characteristics, evaluation, and utility. Mov Disord. 2005;20(3):283-92.

7. de Carvalho Aguiar PM, Ozelius L. Classification and genetics of dystonia. Lancet Neurol.. 2002;1(5):316-25.

8. Geyer HL, Bressman SB. The diagnosis of dystonia. Lancet Neurol. 2006 Sep;5(9):780-90.

9. Coubes P, Cif L, El Fertit H, Hemm S, Vayssiere N, Serrat S, et al. Electrical stimulation of the globus pallidus internus in patients with primary generalized dystonia: Long-term results. J Neurosurg. 2004 Aug;101(2):189-94.

10. Kupsch A, Kuehn A, Klaffke S, Meissner W, Harnack D, Winter C, et al. Deep brain stimulation in dystonia. J Neurol. 2003 Feb;250 Suppl 1:I47-52.

11. Breakefield XO, Blood AJ, Li Y, Hallett M, Hanson PI, Standaert DG. The pathophysiological basis of dystonias. Nat Rev Neurosci. 2008 Mar;9(3):222-34.

12. Conlee JW, Shapiro SM. Morphological changes in the cochlear nucleus and nucleus of the trapezoid body in gunn rat pups. Hear Res. 1991;57(1):23-30.

13. Practice parameter: Management of hyperbilirubinemia in the healthy term newborn. american academy of pediatrics. provisional committee for quality improvement and subcommittee on hyperbilirubinemia. Pediatrics. 1994;94(4 Pt 1):558-65.

14. Shapiro SM, Nakamura H. Bilirubin and the auditory system. J Perinatol. 2001;21 Suppl 1:S52-5.

15. Shapiro SM, Hecox KE. Development of brainstem auditory evoked potentials in heterozygous and homozygous jaundiced gunn rats. Brain Res. 1988;469(1-2):147-57.

16. Ahlfors CE, Shapiro SM. Auditory brainstem response and unbound bilirubin in jaundiced (jj) gunn rat pups. Biol Neonate. 2001 Aug;80(2):158-62.

17. Shapiro S. Bilirubin toxicity in the developing nervous system. Pediatr Neurol. 2003;29(5):410-21.

18. Ahdab-Barmada M, Moossy J. The neuropathology of kernicterus in the premature neonate: Diagnostic problems. J Neuropathol Exp Neurol. 1984 Jan;43(1):45-56.

19. Ahdab-Barmada M, Moossy J. Kernicterus reexamined. Pediatrics. 1983 Mar;71(3):463-4.

20. Blanc WA, Johnson L. Studies on kernicterus; relationship with sulfonamide intoxication, report on kernicterus in rats with glucuronyl transferase deficiency and review of pathogenesis. J Neuropathol Exp Neurol. 1959 Jan;18(1):165,87; discussion 187-9.

21. Johnson L, Sarmiento F, Blanc WA, Day R. Kernicterus in rats with an inherited deficiency of glucuronyl transferase. AMA J Dis Child. 1959 May;97(5, Part 1):591-608.

22. Jew JY, Williams TH. Ultrastructural aspects of bilirubin encephalopathy in cochlear nuclei of the gunn rat. J Anat. 1977 Dec;124(Pt 3):599-614.

23. Jew JY, Sandquist D. CNS changes in hyperbilirubinemia. functional implications. Arch Neurol. 1979 Mar;36(3):149-54.

24. Rose AL, Wisniewski H. Acute bilirubin encephalopathy induced with sulfadimethoxine in gunn rats. J Neuropathol Exp Neurol. 1979;38(2):152-64.

25. Schutta HS, Johnson L. Bilirubin encephalopathy in the gunn rat: A fine structure study of the cerebellar cortex. J Neuropathol Exp Neurol. 1967 Jul;26(3):377-96.

26. Schutta HS, Johnson L, Neville HE. Mitochondrial abnormalities in bilirubin encephalopathy. J Neuropathol Exp Neurol. 1970 Apr;29(2):296-305.

27. Schutta HS, Johnson L. Electron microscopic observations on acute bilirubin encephalopathy in gunn rats induced by sulfadimethoxine. Lab Invest. 1971 Jan;24(1):82-9.

28. Schutta HS, L. Johnson. Clinical signs and morphologic abnormalities in gunn rats treated with sulfadimethoxine. J Pediatr. 1969;75:1070-9.

29. Shapiro SM, Bhutani VK, Johnson L. Hyperbilirubinemia and kernicterus. Clin Perinatol. 2006 Jun;33(2):387-410.

30. Shapiro SM. Brainstem auditory evoked potentials in an experimental model of bilirubin neurotoxicity. Clin Pediatr (Phila). 1994 Aug;33(8):460-7.

31. Shapiro SM. Somatosensory and brainstem auditory evoked potentials in the gunn rat model of acute bilirubin neurotoxicity. Pediatr Res. 2002 Dec;52(6):844-9.

32. Shapiro SM, Hecox KE. Brain stem auditory evoked potentials in jaundiced gunn rats. Ann Otol Rhinol Laryngol. 1989;98(4):308-17.

33. Shapiro SM, Conlee JW. Brainstem auditory evoked potentials correlate with morphological changes in gunn rat pups. Hear Res. 1991 Dec;57(1):16-22.

34. Shapiro SM. Brainstem auditory evoked potentials in an experimental model of bilirubin neurotoxicity. Clin Pediatr. 1994;33(8):460-7.

35. Shapiro SM. Reversible brainstem auditory evoked potential abnormalities in jaundiced gunn rats given sulfonamide. Pediatr Res. 1993;34(5):629-33.

36. Chaniary K, Baron M, Rice A, Wetzel P, Shapiro S. Electromyographic characterization in an animal model of dystonia. Mov Disord. 2008;23(8):1122-9.

37. Strebel, L. and G.B. Odell. Bilirubin uridine disphosphoglucuronyltransferase in rat liver microsomes: Genetic variation and maturation. Pediatr Res. 1971;5:548-59.

38. Cummings JL. Frontal-subcortical circuits and human behavior. Arch Neurol. 1993;50(8):873-80.

39. Bar-Gad I, Morris G, Bergman H. Information processing, dimensionality reduction and reinforcement learning in the basal ganglia. Prog Neurobiol. 2003;71(6):439-73.

40. Hamani C, Lozano A. Physiology and pathophysiology of parkinson's disease. Ann N Y Acad Sci. 2003;991:15-21.

41. Parent A, Hazrati LN. Functional anatomy of the basal ganglia. I. the cortico-basal ganglia-thalamo-cortical loop. Brain Res Rev. 1995;20(1):91-127.

42. Plenz D KS. A basal ganglia pacemaker formed by the subthalamic nucleus and external globuspallidus. Nature. 1999;400(6745):677.

43. Wichmann T, Bergman H, DeLong MR. The primate subthalamic nucleus. I. functional properties in intact animals. J Neurophysiol. 1994;72(2):494-506.

44. Urbain N, Gervasoni D, Soulire F, Lobo L, Rentro N, Windels F, et al. Unrelated course of subthalamic nucleus and globus pallidus neuronal activities across vigilance states in the rat. Eur J Neurosci. 2000;12(9):3361-74.

45. Soares J, Kliem M, Betarbet R, Greenamyre JT, Yamamoto B, Wichmann T. Role of external pallidal segment in primate parkinsonism: Comparison of the effects of 1-methyl-4-phenyl-1,2,3,6-tetrahydropyridine-induced parkinsonism and lesions of the external pallidal segment. J Neurosci. 2004;24(29):6417-26.

46. Matsumura M, Kojima J, Gardiner TW, Hikosaka O. Visual and oculomotor functions of monkey subthalamic nucleus. J Neurophysiol. 1992;67(6):1615-32.

47. Hassani OK, Mouroux M, Fger J. Increased subthalamic neuronal activity after nigral dopaminergic lesion independent of disinhibition via the globus pallidus. Neuroscience. 1996;72(1):105-15.

48. Georgopoulos AP, DeLong MR, Crutcher MD. Relations between parameters of step-tracking movements and single cell discharge in the globus pallidus and subthalamic nucleus of the behaving monkey. J Neurosci. 1983;3(8):1586-98.

49. Bergman H, Wichmann T, Karmon B, DeLong MR. The primate subthalamic nucleus. II. neuronal activity in the MPTP model of parkinsonism. J Neurophysiol. 1994 Aug;72(2):507-20.

50. Fujimoto K, Kita H. Response characteristics of subthalamic neurons to the stimulation of the sensorimotor cortex in the rat. Brain Res. 1993;609(1-2):185-92.

51. Wichmann T, Kliem M, Soares J. Slow oscillatory discharge in the primate basal ganglia. J Neurophysiol. 2002;87(2):1145-8.

52. Parent A, Cicchetti F. The current model of basal ganglia organization under scrutiny. Mov Disord. 1998;13(2):199-202.

53. Albin RL, Young AB, Penney JB. The functional anatomy of basal ganglia disorders. Trends Neurosci. 1989 Oct;12(10):366-75.

54. DeLong MR. Primate models of movement disorders of basal ganglia origin. Trends Neurosci. 1990 Jul;13(7):281-5.

55. Hutchison WD, Lang AE, Dostrovsky JO, Lozano AM. Pallidal neuronal activity: Implications for models of dystonia. Ann Neurol. 2003 Apr;53(4):480-8.

56. Loscher W, Fisher JE,Jr, Schmidt D, Fredow G, Honack D, Iturrian WB. The sz mutant hamster: A genetic model of epilepsy or of paroxysmal dystonia? Mov Disord. 1989;4(3):219-32.

57. Gernert M, Richter A, Loscher W. In vivo extracellular electrophysiology of pallidal neurons in dystonic and nondystonic hamsters. J Neurosci Res. 1999 Sep 15;57(6):894-905.

58. Gernert M, Bennay M, Fedrowitz M, Rehders JH, Richter A. Altered discharge pattern of basal ganglia output neurons in an animal model of idiopathic dystonia. J Neurosci. 2002 Aug 15;22(16):7244-53.

59. Gernert M, Hamann M, Bennay M, Loscher W, Richter A. Deficit of striatal parvalbumin-reactive GABAergic interneurons and decreased basal ganglia output in a genetic rodent model of idiopathic paroxysmal dystonia. J Neurosci. 2000 Sep 15;20(18):7052-8.

60. Nobrega JN, Richter A, Tozman N, Jiwa D, Lscher W. Quantitative autoradiography reveals regionally selective changes in dopamine D1 and D2 receptor binding in the genetically dystonic hamster. Neuroscience. 1996;71(4):927-37.

61. LeDoux MS, Lorden JF, Ervin JM. Cerebellectomy eliminates the motor syndrome of the genetically dystonic rat. Exp Neurol. 1993;120(2):302-10.

62. Lorden JF, McKeon TW, Baker HJ, Cox N, Walkley SU. Characterization of the rat mutant dystonic (dt): A new animal model of dystonia musculorum deformans. J Neurosci. 1984 Aug;4(8):1925-32.

63. Lorden JF, Oltmans GA, Stratton S, Mays LE. Neuropharmacological correlates of the motor syndrome of the genetically dystonic (dt) rat. Adv Neurol. 1988;50:277-97.

64. Perlmutter JS, Tempel LW, Black KJ, Parkinson D, Todd RD. MPTP induces dystonia and parkinsonism. clues to the pathophysiology of dystonia. Neurology. 1997;49(5):1432-8.

65. Byl NN, Merzenich MM, Jenkins WM. A primate genesis model of focal dystonia and repetitive strain injury: I. learning-induced dedifferentiation of the representation of the hand in the primary somatosensory cortex in adult monkeys. Neurology. 1996;47(2):508-20.

66. Grosse P, Edwards M, Tijssen MA, Schrag A, Lees AJ, Bhatia KP, et al. Patterns of EMG-EMG coherence in limb dystonia. Mov Disord. 2004 Jul;19(7):758-69.

67. Deuschl G, Heinen F, Kleedorfer B, Wagner M, Lcking CH, Poewe W. Clinical and polymyographic investigation of spasmodic torticollis. J Neurol. 1992;239(1):9-15.

68. Dressler D. Electromyographic evaluation of cervical dystonia for planning of botulinum toxin therapy. Eur J Neurol. 2000;7(6):713-8.

69. Tijssen MAJ, Mnchau A, Marsden J, Lees A, Bhatia K, Brown P. Descending control of muscles in patients with cervical dystonia. Mov Disord. 2002;17(3):493-500.

70. Shaia W, Shapiro S, Heller A, Galiani D, Sismanis A, Spencer R. Immunohistochemical localization of calcium-binding proteins in the brainstem vestibular nuclei of the jaundiced gunn rat. Hear Res. 2002;173(1-2):82-90.

71. Wang SY, Liu X, Yianni J, Tailor JK, Aziz TZ, Stein JF. Detecting functional coupling between electromyogram and local field potentials in dystonia using discrete wavelet transform and coherence estimation. Proceedings of the 1st International IEEE EMBS. 2003.

72. Wang S, Liu X, Yianni J, Aziz T, Stein J. Extracting burst and tonic components from surface electromyograms in dystonia using adaptive wavelet shrinkage. J Neurosci Methods. 2004;139(2):177-84.

73. Mallat SG. A theory for multiresolution signal decomposition: The wavelet representation. IEEE Trans Pattern Anal Mach Intell. 1989;11:674-93.

74. Polikar R. the wavelet tutorial http://users.rowan.edu/~polikar/WAVELETS/ WTtutorial.html.

75. Myers LJ, Lowery M, O'Malley M, Vaughan CL, Heneghan C, St Clair Gibson A, et al. Rectification and non-linear pre-processing of EMG signals for cortico-muscular analysis. J Neurosci Methods. 2003;124(2):157-65.

76. Carter GC. Coherence and time delay estimation. Proceedings of the IEEE. 1987;75:236-55.

77. Bazzucchi I, Sbriccoli P, Marzattinocci G, Felici F. Coactivation of the elbow antagonist muscles is not affected by the speed of movement in isokinetic exercise. Muscle Nerve. 2006;33(2):191-9.

78. Malfait N, Sanger T. Does dystonia always include co-contraction? A study of unconstrained reaching in children with primary and secondary dystonia. Exp Brain Res. 2007;176(2):206-16.

79. Fahn S. Concept and classification of dystonia. Adv Neurol. 1988;50:1-8.

80. Snijders A, van de Warrenburg B, Giladi N, Bloem B. Neurological gait disorders in elderly people: Clinical approach and classification. Lancet Neurol. 2007;6(1):63-74.

81. Watts RL KW. Movement disorders: Neurologic principles and practice. In: second ed. McGraw-Hill; 2004.

82. Vitek JL, Giroux M. Physiology of hypokinetic and hyperkinetic movement disorders: Model for dyskinesia. Ann Neurol. 2000 Apr;47(4 Suppl 1):S131-40.

83. Zhang JG, Zhang K, Wang ZC, Ge M, Ma Y. Deep brain stimulation in the treatment of secondary dystonia. Chin Med J (Engl). 2006 Dec 20;119(24):2069-74.

84. Richter A, Lscher W. Pathology of idiopathic dystonia: Findings from genetic animal models. Prog Neurobiol. 1998;54(6):633-77.

85. Jinnah HA, Sepkuty JP, Ho T, Yitta S, Drew T, Rothstein JD, et al. Calcium channel agonists and dystonia in the mouse. Mov Disord. 2000;15(3):542-51.

86. LeDoux MS, Lorden JF, Meinzen-Derr J. Selective elimination of cerebellar output in the genetically dystonic rat. Brain Res. 1995;697(1-2):91-103.

87. Dang M, Yokoi F, Pence M, Li Y. Motor deficits and hyperactivity in Dyt1 knockdown mice. Neurosci Res. 2006;56(4):470-4.

88. Cheng H, Almstrm S, Gimnez-Llort L, Chang R, Ogren SO, Hoffer B, et al. Gait analysis of adult paraplegic rats after spinal cord repair. Exp Neurol. 1997;148(2):544-57.

89. Metz GA, Merkler D, Dietz V, Schwab ME, Fouad K. Efficient testing of motor function in spinal cord injured rats. Brain Res. 2000 Nov 17;883(2):165-77.

90. Yu P, Matloub HS, Sanger JR, Narini P. Gait analysis in rats with peripheral nerve injury. Muscle Nerve. 2001;24(2):231-9.

91. Amende I, Kale A, McCue S, Glazier S, Morgan J, Hampton T. Gait dynamics in mouse models of parkinson's disease and huntington's disease. J Neuroeng Rehabil. 2005;2:20-26.

92. de Medinaceli L, Freed WJ, Wyatt RJ. An index of the functional condition of rat sciatic nerve based on measurements made from walking tracks. Exp Neurol. 1982;77(3):634-43.

93. Kunkel-Bagden E, Dai HN, Bregman BS. Recovery of function after spinal cord hemisection in newborn and adult rats: Differential effects on reflex and locomotor function. Exp Neurol. 1992;116(1):40-51.

94. Nessler J, De Leon R, Sharp K, Kwak E, Minakata K, Reinkensmeyer D. Robotic gait analysis of bipedal treadmill stepping by spinal contused rats: Characterization of intrinsic recovery and comparison with BBB. J Neurotrauma. 2006;23(6):882-96.

95. Dorner H, Otte P, Platt D. Training influence on age-dependent changes in the gait of rats. Gerontology. 1996;42(1):7-13.

96. Hicks SP, D'Amato CJ. Motor-sensory cortex-corticospinal system and developing locomotion and placing in rats. Am J Anat. 1975;143(1):1-42.

97. Hamm RJ, Pike BR, O'Dell DM, Lyeth BG, Jenkins LW. The rotarod test: An evaluation of its effectiveness in assessing motor deficits following traumatic brain injury. J Neurotrauma. 1994;11(2):187-96.

98. Howard CS, Blakeney DC, Medige J, Moy OJ, Peimer CA. Functional assessment in the rat by ground reaction forces. J Biomech. 2000;33(6):751-7.

99. Ballermann M, Tse ADY, Misiaszek J, Fouad K. Adaptations in the walking pattern of spinal cord injured rats. J Neurotrauma. 2006;23(6):897-907.

100. Scholle HC, Schumann NP, Biedermann F, Stegeman DF, Grassme R, Roeleveld K, et al. Spatiotemporal surface EMG characteristics from rat triceps brachii muscle during treadmill locomotion indicate selective recruitment of functionally distinct muscle regions. Exp Brain Res. 2001;138(1):26-36.

101. Dubost V, Kressig R, Gonthier R, Herrmann F, Aminian K, Najafi B, et al. Relationships between dual-task related changes in stride velocity and stride time variability in healthy older adults. Hum Movement Sci. 2006;25(3):372-82.

102. Comella C, Leurgans S, Wuu J, Stebbins G, Chmura T. Rating scales for dystonia: A multicenter assessment. Mov Disord. 2003;18(3):303-12.

103. Wilson CJ, Kawaguchi Y. The origins of two-state spontaneous membrane potential fluctuations of neostriatal spiny neurons. J Neurosci. 1996;16(7):2397-410.

104. Goto Y, O'Donnell P. Network synchrony in the nucleus accumbens in vivo. J Neurosci. 2001;21(12):4498-504.

105. Kasanetz F, Riquelme L, O'Donnell P, Murer MG. Turning off cortical ensembles stops striatal up states and elicits phase perturbations in cortical and striatal slow oscillations in rat in vivo. J Physiol (Lond). 2006;577(1):97-113.

106. Nicoll RA, Madison DV. General anesthetics hyperpolarize neurons in the vertebrate central nervous system. Science. 1982;217(4564):1055-7.

107. Alkire M, Hudetz A, Tononi G. Consciousness and anesthesia. Science. 2008;322(5903):876-80.

108. Schonewille M, Khosrovani S, Winkelman BHJ, Hoebeek F, De Jeu MTG, Larsen I, et al. Purkinje cells in awake behaving animals operate at the upstate membrane potential. Nat Neurosci. 2006;9(4):459-61.

109. Korshunov VA. Miniature microdrive for extracellular recording of neuronal activity in freely moving animals. J Neurosci Methods. 1995;57(1):77-80.

110. Jackson A, Fetz E. Compact movable microwire array for long-term chronic unit recording in cerebral cortex of primates. J Neurophysiol. 2007;98(5):3109-18.

111. Eliades S, Wang X. Chronic multi-electrode neural recording in free-roaming monkeys. J Neurosci Methods. 2008;172(2):201-14.

112. Pager J. A removable head-mounted microdrive for unit recording in the free-behaving rat. Physiol Behav. 1984;33(5):843-8.

113. Parry TJ, McElligott JG. A method for restraining awake rats using head immobilization. Physiol Behav. 1993;53(5):1011-5.

114. Soulire F, Urbain N, Gervasoni D, Schmitt P, Guillemort C, Fort P, et al. Single-unit and polygraphic recordings associated with systemic or local pharmacology: A multi-purpose stereotaxic approach for the awake, anaesthetic-free, and head-restrained rat. J Neurosci Res. 2000;61(1):88-100.

115. Heck D, Kmmell F, Thach W, Aertsena A. Dynamic correlation of neuronal activity in rat cerebellar cortex modulated by behavior. Ann N Y Acad Sci. 2002;978:156-63.

116. Fà M, Mereu G, Ghiglieri V, Meloni A, Salis P, Gessa G. Electrophysiological and pharmacological characteristics of nigral dopaminergic neurons in the conscious, head-restrained rat. Synapse. 2003;48(1):1-9.

117. Paxinos G WC. The rat brain in stereotaxic coordinates. San Diego, CA: Academic Press; 1998.

118. Bryant J, Roy S, Heck D. A technique for stereotaxic recordings of neuronal activity in awake, head-restrained mice. J Neurosci Methods. 2009;178(1):75-9.

119. Mahon S, Vautrelle N, Pezard L, Slaght S, Deniau J, Chouvet G, et al. Distinct patterns of striatal medium spiny neuron activity during the natural sleep-wake cycle. J Neurosci. 2006;26(48):12587-95.

120. Lee MS, Marsden CD. Movement disorders following lesions of the thalamus or subthalamic region. Mov Disord. 1994 Sep;9(5):493-507.

121. Merello M, Cerquetti D, Cammarota A, Tenca E, Artes C, Antico J, et al. Neuronal globus pallidus activity in patients with generalised dystonia. Mov Disord. 2004 May;19(5):548-54.

122. Vitek JL. Surgery for dystonia. Neurosurg Clin N Am. 1998 Apr;9(2):345-66.

123. Sanghera MK, Grossman RG, Kalhorn CG, Hamilton WJ, Ondo WG, Jankovic J. Basal ganglia neuronal discharge in primary and secondary dystonia in patients undergoing pallidotomy. Neurosurgery. 2003 Jun;52(6):1358,70; 1370-3.

124. Starr PA, Rau GM, Davis V, Marks WJ,Jr, Ostrem JL, Simmons D, et al. Spontaneous pallidal neuronal activity in human dystonia: Comparison with parkinson's disease and normal macaque. J Neurophysiol. 2005 Jun;93(6):3165-76.

125. Schrock L, Ostrem J, Turner R, Shimamoto S, Starr P. The subthalamic nucleus in primary dystonia: Single-unit discharge characteristics. J Neurophysiol. 2009;102(6):3740-52.

126. Lenz FA, Jaeger CJ, Seike MS, Lin YC, Reich SG, DeLong MR, et al. Thalamic single neuron activity in patients with dystonia: Dystonia-related activity and somatic sensory reorganization. J Neurophysiol. 1999 Nov;82(5):2372-92.

127. Bhatia KP. Familial (idiopathic) paroxysmal dyskinesias: An update. Semin Neurol. 2001;21(1):69-74.

128. Richter A, Loscher W. Alterations in pharmacological sensitivity of GABAergic but not dopaminergic and glutamatergic systems during ontogenesis in dystonic mutant hamsters. Eur J Pharmacol. 1993 Jan 26;231(1):111-9.

129. Chaniary K, Baron M, Rice A, Wetzel P, Ramakrishnan V, Shapiro S. Quantification of gait in dystonic gunn rats. J Neurosci Methods. 2009;180(2):273-7.

130. Lewicki MS. A review of methods for spike sorting: The detection and classification of neural action potentials. Network. 1998 Nov;9(4):R53-78.

131. Kaneoke Y, Vitek JL. Burst and oscillation as disparate neuronal properties. J Neurosci Methods. 1996 Oct;68(2):211-23.

132. Legendy CR, Salcman M. Bursts and recurrences of bursts in the spike trains of spontaneously active striate cortex neurons. J Neurophysiol. 1985 Apr;53(4):926-39.

133. Jackson ME, Homayoun H, Moghaddam B. NMDA receptor hypofunction produces concomitant firing rate potentiation and burst activity reduction in the prefrontal cortex. Proc Natl Acad Sci U S A. 2004 Jun 1;101(22):8467-72.

134. Kita H, Chiken S, Tachibana Y, Nambu A. Serotonin modulates pallidal neuronal activity in the awake monkey. J Neurosci. 2007;27(1):75-83.

135. Wichmann T, Soares J. Neuronal firing before and after burst discharges in the monkey basal ganglia is predictably patterned in the normal state and altered in parkinsonism. J Neurophysiol. 2006;95(4):2120-33.

136. Lenz FA, Suarez JI, Metman LV, Reich SG, Karp BI, Hallett M, et al. Pallidal activity during dystonia: Somatosensory reorganisation and changes with severity. J Neurol Neurosurg Psychiatry. 1998 Nov;65(5):767-70.

137. DeLong MR. Activity of pallidal neurons during movement. J Neurophysiol. 1971;34(3):414-27.

138. Wichmann T, Bergman H, DeLong MR. The primate subthalamic nucleus. III. changes in motor behavior and neuronal activity in the internal pallidum induced by subthalamic inactivation in the MPTP model of parkinsonism. J Neurophysiol. 1994;72(2):521-30.

139. Alexander GE, Crutcher MD. Neural representations of the target (goal) of visually guided arm movements in three motor areas of the monkey. J Neurophysiol. 1990;64(1):164-78.

140. Hamada I, DeLong MR, Mano N. Activity of identified wrist-related pallidal neurons during step and ramp wrist movements in the monkey. J Neurophysiol. 1990;64(6):1892-906.

141. Turner RS, Anderson ME. Pallidal discharge related to the kinematics of reaching movements in two dimensions. J Neurophysiol. 1997;77(3):1051-74.

142. Turner R, Anderson M. Context-dependent modulation of movement-related discharge in the primate globus pallidus. J Neurosci. 2005;25(11):2965-76.

143. Mink JW, Thach WT. Basal ganglia motor control. II. late pallidal timing relative to movement onset and inconsistent pallidal coding of movement parameters. J Neurophysiol. 1991;65(2):301-29.

144. Mink JW, Thach WT. Basal ganglia motor control. III. pallidal ablation: Normal reaction time, muscle cocontraction, and slow movement. J Neurophysiol. 1991;65(2):330-51.

145. Brotchie P, Iansek R, Horne MK. Motor function of the monkey globus pallidus. 1. neuronal discharge and parameters of movement. Brain. 1991;114(4):1667-83.

146. van Donkelaar P, Stein JF, Passingham RE, Miall RC. Neuronal activity in the primate motor thalamus during visually triggered and internally generated limb movements. J Neurophysiol. 1999;82(2):934-45.

147. Cunnington R, Windischberger C, Deecke L, Moser E. The preparation and execution of self-initiated and externally-triggered movement: A study of event-related fMRI. Neuroimage. 2002;15(2):373-85.

148. Kimura M, Aosaki T, Hu Y, Ishida A, Watanabe K. Activity of primate putamen neurons is selective to the mode of voluntary movement: Visually guided, self-initiated or memory-guided. Exp Brain Res. 1992;89(3):473-7.

149. DeLong MR, Crutcher MD, Georgopoulos AP. Primate globus pallidus and subthalamic nucleus: Functional organization. J Neurophysiol. 1985;53(2):530-43.

150. Anderson ME, Horak FB. Influence of the globus pallidus on arm movements in monkeys. III. timing of movement-related information. J Neurophysiol. 1985;54(2):433-48.

151. Hashimoto T, Tada T, Nakazato F, Maruyama T, Katai S, Izumi Y, et al. Abnormal activity in the globus pallidus in off-period dystonia. Ann Neurol. 2001;49(2):242-5.

152. Bergman H, Feingold A, Nini A, Raz A, Slovin H, Abeles M, et al. Physiological aspects of information processing in the basal ganglia of normal and parkinsonian primates. Trends Neurosci. 1998;21(1):32-8.

153. Levy R, Hutchison WD, Lozano AM, Dostrovsky JO. Synchronized neuronal discharge in the basal ganglia of parkinsonian patients is limited to oscillatory activity. J Neurosci. 2002 Apr 1;22(7):2855-61.

154. Levy R, Hutchison WD, Lozano AM, Dostrovsky JO. High-frequency synchronization of neuronal activity in the subthalamic nucleus of parkinsonian patients with limb tremor. J Neurosci. 2000 Oct 15;20(20):7766-75.

155. Nini A, Feingold A, Slovin H, Bergman H. Neurons in the globus pallidus do not show correlated activity in the normal monkey, but phase-locked oscillations appear in the MPTP model of parkinsonism. J Neurophysiol. 1995;74(4):1800-5.

156. Raz A, Feingold A, Zelanskaya V, Vaadia E, Bergman H. Neuronal synchronization of tonically active neurons in the striatum of normal and parkinsonian primates. J Neurophysiol. 1996;76(3):2083-8.

157. Deller T, Haas C, Freiman T, Phinney A, Jucker M, Frotscher M. Lesion-induced axonal sprouting in the central nervous system. Adv Exp Med Biol. 2006;557:101-21.

158. Kaas JH, Krubitzer LA, Chino YM, Langston AL, Polley EH, Blair N. Reorganization of retinotopic cortical maps in adult mammals after lesions of the retina. Science. 1990;248(4952):229-31.

159. Gilbert CD, Wiesel TN. Receptive field dynamics in adult primary visual cortex. Nature. 1992;356(6365):150-2.

160. Darian-Smith C, Gilbert CD. Axonal sprouting accompanies functional reorganization in adult cat striate cortex. Nature. 1994;368(6473):737-40.

161. Calford M, Wright L, Metha A, Taglianetti V. Topographic plasticity in primary visual cortex is mediated by local corticocortical connections. J Neurosci 2003;23(16):6434-42.

## **APPENDIX A**

Matlab code for Discrete Wavelet Transform analysis:

```
load nj1a.txt               % load first 30 sec of data into matlab
ampext1=nj1a(:,2)           % select extension amplitudes from file
ampflx1=nj1a(:,4)           % select flexion amplitudes from file
save ampext1 ampext1        % save
save ampflx1 ampflx1
load nj1b.txt               % load the next 30 sec of data into matlab
ampext2
ampext2=nj1b(:,2)
ampflx2=nj1b(:,4)
save ampext2 ampext2
save ampflx2 ampflx2
load nj1c.txt               %load the next 30 sec of data into matlab
ampext3=nj1c(:,2)
ampflx3=nj1c(:,4)
save ampext3 ampext3
save ampflx3 ampflx3
wavemenu
% The wavelet toolbox will appear. Select File>>1D DWT.
```
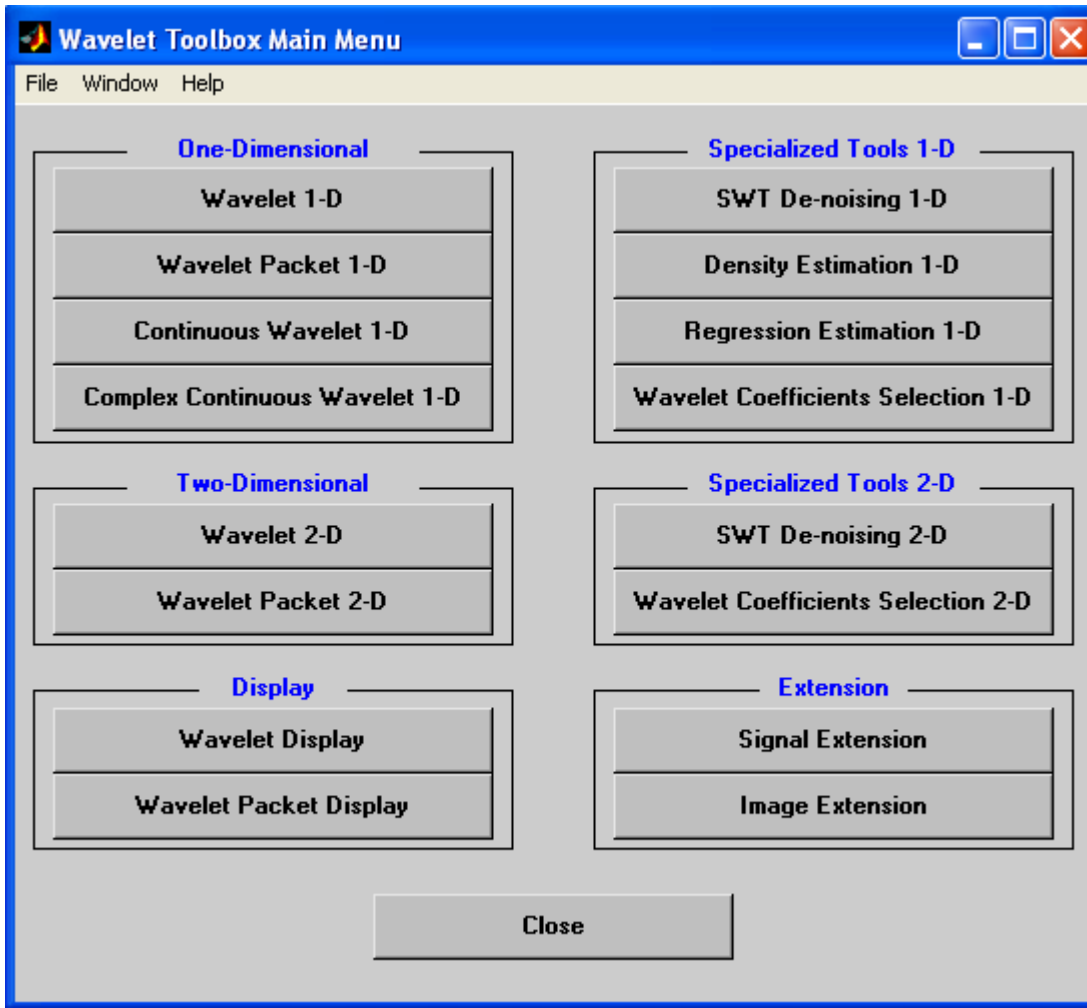
%Next load the extensor muscle data into the system for wavelet analysis

load('C:\Documents and Settings\Kunal Chaniary\Desktop\filesforanalysis\L07-002\Nj1\coeffampext1.mat'). Use coif 4 wavelet/ 8 level decomposition for analysis

c=coefs'

d=abs(c)

a18e=d(1:261)   % approximate coefficient a8

d18e=d(262:522)   % detail coefficient d8

d17e=d(523:1021)   % detail coefficient d7

```
d16e=d(1022:1997)              % detail coefficient d6
d15e=d(1998:3927)              % detail coefficient d5
d14e=d(3928:7765)              % detail coefficient d4
d13e=d(7766:15418)             % detail coefficient d3
d12e=d(15419:30701)            % detail coefficient d2
d11e=d(30702:61244)             % detail coefficient d1
save d11e.dat d11e /ascii       % save the coefficients in ascii format
save d12e.dat d12e /ascii
save d13e.dat d13e /ascii
save d14e.dat d14e /ascii
save d15e.dat d15e /ascii
e=synampext1'
f=abs(e)
save synext3.dat f /ascii


%Next load the extensor flexor data into the system for wavelet analysis
load('C:\Documents and Settings\Kunal Chaniary\Desktop\filesforanalysis\L07-
002\Nj1\coeffampflx1.mat')
c=coefs'
d=abs(c)
d15f=d(1998:3927)
d14f=d(3928:7765)
d13f=d(7766:15418)
d12f=d(15419:30701)
save d12f.dat d12f /ascii
save d13f.dat d13f /ascii
save d14f.dat d14f /ascii
save d15f.dat d15f /ascii
e=synampflx1'
```

f=abs(e)

save synflx1.dat f /ascii

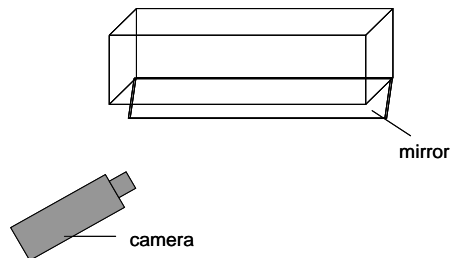% Repeat the process for each set of 30 sec data in file.

APPENDIX B

Gait analysis study

Procedure description:

The entire experiment was carried out inside a darkened room. Diffuse external lighting

was used to illuminate the chamber. A Plexiglas chamber 80cm long, 10 cm wide and 12

cm in height was used for this study. The experimental setup is described below.

Rats entered the Plexiglas chamber at one end and the other end of the chamber was

connected to a dark goal box filled with bedding. Rats were exposed to a brief stimulus of

bright light (40W bulb) and loud noise (radio), which would encourage them to run down

the chamber towards the goal box. Animals used for the gait study had to be trained (2-3

days prior to recording) to acclimatize them to the experimental conditions. The rats were

trained to walk inside a Plexiglas chamber towards a darkened goal box. At the end of each

satisfactory run across the chamber the rats were given a food reward (kitten's milk).

Note: Some severely dystonic animals (C.S> 3.0) were not capable of walking across the

chamber because of their motor disability. As a result, video recording of their gait was not

performed and the animals were marked severe.

<u>VITA</u>

Kunal Chaniary was born on May 5, 1984, in Mumbai, India. He is Indian by birth. He graduated from University of Mumbai in 2005 with a Bachelors degree in Biomedical Engineering. He received his Masters of Science degree in Biomedical Engineering from Virginia Commonwealth University in May 2008, followed by a Doctor of Philosophy in Biomedical Engineering in May 2010. He is an inducted member of Alpha Eta Mu Beta Biomedical Engineering Honor Society since 2009. Two of his publications have already been published in Movement Disorders and Journal of Neuroscience Methods. Work on three more publications is currently under way.